Application of fractals in condensed-matter physics

A. I. Olemskoi and A. Ya. Flat

Physicotechnical Institute, Sumy, Ukraine and Scientific-Production Enterprise RÉTO, Tomsk, Russia
(Submitted 16 June 1993; resubmitted 24 September 1993)
Usp. Fiz. Nauk **163**, 1–50 (December 1993)

Basic information about the theory of mono- and multifractal sets is presented. Geometric and thermodynamic descriptions are developed. The geometric picture is presented on the basis of the simplest examples of the Koch and Cantor fractal sets. An ultrametric space, representing the metric of a fractal set, is introduced on the basis of Cayley's hierarchical tree. The spectral characteristics of a multifractal formation are described. Attention is focused mainly on the application of the fractal concept for a thermodynamic system with partial memory loss, turbulent fluid flow, hierarchically coordinated set of statistical ensembles, Anderson's transition, and incommensurable and quasicrystalline structures.

1. INTRODUCTION

The concept of a fractal, recognized already at the beginning of the century and popularized by Mandelbrot in the 1960s,[1] is now widely disemminated in different fields of knowledge (see Refs. 2–25). Several books and reviews have now been published.[2–9] In our view, however, inadequate attention is devoted to application of the fractal concept in condensed-matter (and especially solid-state) physics. This is apparently attributable to the unusual nature of the geometric image of a fractal, the representation of which requires unaccustomed, seemingly abstract concepts. In addition, in solid-state physics real fractal formations of the type dislocation structures[12] and fractal clusters of microcracks[13] have become an object of investigation only very recently—after the introduction of the concept of scale (structural) levels of strain and fracture.[14] A characteristic feature of such formations is that the fractal structure is manifested only with simultaneous allowance of several levels, the difference of whose scales makes it difficult to represent a geometric image such as a broken coastline. Although it is difficult to observe multiscale structures themselves, they can, however, be described systematically only within a fractal ideology. This is because such nonequilibrium systems are represented as super-ensembles, consisting of hierarchically coordinated statistical ensembles, which, in turn, consist of a collection of subensembles, and so on.[15] For this reason, a fractal in a condensed medium must refer more to the application of the concept and not the description of the observed geometric image. This circumstance, which is the central idea of our exposition, is reflected in the title.

It should not be forgotten, however, that fractals were initially introduced as a geometric object in ordinary physical space.[1,2] For this reason, from the methodological standpoint it is best to start the analysis with the graphic constructions of Koch and Cantor (Sec. 2.1.1). This choice is made due to the fact that in the first case the fractal dimension D is greater than the topological dimension d and in the second case $D<d$. By gradually increasing the complexity of the procedure for constructing a fractal it is possible to find a general expression for the fractal dimension of an arbitrary monofractal, characterized by a single value D. The construction scheme itself is conveniently represented by a hierarchical Cayley tree, which is studied in Sec. 2.1.2. It turns out that the introduction of a metric on this tree makes it possible to find the distance between arbitrary points of the set. Since its value is prescribed by the branching ratio of the tree, this means that the branching ratio determines the dimension of the corresponding fractal. This result is true for both a regular tree with constant branching ratio and for a fractal, where the branching ratio changes from node to node, and one can talk only about an average branching ratio. Questions concerning the determination of the branching ratio are considered at the end of Sec. 2.1.2 and in Sec. 3.3.2.

The question of determining the dimension D of fractals occupies a central place in the theory of fractals. In Secs. 2.1.1 and 2.1.2 graphic methods are employed for the simplest formations. For the general case, however, these methods break down, and there arises the question of finding an algorithm for determining the fractal dimension of an arbitrary set. In order to construct it, in Sec. 2.2 a formal procedure is presented for determining the length, area, and volume of an ordinary surface. It is shown that extension of this procedure to an arbitrary set enables introducing a generating function, the condition of finiteness of which prescribes the fractal dimension D. The basic methods for determining the fractal dimension experimentally are presented in Sec. 2.3.

The exposition of the material of Sec. 2, which is devoted to monofractals, is completed in Sec. 2.4 with an examination of specific physical situations. Investigation of the simplest model of nonideal memory in Sec. 2.4.1 shows that in order to describe such memory the concept of degree of an integral and derivative must be extended to fractional numbers. From the physical standpoint this re-

 1063-7869/93/121087-42$10.00

duction of the order of integration/differentiation is associated with closing of some memory channels which operate in parallel. A similar situation is also observed if nondissipative dynamical and dissipative thermodynamic channels operative in parallel. In this case increasing the fraction of the former results in gradual transformation of a heat-conduction type equation into a wave equation. The character of the temporal evolution of such nonequilibrium systems is described in Sec. 2.4.2.

As experience in studying turbulence shows (see, for example, Refs. 8 and 9), fractal sets, representing real physical formations and processes, are characterized not by one value of the dimension D but rather by an entire spectrum of values. This makes it necessary to introduce the concept of a multifractal, which can be represented as a superposition of monofractals with different dimensions D. Section 3 is devoted to such sets. Since the concept of a multifractal is itself significantly more complicated than that of a monofractal (the former, in contrast to the latter, cannot be represented in the form of a regular Cayley tree), the exposition in Sec. 3 is unavoidably more difficult than in Sec. 2. For this reason we thought it would be convenient to present the material on mono- and multifractal separately.

In our exposition of the concept of a multifractal we started from the fact that a multifractal can be generated in two possible ways: 1) a geometric construction, in the process of which the initial fragment is divided into several blocks, whose number and relative position are then changed and the process is repeated many times; 2) the curdling method, where, in contrast to the preceding construction, both the number of blocks and the total magnitude of the physical measure (for example, the mass) remain constant; the construction process itself reduces to compressing the blocks (curdling). In this connection, there also exist two methods for describing multifractal sets: geometric, which is described in Sec. 3.1., and thermodynamic, which is described in Sec. 3.2. In the first method attention is focused on the investigation of the distribution of distances between points of the set and in the second method attention is centered on the distribution of measure on these points.

Just as in the analysis of monofractals, we start our exposition in Sec. 3 with investigation of the simplest two-scale Cantor multifractal (Sec. 3.1.1). This makes it possible to investigate within an analytical approach the spectrum of dimensions, trace how a multifractal is formed from a set of monofractals, and determine conveniently the required set of characteristics of a multifractal set. In Sec. 3.1.2 the results obtained for a Cantor set are extended to the arbitrary case. It is shown that the measure can be defined in two ways: One way extends to multifractal sets the concept of a generating function, introduced in Sec. 2.2, and the second method takes into account the fact that after arbitrarily fine fragmentation of the carrying space, some of the blocks will contain more than one point of the fractal set (the latter leads to the appearance of an additional free parameter τ). The basic relations between the spectral characteristics of a multifractal are established in Sec. 3.1.2 and their characteristic features are investigated in Sec. 3.1.3.

The thermodynamic formalism presented in Sec. 3.2 makes it possible to describe a multifractal set by analogy to statistical ensembles of many particles. In order to implement such an approach it is sufficient to assume that the set of elementary distances between the points of the set corresponds to the spectrum of effective energies, and the free parameter of the multifractal, determining the "coordinate" of one of the constituent monofractals, reduces to a thermodynamic state parameter. Just as in ordinary thermodynamics, here two mutually complementary approaches, related by a Legendre transformation, are possible. The formalism corresponding to the choice of temperature as the independent parameter is described in Sec. 3.2.1. It is found that this approach describes a set with a constant probability of realization of a measure. If the effective energy is taken as the free parameter, then the additional approach, describing the distribution of measure, provided by the curdling procedure (Sec. 3.2.2), is realized. Of course, the thermodynamic formalism makes it possible to retrieve the entire collection of parameters and spectral distributions of the geometric method. However, the thermodynamic representations provide not only a convenient and familiar language of description, but they also open up the possibility for application of the fruitful concepts of thermodynamics. Thus, for example, it is evident from Sec. 3.3.2 that the transformation of a long-period structure into a quasicrystalline structure can be represented as a phase transition between monofractals, belonging to the opposite ends of the spectrum of a multifractal, corresponding to the superposition of two incommensurable structures.

The last section (Sec. 3.3), just as Sec. 2, is devoted to specific examples of applications of the concept of a multifractal. Since the properties of a multifractal are largely determined by the symmetry of the function generating the set, a symmetric map, given by a parabola (the logistic sequence), is considered in Sec. 3.3.1 and incommensurable structures, generated by an antisymmetric function, are investigated in Sec. 3.3.2. The most important of them is realized in quasicrystals, in which the ordering of the atoms is described by a Fibonacci sequence. In Sec. 3.3.3 it is shown how the geometric characteristics of a multifractal enable describing a stochastic system consisting of hierarchically coordinated statistical ensembles.

In the concluding section the main ideas are presented and future prospects are discussed.

2. MONOFRACTALS

So, naturalists observe, a flea
Hath smaller fleas that on him prey;
And these have smaller still to bite 'em;
And so proceed *ad infinitum*
Daniel Defoe

We start the exposition with an original definition of a fractal, given by Mandelbrot:[2] a fractal is a self-similar (in the sense of a change in scale) set, whose dimension is different from the topological dimension.

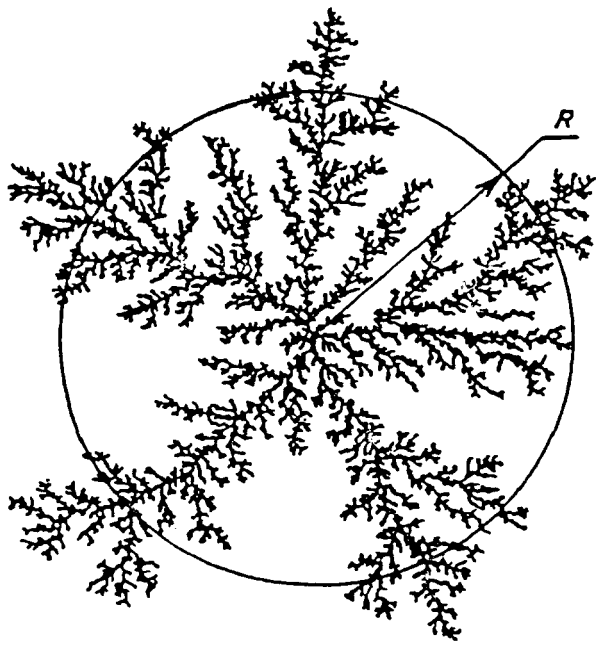

FIG. 1. Cluster with dimension $D=1.71$, arising as a result of two-dimensional diffusion-limited aggregation.[3]

Since this definition is more a mathematical than physical definition, we give some convenient considerations which demonstrate the concept of a fractal. To this end, we consider condensation of microparticles into a formation of a new phase. Such a formation is usually compact, and for this reason the number of particles in the formation of size R is given by the relation

$$N \propto R^d, \tag{2.1}$$

where d is the dimension of the space. The volume V of the formation has the same form

$$V=A_d R^d, \tag{2.2}$$

where A_d is a geometric factor that takes into account the shape (for an equiaxial shape $A_1=2\pi$, $A_2=4\pi$, $A_3=4\pi/3$). Correspondingly, the density of particles of a compact formation $\rho=N/V$ is independent of the size of the formation.

A completely different situation is observed for fractals, which are not compact formations (Fig. 1). It is evident that as the size R of the formation increases, the number of particles

$$N \propto R^D \tag{2.3}$$

increases more slowly. The exponent D is the main quantitative characteristic of a fractal and is called the fractal (Hausdorff) dimension. The anomalous character of the function (2.3) arises because the fractal dimension D is different from the dimension d of the physical space in the relation (2.1) for the dense formation. Accordingly, the density of a fractal

$$\rho \propto R^{-(d-D)}, \quad d>D \tag{2.4}$$

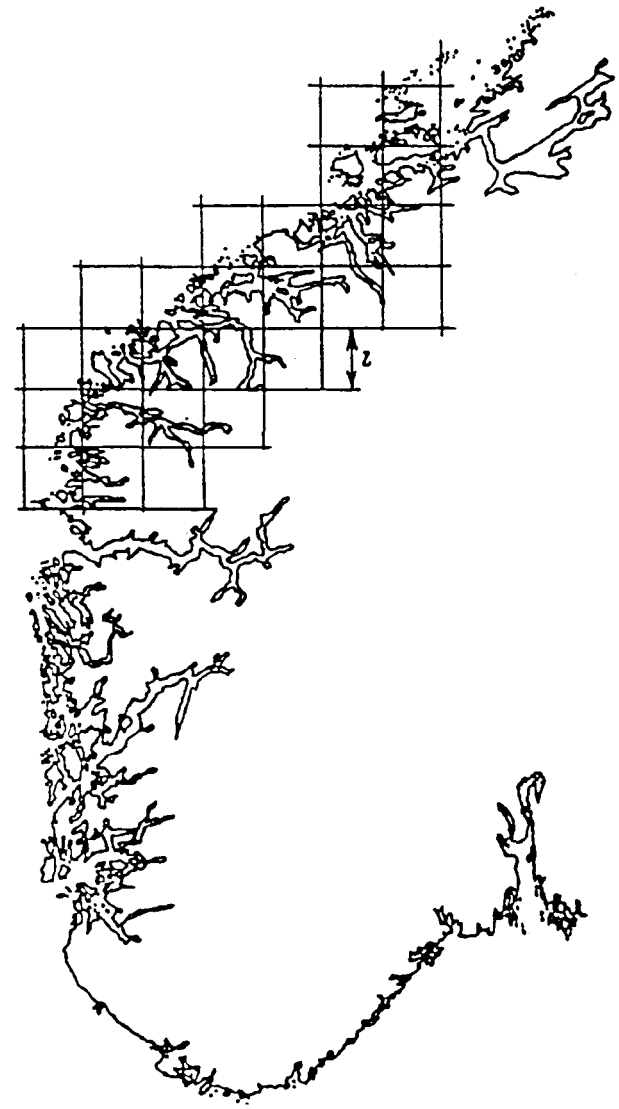

FIG. 2. Southern coastline of Norway (the resolution of the grid shown at the top is $l\sim 50$ km).[3]

becomes a decreasing function of size, which is what reflects the noncompact character of a fractal. Obviously, the larger the difference between the topological d and fractal D dimensions, the more open the fractal object is.

The concept of a fractal was first encountered in measurements of the length of a coastline. Although intuitively it seems obvious that the length L of the coastline should not depend on the choice of measurement scale $l\to 0$, measurements showed that in reality the relation

$$L \propto l^{1-D}, \tag{2.5}$$

where the fractal dimension $D>1$, holds (for example, for the British Islands $D\approx 1.3$ and for Norway $D\approx 1.5$). This indicates that the coastline is a set occupying a position intermediate between the ordinary line ($d=1$) and a surface ($d=2$), and the quantity $1<D<2$ is all the larger, the

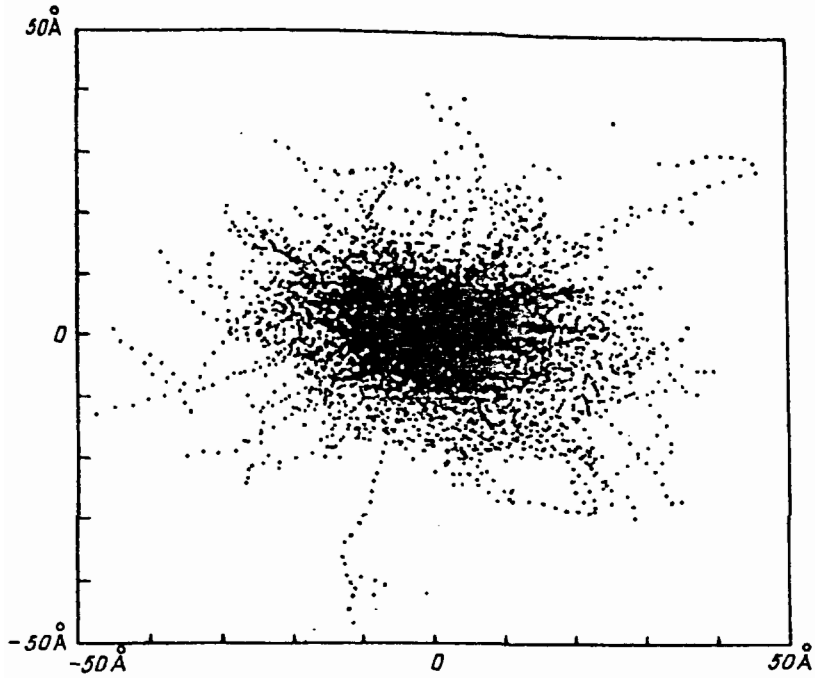

FIG. 3. Two-dimensional pattern of point defects arising in a beryllium crystal after passage of 25-MeV uranium ions in a direction perpendicular to the plane of the figure (data obtained by A. I. Kul'ment'ev).

more irregular the coastline is. This circumstance is demonstrated graphically in Fig. 2, where the coastline of Norway is displayed.

A physical example of a fractal are clusters of gels, formed when sols merge (see Fig. 1). In a solid, defect fractal structures arise, for example, when heavy particles pass through crystals (Fig. 3). An example of fundamental importance are defect structures in solids subjected to an intense external load, resulting in significant defect densities. As a result, there appear collective effects, which lead to the inclusion of new structural levels of plastic strain. The carriers are first fractal clusters, whose compactification leads to formation of superdefects, comprising structural elements on a new level.[15] Thus, Fig. 4 displays the basic stages of the evolution of a high-density ensemble of dislocations: At first their distribution is uniform, but then clusters in the form of clumps and open walls of blocks form, and at the final stage a distinct block structure is formed.[12] Evidently, it is the accumulations of dislocations, forming block walls, that represent fractals, whose dimension at first increases from $d=1$ (uniform distribution of dislocations) up to a dimension $1<D<2$ (open accumulations) and then increases up to $d=2$ (geometric wall of a block).

As one can see from the examples presented above, the basic characteristic of a fractal is its dimension D. In this section we consider the idealized case of a monofractal, which is characterized by a single value of D. First we present convenient geometric models, which make it possible to find the dimension D in an intuitive manner. Next, an algorithm making it possible to determine D analytically for an arbitrary monofractal is formulated. The exposition is completed by an examination of specific cases arising in condensed-matter physics.

2.1. Geometric models of fractals

We consider first convenient models of the simplest fractal Koch and Cantor sets (Sec. 2.1.1). This will enable us to find a general expression for the dimension of a fractal geometric object, represented in the ordinary physical space. In Sec. 2.1.2 an extension is made to the hypothetical space with ultrametric topology.[17,18] The use of this

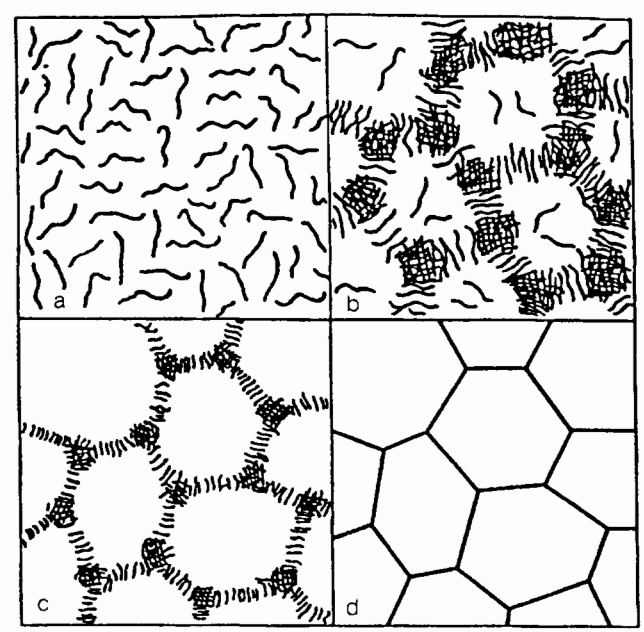

FIG. 4. Schematic representation of the restructuring of a dislocation structure into a block structure. a—Chaotic distribution of dislocations. b, c—Formation of dislocation clumps and open walls. d—Block structure.[12]

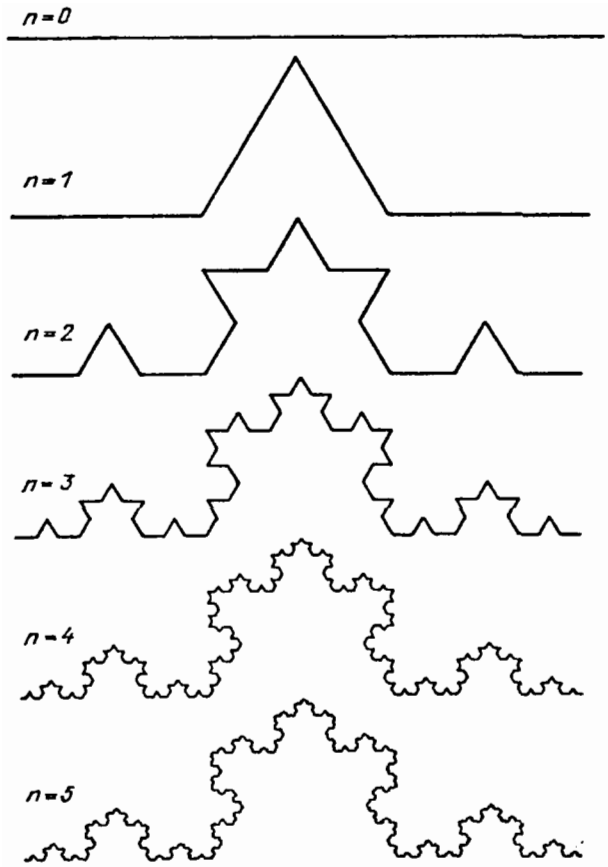

FIG. 5. Construction of a triadic Koch figure.[3]

space has made it possible to explain, in the last few years, the behavior of hierarchically coordinated structures arising in spin[18,19] and structural[20] glasses, in the process of plastic strain[21] and fracture[22] in structural[23] and, in particular, martensite[24] transformations, in high-T_c oxides,[25,26] and so on.

2.1.1. Koch and Cantor fractal sets

We consider first Koch's triadic figure. As one can see from Fig. 5, in order to construct this figure a segment of unit length is taken at the step $n=0$. At the next step $n=1$ an interval of length 1/3 is cut out of the center of the segment, and an equilateral triangle without a base is constructed on the segment. At the next step, an interval of length $(1/3)^2$ is cut out on each of the four segments obtained and the same construction as performed above is made. Then the procedure is repeated $n\to\infty$ times.

Let L be the length of the fractal obtained. Since after each step the length increases by 4/3 times, at the nth step we obtained $L_n=(4/3)^n$. Since the length of each link is $l_n=(1/3)^n$, we have $n=-\ln l_n/\ln 3$, and it is evident that the relation (2.5), where the fractal dimension is

$$D=\ln 4/\ln 3=1.263, \tag{2.6}$$

holds between the total length L_n and the elementary length l_n. The number of segments $N_n=L_n/l_n$, comprising a Koch figure, is determined by the relation (we temporarily drop the index n)

$$N(l)\propto l^{-D}. \tag{2.7}$$

As one can see from Fig. 5, in the limit $n\to\infty$ Koch's curve is a formation intermediate between an ordinary line and an ordinary surface. For this reason, its fractal dimension (2.6) lies in the interval $1<D<2$.

According to the definition given above, a fractal is a self-similar set. This is easily seen from Fig. 5, by noting that the identical construction, but at a reduced scale, is performed at each step n. For this reason, any fragment of Koch's figure can be obtained by simply increasing any of its components up to the required scale. This circumstance is formally reflected in the equality of the type (7). Indeed, if the length l of an elementary section is reduced by ξ^{-1} times, then the number of segments $N(l)$ will also increase. Then we obtain from Eq. (7)

$$N(\xi l)=\xi^{-D}N(l), \quad \xi<1. \tag{2.8}$$

By definition the function $N(l)$, satisfying an equation of the type (2.8), is a homogeneous function of order D, whose value is equal to the fractal dimension. A characteristic function of homogeneous functions $N(l)$ is that a decrease of the measurement scale of the argument l by a factor ξ^{-1} is equivalent to increasing the function N by a factor ξ^{-D}.

This self-similarity property is characteristic not only of Koch's figure, but also all fractal formations. The similarity relation (8) is itself more general than the expressions (2.6) and (2.7) for a triadic Koch figure. Indeed, fixing in Eq. (2.8) the similarity parameter ξ by the condition $\xi l=1$, we immediately obtain the relation (2.7). On the other hand, it is evident hence that with an arbitrary scale ξ the elementary length $l_n=\xi^n$ does not reduce to $(1/3)^n$ and Eq. (2.6) must be generalized as follows:

$$D=\ln 4/\ln \xi^{-1}, \tag{2.9}$$

where the similarity parameter $\xi<1$ shows the amount by which the length of each of the four segments of the block forming the Koch figure is shortened.

We now consider an example of a fractal set with dimension $D<1$—"Cantor dust." As one can see from Fig. 5, its construction is different from the Koch curve only in that at the n-th step one does not add but rather removes n intervals of length $l_n=(1/3)^n$. Accordingly, the length of the remaining set is $L_n=(2/3)^n$, and each link l_n remains the same as in Koch's figure. As a result the relation $L_n(l_n)$ is expressed by the previous function (5), where, however, the fractal dimension is

$$D=\ln 2/\ln 3=0.631. \tag{2.10}$$

The condition $D<1$, as one can see from Fig. 6, means that "Cantor dust" is a formation intermediate between a point and a line. It is easy to see that the number $N_n=L_n/l_n$ of segments of length l_n is determined by the same formula (2.7) as in the case of a Koch curve.

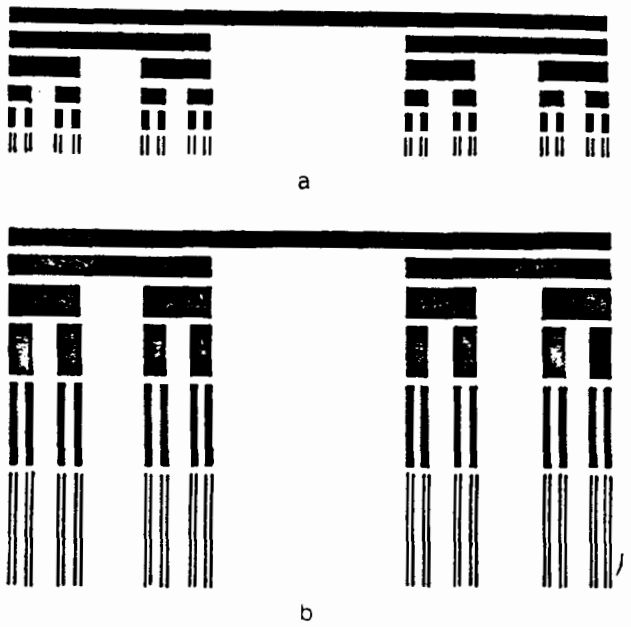

FIG. 6. Construction of a triadic Cantor set. a—Geometric method. b—Curdling method.[3]

The equation (2.10) corresponds to the simplest case of a symmetric Cantor set, shown in Fig. 5. Just as for Koch's figure, it is evident that if after each step n of the construction the length of the segments l_n is taken to be ξ and not 1/3, then in the denominator of Eq. (2.10) ln 3 is replaced by $\ln \xi^{-1}$. On the other hand, comparing the numerators of the expressions (2.6) and (2.10) shows that in the general case ln j should apparently occur there, where j is the number of blocks participating in the construction of the elementary figure of the fractal (for a Koch curve and Cantor dust, shown in Figs. 5 and 6, we have $j=4$ and 2, respectively). Thus it can be inferred that the expression for the fractal dimension, generalizing Eqs. (2.6), (2.9), and (2.10), has the form

$$D=\ln j/\ln \xi^{-1}, \tag{2.11}$$

where j is the number of blocks representing an elementary fragment of the fractal and ξ is the similarity index, determining by how many times the size of the block is diminished at each step of the construction. Since for a Cantor set the size of the obtained fragment must not exceed the size of the initial block, the value of the similarity parameter is limited by the condition $\xi j \leqslant 1$, which in turn leads to the result $D \leqslant 1$. As found above, it corresponds to the fractal sets for which at each step of the construction separate blocks are removed. In the case when blocks are added, as in the Koch figure, we have $D>1$, and according to Eq. (2.11) the similarity parameter assumes the value $\xi > j^{-1}$.

2.1.2. Hierarchical Cayley tree

It is easy to see that the above-described procedure for constructing a Cantor set (see Fig. 6) can be represented by a hierarchical Cayley tree, shown in Fig. 7a. We shall show that the topological equivalence of the figures presented in Fig. 6 and 7a[1)] makes it possible to associate to each element of a fractal set a point in an ultrametric space, whose geometric image is a Cayley tree. To this end, we must introduce a parameterization of the hierarchical tree, i.e., we must construct a method for describing the tree analytically.[17]

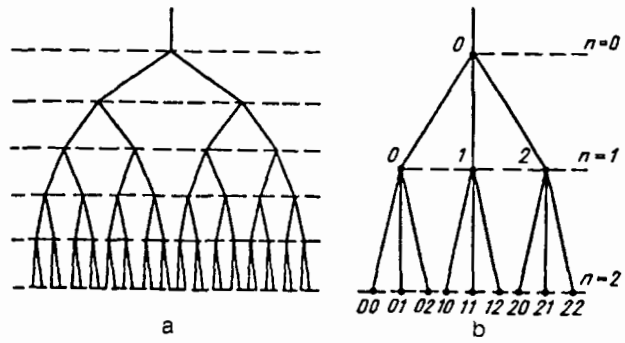

FIG. 7. Simplest regular Cayley trees. a—Tree describing a chain of bifurcations (degree of branching $j=2$). b—Parameterization of a Cayley tree with $n=2$ hierarchical levels and ratio $j=3$.

We begin with the simplest example of a one-dimensional tree, presented in Fig. 7b. It is characterized by the number of levels $n=2$ and the branching ratio $j=3$. It is evident from the figure that each node of the tree at the lower level $n=2$ can be prescribed by n numbers a_l, where the index l runs through the values 0 up to $n-1$, and the numbers a_l themselves vary from 0 to $j-1$. In other words, the coordinates of the nodes at the level n

$$\{a_l\}_n^j = a_0 a_1 \ldots a_l \ldots a_{n-1}, \quad a_l = 0,1,\ldots,j-1 \tag{2.12}$$

are n-digit numbers in a j-adic number system. They also determine the space with ultrametric topology. The characteristic feature of the space is that its points cannot form triangles all of whose sides are different.[17] This property can be easily checked by assuming that the distance l between any nodes of a Cayley tree, which belong to a given level n, is determined by the number of steps up to the common ancestor, lying at the level $n-l$. For example, the distance between the nodes and 10 and 12 in Fig. 7b is 1, and the distance between nodes 01 and 12 is 2; the points 01, 12, and 20 form an equilateral triangle, and the points 01, 11, and 12 form an isosceles triangle. It follows from the examples presented that if two nodes are enumerated by the collections (2.12) of numbers a_l and b_l, then the distance between the nodes depends only on which of the numbers differ first. Thus for the tree shown in Fig. 7b the distance is 2 if $a_0 \neq b_0$ and 1 if $a_0 = b_0$, but $a_1 \neq b_1$. For an arbitrary collection of numbers n and j the distance between given points is $l=0,1,\ldots,n+1$ if $a_m = b_m$, $m=0,1,\ldots,n-l-1$, but $a_{n-l} \neq b_{n-l}$.

The importance of the concept of an ultrametric space is determined by the fact that, being a reflection of the hierarchical structure of the system, it realizes a so-called logarithmic metric for physically observable quantities. This means that in such a space the distance l is a linear function of the logarithm of the observed quantity ρ. Since

it is more convenient to manipulate $\ln \rho$ than a linear function of l, it is convenient to introduce, instead of the ordinary axis of the values of ρ, the corresponding ultrametric space, characterized by the distance l, and then perform all calculations in this space.[17-18]

In order to determine the function $\rho(l)$ we represent ρ in the j-adic number system (2.12). This is done by expanding in a power series

$$\rho(a-b)=(a_0-b_0)j^n+(a_1-b_1)j^{n-1}+\cdots+(a_{n-1}-b_{n-1})j^l+\cdots+(a_{n-1}-b_{n-1})j+(a_n-b_n), \quad (2.13)$$

the first n coefficients of which are given by the n-digit numbers (2.12), and the last coefficients determine the origin with respect to which ρ is measured. It is easy to see from Fig. 7b that the representation (2.13) corresponds to partitioning j^n nodes of Cayley's tree into $n+1$ groups, each of which consists of clusters of nodes characterized by the same values l of the maximum distance between them. Thus the first term in the series (2.13) corresponds to the group consisting of j^n isolated nodes, for which $l=0$. The second term in Eq. (2.13) describes the contribution of clusters whose nodes are separated by a distance $l=1$ (in Fig. 7b three such clusters can be singled out: 00, 01, 02; 10, 11, 12 and 20, 21, 22). Since each of these clusters is engendered by a node lying at the preceding hierarchical level $n-1$, it is easy to see that in the general case any such cluster consists of j nodes, and there are j^{n-1} clusters. The group of clusters engendered by the hierarchical level $n-l$ corresponds to an arbitrary distance l. For this reason, the number of such clusters is j^{n-l}, and each of them contains j^l nodes. These nodes are grouped into j subclusters, corresponding to the shorter distance $l-1$. Thus it can be concluded that the degree of the factor of j^{n-l} of any arbitrary term in the series (2.13) is given by the number of clusters of nodes the maximum distance between which is l, and the magnitudes of the coefficients a_l-b_l are limited by the number j of subclusters, corresponding to the distance $l-1$, contained in them.

A remarkable property of the expansion (2.13) is that for $j\gg 1$ only one term dominates in it. Indeed, if the distance between the points of the ultrametric space is l, then the first $n-l$ terms, containing the maximum powers of the large number j, are zero, since by definition $a_m=b_m$ for $m=0,1,\ldots,n-l-1$. The last l terms of the series contain the powers j^k, $k=l-1, l-2, \ldots, 0$, whose values are negligibly small compared to j^l. Thus the only remaining term is $(a_{n-l}-b_{n-l})j^l\leqslant j^{n+1}$, and to logarithmic accuracy the series (2.13) reduces the form

$$\ln \rho\approx(l+1)\ln j\approx l\ln j, \quad n,j,l\gg 1. \quad (2.14)$$

It is this equality that specifies the logarithmic metric of the ultrametric space.

We considered above a discrete ultrametric space, since it is only in this case that a definite Cayley tree can be associated to it. However, just as in ordinary space, it is possible to pass to the corresponding continuous limit

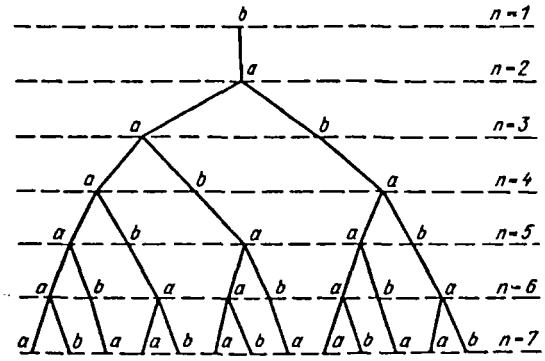

FIG. 8. Irregular Fibonacci tree with variable degree of branching.

(such a limit visually looks like smearing of a set of points uniformly filling the area of a sheet of paper). In the Cayley tree representation this smearing is achieved by an infinite increase in the number of levels n and/or branching ratio j. Then the number of nodes

$$N_n=j^n, \quad (2.15)$$

at each level n becomes so large that the interval $l_n=N_n^{-1}=j^{-n}$ between the closest points of a discrete space becomes infinitely small, and the ultrametric space itself becomes continuous. Correspondingly, the distance l in Eq. (2.14) becomes continuous. The transition to the continuum on Cayley's tree means infinite bunching of hierarchical levels.

Everywhere above we had in mind a uniform Cayley tree, whose degree of branching is the same at all nodes. Obviously, the dimension of the corresponding ultrametric space will be $d=1$. Indeed, since here the similarity parameter $\xi=j^{-1}$, we obtain the elementary length $l_n=\xi^n=j^{-n}$, and Eq. (2.15) acquires the form (2.7), where $D=1$. It is easy to see that the fractional dimension $D<1$ is obtained only in the case if at each level n the branching vanishes for some nodes. Such a situation is realized, for example, for the Fibonacci sequence, studied in Sec. 3.3.2. It is evident from the corresponding Cayley tree, shown in Fig. 8, that aperiodic (but completely regular!) alternation of nodes with branching ratios $j=1,2$, is observed. In Sec. 3.3.2 it will be shown that here for each nonbranching node the number of doubly branching nodes is equal to the so-called golden mean $\tau=(\sqrt{5}+1)/2\approx 1.618$. It turns out that this results in a reduction of the dimension of the ultrametric space, corresponding the Fibonacci tree, to the value $D=\ln\tau/\ln 2\approx 0.694$. In the general case we have

$$D=\ln\rho/\ln j, \quad (2.16)$$

where ρ is the number of nodes, per nonbranching node, with branching ratio $j=2,3,\ldots$.

Of course, just as for ordinary space, the dimension of the ultrametric space can take on values $D>1$. Thus Fig. 9a displays an example of the two-dimensional uniform Cayley tree, whose dimension $d=2$. The characteristic feature of this tree is that branches from both the vertical and horizontal components of the tree enter into all nodes at

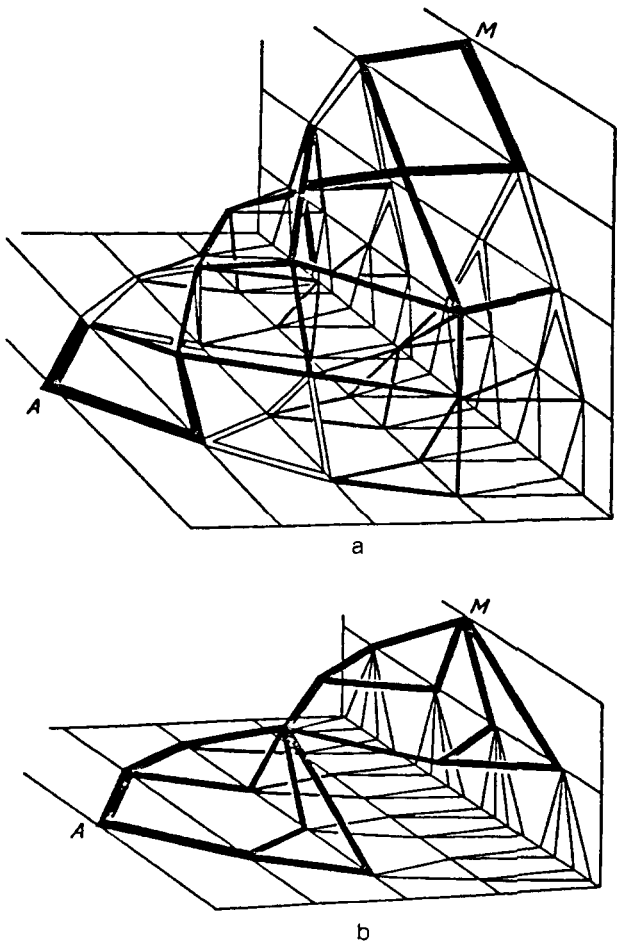

FIG. 9. Regular (a) and irregular (b) two-dimensional Cayley trees.

lower hierarchical levels. When this rule is violated (Fig. 9b) the dimension of the space decreases to $D=\ln(j\sigma)/\ln j$, where the parameter $\sigma\leqslant j$ determines the fraction of the nodes where branches from both components of the two-dimensional tree converge. As the topological dimension increases to values $d>2$, the parameter σ coupling different components acquires the exponent $d-1$. If, besides incomplete merging of the components, the components themselves have a fractal character such as the Fibonnaci tree in Fig. 8, then in accordance with Eq. (2.16) $j\sigma^{d-1}$ must be replaced by $\rho\sigma^{d-1}$, where the parameter ρ determines the fraction of the branching nodes. As a result the fractal dimension of the ultrametric space corresponding to nodes of the d-dimensional Cayley tree assumes the form

$$D=\frac{\ln\rho}{\ln j}+(d-1)\frac{\ln\sigma}{\ln j}. \tag{2.17}$$

The foregoing analysis refers to a rarefied ultrametric space, for which the fractal dimension D is less than the topological dimension d. The inverse case $D>d$ occurs if not only the nearest hierarchical levels but also distant hierarchical levels are connected (Fig. 10). In other words, the condition $D>d$ is realized for non-Markovian hierar-

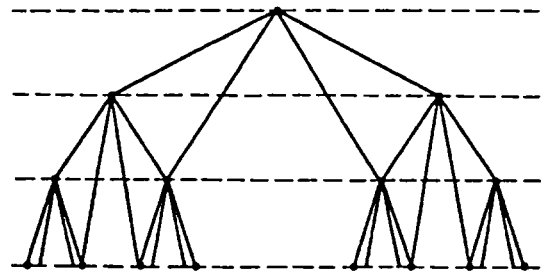

FIG. 10. Cayley tree corresponding to non-Markovian generation of scale levels.

chical systems exhibiting memory. It is obvious that Eqs. (2.16) and (2.17) are also applicable to this situation, if it is assumed that the parameters ρ and σ assume the values $\rho,\sigma>j$.

2.2. Determination of fractal dimension

In the examples presented above the fractal dimension was determined from graphical considerations. In the general case, however, the situation becomes so complicated that the arguments are no longer obvious and the constructions indicated above must be generalized. The crux of the constructions is that the fractal set is covered by elementary d-dimensional cubes with edge length $l\to 0$ and the number $N(l)$ of the cubes is counted. The fractal dimension is then determined from a relation of the type (2.7). A formal device, enabling implementation of this procedure, is to introduce a generating function, whose meaning can be seen from the following example.

Consider an ordinary (nonfractal) surface with dimension $d=2$ and area S_0 (Fig. 11). First we cover it with squares with side $l\to 0$, whose number is

$$N(l)=S_0/l^2. \tag{2.18}$$

The total area of the squares is determined by the formula

$$S(l)=N(l)l^2. \tag{2.19}$$

Although from the algebraic standpoint the equations (2.18) and (2.19) seem to be identical, it should be kept in mind that the first equation is applicable only to ordinary surfaces, whereas the second is applicable only to fractal surfaces. Substituting Eq. (2.18) into Eq. (2.19) obviously gives

$$S(l)=S_0. \tag{2.20}$$

It appears that an elementary square is the most natural element to use in determining the surface area. But this is not the only possible choice. Thus our surface can also be covered with elementary cubes, as shown in Fig. 11. Their total volume is expressed by the obvious equality of the type (2.19)

$$V(l)=N(l)l^3. \tag{2.21}$$

Substituting here the number of cubes (2.18)

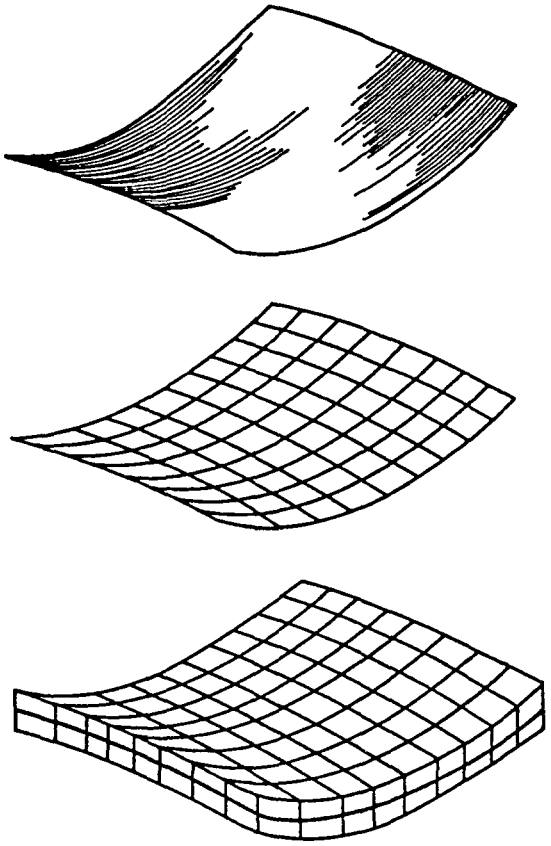

FIG. 11. Definition of surface measure.[3]

$$V(l)=S_0 l. \tag{2.22}$$

Continuing the list of elementary figures with whose help the surface of interest is covered, we can, in principle, also use a broken line, consisting of $N(l)$ segments of length $l\to 0$. The total length of the line is determined by the formula

$$L(l)=N(l)l, \tag{2.23}$$

leading, after substituting Eq. (2.18), to the relation

$$L(l)=S_0 l^{-1}. \tag{2.24}$$

The equations (2.24), (2.20), and (2.22) have in common the fact that they express the measure χ_q of sets with dimensions $q=1,2,3$, covering the set of interest—a surface with dimension $d=2$. It can be represented in the general form

$$\chi_q(l)=S_0 l^{q-d}. \tag{2.25}$$

A characteristic feature of this equality is that in the limit $l\to 0$ the function $\chi_q(l)\to\infty$ for $q<d$ [Eq. (2.24)] and $\chi_q(l)\to 0$ for $q>d$ [Eq. (2.22)]. The measure (2.25) assumes a finite value $\chi_q(l)\to S_0$ only if $q=d$, which condition gives the dimension of the surface of interest.

The graphic example considered above shows how to construct the generating function which makes it possible to find the fractal dimension D of an arbitrary set (in the example considered above, it reduced to an ordinary surface with $d=2$). Evidently, the general form of this function can be represented as the equation

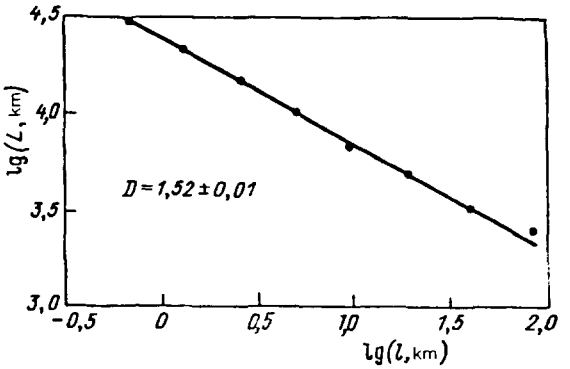

FIG. 12. Graph of the length of the coastline of Norway versus the resolution of the covering square grid.[3]

$$\chi_q=\sum_i l_i^q, \tag{2.26}$$

where the summation extends over elementary formations characterized by the length l_i and dimension q. In contrast to the previously considered examples, where $l_i=\text{const}\equiv l$ and $q=1,2,3$, here, first of all, it is assumed that the partitioning into elementary sets is nonuniform (l_i is not a constant) and, second, the parameter q is assumed to be continuous. If uniform partitioning is employed, then the definition (2.26) assumes the simpler form

$$\chi_q(l)=N(l)l^q. \tag{2.27}$$

Taking into account Eq. (2.27) we obtain the relation

$$\chi_q(l)\propto l^{q-D}, \tag{2.28}$$

extending the result (2.25) for fractal objects. The formula (2.7) for the length of a coastline is an example of such a relation with $q=1$.

Thus in order to determine the fractal dimension analytically the fractal must be covered with elementary q-dimensional blocks with edge length l_i and the generating function must be found using the formula (2.26). Changing the exponent q, we must find next the value $q=D$ that gives the generating function a finite value. This will be the fractal dimension D. The generating function $\chi_q(l)$ itself is the main characteristic of a fractal of a type such as the length of a coastline.

2.3. Experimental methods for determining fractal dimension

The most convenient method for determining D is based on direct computation of the generating function (2.26). For example, in determining the length of a coastline the coastline is covered by a collection of squares with side $l\to 0$ and the number of squares $N(l)$ is calculated for different values of l. Next, the function $N(l)$ (Fig. 12) is

constructed in double logarithmic coordinates and the fractal dimension is determined, using Eq. (2.7), from the slope

$$D=\frac{\text{const}-\ln N}{\ln l}. \tag{2.29}$$

Another variant of the geometric method is to determine D from the relations between the characteristics of sets of different topological dimension. For example, if for the figure bounded by the fractal boundary the area $S\propto R^2$ and the perimeter length $L\propto R^n$, where R is a characteristic length, is measured, then the following formula follows from the relations $S^{1/2}\propto R\propto L^{1/D}$:

$$D=\frac{\text{const}+\ln L^2}{\ln S}, \tag{2.30}$$

according to which the fractal dimension D of the boundary is defined as the tangent of the slope angle of the function of the square with perimeter L^2 versus the area S, constructed in double logarithmic coordinates.[2)] The length of the perimeter is measured either directly (for example, with a curvimeter) or in the same way as in the coastline problem.

For all their convenience, the methods presented above have the drawback that the quantity l must be determined empirically: On the one hand, it must not be so small that it would be impossible to count the number of elements and, on the other hand, it cannot be so large that the relation (2.7) is not applicable. For this reason, methods based on direct experimental determination of $N(l)$ are more reliable. Thus, if a large number of identical fractal clusters, displayed on a transparent photographic plate, are available, then passing a light beam of thickness r through the transparent and measuring the intensity I of the transmitted light Eq. (2.29) can be replaced by the formula

$$D=\frac{\text{const}-\ln I}{\ln r}. \tag{2.31}$$

This formula is applicable not only for a uniform distribution of identical fractal clusters, but also for investigating a single fractal. The centers of the beam and cluster must coincide, and the size r of the diaphragm must not exceed the size R of the cluster.

In a real experiment the most reliable structural data are obtained by determining the correlation function, whose spatial Fourier transform is proportional to the intensity of the scattered radiation. For this reason, when measuring fractal dimension preference should be given to the method of small-angle scattering of the transmitted radiation (for large clusters ordinary light can be used, but as the cluster size decreases, x-rays, electrons, or thermal neutrons must be used). If the value of the scattering vector q falls in the range $R^{-1}\ll q\ll a^{-1}$, where R is the cluster size and a is the size of the particles forming the cluster, then the intensity I of small-angle scattering is determined by the formula[27]

$$I(q)=I_0q^{-n},\quad q=(4\pi/\lambda)\sin(\theta/2). \tag{2.32}$$

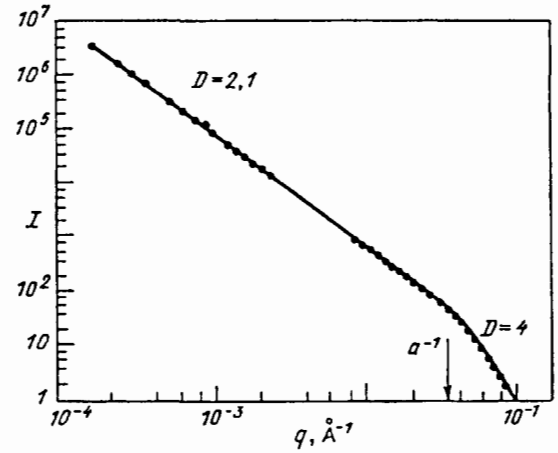

FIG. 13. Intensity of scattered light (small q) and 2 small-angle scattering of x-rays (large q) versus the scattering wave vector q.[3]

where I_0 is the intensity of the incident beam, λ is the wavelength, and θ is the scattering angle. Constructing the function $I(q)$ in logarithmic coordinates, we find the fractal dimension from the slope angle of the obtained straight line

$$D=\frac{\ln I_0-\ln I(q)}{\ln q}. \tag{2.33}$$

Here it is important to work in the region of scattering vectors q that reflects the fractal structure. As the scattering vectors increase up to values $qa\sim 1$, for which Porod's regime[21]

$$I(q)=I_0q^{-(d+1)} \tag{2.34}$$

is realized, the measurements will give the topological dimension d of the cluster (Fig. 13).

2.4. Examples of application of the concept of a fractal

In describing fractals one usually has in mind real formations (fractal gels, ball lightning, mixture of liquids with different viscosity, fractal surface of a fracture, fractal formations obtained by sintering powders, defect structures, and so on).[3–7] In the present section we shall not describe their structure, but rather we shall consider the theoretical aspects based on fractal representations.

2.4.1. Fractional integral and fractional derivative

Consider a medium exhibiting memory. Such a situation arises when describing a structure of a solid far from thermodynamic equilibrium: in amorphous materials,[18–20] in the description of structural relaxation of high-T_c oxide superconductors,[25] in the process of plastic deformation[15] and fracture of solids,[13] in the description of solid solutions[23] and the macrostructure of martensite,[24] and so on. The existence of memory means that if at time t' a force $f(t')$ acts on the system, then there arises a flux J whose magnitude at time $t>t'$ is given by the equation

$$J(t)=\int_0^t M(t-t')f(t')\,dt'. \tag{2.35}$$

For a system which does not exhibit memory the time dependence of the memory function $M(t-t')$ has the form

$$M(t-t')=\gamma\delta(t-t'), \tag{2.36}$$

where γ is a positive constant and $\delta(t-t')$ is the Dirac delta function. Substituting Eq. (2.36) into Eq. (2.35) we obtain the relation

$$J(t)=\gamma f(t), \tag{2.37}$$

according to which in the absence of memory the flux $J(t)$ is affected only by the value of the force $f(t)$ acting at the same time t. When memory is switched on the delta function in Eq. (2.36) spreads into a dome-shaped function, whose width determines the time interval τ during which the action of the force f affects the flux J. For systems with ideal memory we have $\tau\to\infty$, i.e., the flux $J(t)$ is formed throughout the entire duration of action of the force $f(t')$ up to the moment t. This is expressed formally by prescribing the kernel of the integral relation (2.35) in the form

$$M(t-t')=\gamma/t. \tag{2.38}$$

Here there is no dependence on the time t' at which the force f acts, and the dependence of the memory function on the time t at which the flux J is measured is taken in a form so as to satisfy the normalization condition

$$\int_0^t M(t-t')\mathrm{d}t'=\gamma. \tag{2.39}$$

The relation (2.35) written in the temporal representation, is inconvenient due to the presence of the convolution (integral over t'). It can be eliminated by using the Laplace transform

$$f(t)=\int_{-i\infty}^{+i\infty} f(\lambda)e^{-\lambda t}\frac{\mathrm{d}\lambda}{2\pi i},$$
$$f(\lambda)=\int_0^\infty f(t)e^{\lambda t}\mathrm{d}t, \tag{2.40}$$

which enables switching from the time t to the complex frequency λ. Applying it to both sides of the definition (2.35) we obtain the algebraic form of this relation

$$J(\lambda)=M(\lambda)f(\lambda). \tag{2.41}$$

It is easy to see that the Laplace transform of the kernel (2.36), corresponding to the absence of memory, reduces to a constant:

$$M(\lambda)=\gamma. \tag{2.42}$$

In the case of ideal memory, in the limit $|\lambda|t\gg 1$, we obtain from Eq. (2.38) correspondingly

$$M(\lambda)=\gamma/\lambda t. \tag{2.43}$$

Thus when memory is switched on, the constant kernel (2.42) is transformed into the hyperbolic function (2.43).

In this connection there arises the following question: What will the function $M(\lambda)$ look like if memory is complete but not ideal? This means that memory is manifested on an infinite interval preceding the time t, but not at all times t'. Suppose, for example, that memory is preserved only at points of a Cantor set. It can then be expected that its fractal dimension D will be related to the measure of memory preservation.

Calculating the Laplace transforms of the simplest time dependences (2.36) and (2.38) is an elementary problem. For memory operating at the points of a Cantor set, however, the calculations are much more difficult. They were performed in Ref. 16 and lead to the result

$$M(\lambda)\propto z^{-D},\quad z=(1-\xi)\lambda t, \tag{2.44}$$

where the fractal dimension D is determined by Eq. (2.11) and ξ is the similarity parameter, determined in Sec. 2.1.1.

It is easy to see that the obtained memory function (2.44) satisfies the similarity condition (2.8) with the exponent D. Reducing to the fractal dimension at the Cantor set at whose points memory is switched on, this exponent is thus a quantitative measure of the manifestation of memory effects. For an empty Cantor set ($\xi=0$) Eq. (2.11) gives $D=0$, and the function (2.44) reduces to a constant (2.42), corresponding to complete absence of memory. As the similarity parameter $\xi>0$ increases the exponent (11) increases, and the Laplace transform (44) of the memory function becomes an increasingly more rapidly varying function. The limiting value $\xi=j^{-1}$ of the similarity parameter gives the dimension $D=1$, corresponding to ideal memory described by the function (2.43).

Thus systems exhibiting residual memory are described by the Laplace transform (2.44), where the exponent $0\leqslant D\leqslant 1$ determines the measure of memory preservation. Inverting the Laplace transform (2.40) we find for the time dependence of the memory function[16]

$$M(t-t')\propto[\sqrt{2}(1-\xi)t]^{-D}(\Gamma(D))^{-1}(t-t')^{D-1}, \tag{2.45}$$

where $\Gamma(D)$ is the gamma function. Substituting this expression into Eq. (2.35) we obtain

$$J(t)=[\sqrt{2}(1-\xi)]^{-D}\hat{D}^{-D}f(t), \tag{2.46}$$

where we have introduced the integral

$$\hat{D}^{-D}f(t)=(\Gamma(D))^{-1}\int_0^1(1-u)^{D-1}f(ut)\mathrm{d}u$$
$$=[D\Gamma(D)]^{-1}\int_0^1 f((1-u)t)\mathrm{d}u^D, \tag{2.47}$$

whose fractional character is reflected by the presence of the affix in the differential argument u.[29]

We employed above the integral representation of memory effects. It is easy to show, however, that it can be associated to an equivalent differential representation. Thus, if we have a conserved quantity n (such as the density of atoms of a given type), then its space and time dependence $n(r,t)$ is determined by the continuity equation

$$\frac{\partial n}{\partial t}=-\nabla J, \tag{2.48}$$

where the flux J is given by Eq. (2.35). In the absence of memory effects Eq. (2.37) holds, where the force f is given by the relation

$$f=-\nabla\mu, \tag{2.49}$$

μ being the chemical potential, and the expression (2.48) leads to the standard equation

$$\frac{\partial n}{\partial t}=\nabla(\gamma\nabla\mu) \tag{2.50}$$

of the diffusion type.[30] According to the analysis made above, when memory is switched on a fractional integral appears on the right-hand side of Eq. (2.50). Analysis of the obtained integral partial differential equation, which is of fractional order, is a very difficult problem.

The problem can be simplified, however, by taking into account the fact that if the memory function $M(t-t')$ vanishes in some time intervals, the flux J in Eq. (2.48) will be fixed, so that the rate $\partial n/\partial t$ is 0. For this reason, it is natural to assume that memory loss can be taken into account by the fractional character not only of the flux integral (2.35) but also for the time derivative in Eq. (2.48). Since the form of Eq. (2.50) corresponds to complete absence of memory ($D=0$) and when memory is switched on, as is reflected by an increase in the exponent D, the rate of change of n should decrease, it is natural to postulate a fractional-differential equation of the form

$$\frac{\partial^{\nu} n}{\partial t^{\nu}}=\nabla(\gamma\nabla\mu), \quad \nu=1-D. \tag{2.51}$$

As should happen, the order ν of this equation decreases as the memory parameter D increases. In systems with ideal memory ($D=1$) the derivative on the left-hand side of Eq. (2.51) vanishes and one must study the behavior of the flux (2.34) itself, as was done above.

The foregoing considerations in favor of the specific form $\nu=-1-D$ of the fractional degree of Eq. (2.51) serve only as a guide. In order to confirm them we show that the expression (2.46) for the flux, determined in the form of the fractional integral (2.47), agree with the solution of the fractional-order differential equation (2.51). Indeed, it is easy to show, by substituting $(1-u)t$ for the variable u in the integrand of the second integral in Eq. (2.47), that the time dependence of the flux has the form $J\propto t^{-D}$. Substituting this function into Eq. (2.48), we find the solution

$$n\propto t^{1-n}, \tag{2.52}$$

satisfying the equation (2.51) being tested. This confirms finally the equivalence of the mutually complementary concepts of a fractional integral (2.47) and the fractional differential equation (2.51). We call attention to the fact that the form of the geometric relation (2.5) for the length $L(l)$ of the coastline is the same as that of the physical dependence $n(t)$ obtained above. Hence it follows, in particular, that the time t plays the role of the size of segments covering in the state space a D-dimensional fractal set, whose points determine the memory of the system.

In order to interpret the equation (2.51) in fractional derivatives, we start from the fact that in the ordinary case $D=0$ the equation describes irreversible processes such as diffusion, heat conduction, and so on.[30] These processes are characterized by the fact that microscopic memory is completely lost under time inversion: If the equation of mechanics of an isolated object exhibits ideal memory, reflected in invariance under the substitution $t\to -t$, then in the thermodynamic equation (2.50) such invariance breaks down completely. Hence it can be concluded that the decrease of the order $\nu=1-D$ of the derivative in Eq. (2.51) reflects the switching on of memory channels, whose fraction is determined by the fractal dimension D. The remaining part $\nu=1-D$ of the channels makes the system irreversible. The residual irreversibility can be taken into account in the initial form by writing the Liouville equation in the fractional form[16]

$$\frac{i\hbar}{t}\cdot\frac{\partial^{D}\rho}{\partial u^{D}}=[H,\rho], \tag{2.53}$$

where $\hbar$ is Planck's constant, H is the Hamiltonian, ρ is the nonequilibrium density-matrix operator, t is the evolution time of the macroscopic system, and $u=t'/t$ is the dimensionless microscopic time, bounded by the condition $u<1$. Evidently, the condition $D<1$ makes it possible to take into account, on the basis of Eq. (2.53), irreversibility effects in the interval $[0,t]$ which are associated with the loss of $\nu=1-D$ deterministic channels. This scenario of taking into account irreversibility is, evidently, preferable to the phenomenological method of adding to the right-hand side of Eq. (2.53) the relaxation term $-\rho/\tau$, where τ is the relaxation time,[30] or by introducing an infinitesimal source.[31]

Besides equations of the diffusion type, the appearance of fractional derivatives can be expected in the description of the motion of particles colliding inelastically with one another. Carrying out calculations of the type that led to the expression for the flux (2.46), it can be shown[16] that if in each collision a force F acts on a particle of mass m, then the change in the velocity of the particle

$$\Delta v=[\sqrt{2}(1-\xi)]^{-D}(t/m)\hat{D}^{-D}F \tag{2.54}$$

is determined by a fractional integral of the type (2.47). The above example of the diffusion equation shows that in order to switch to the corresponding fractional-differential equation it is sufficient to operate on Eq. (2.54) with the operator $\hat{D}^{D}=\partial^{D}/\partial u^{D}$, inverse to the fractional integral $\hat{D}^{-D}$. Then, in the case of an elastic force $\mathbf{F}=-\lambda\Omega\nabla^{2}r$, where λ is the elastic constant and Ω is the atomic volume, we obtain[16] the following generalized transport equation for the coordinate r of the particle:

$$\frac{d^{1+D}r}{du^{1+D}}+(ct)^{2}\nabla^{2}r=0, \tag{2.55}$$

where the dimensionless time $u=t'/t<1$, and we have introduced the speed defined as

$$c^{2}=(\lambda\Omega/m)[\sqrt{2}(1-\xi)]^{-D}. \tag{2.56}$$

The equation (2.55) describes a new type of wave motion, occupying a position intermediate between ordinary diffusion ($D=0$) and classical waves $D=1$. Correspondingly,

the expression (2.56) defines the diffusion coefficient $D=c^2t$ in the first case and the wave speed c in the second case.

Fractional-differential equations of the type (2.51) and (2.55) were written in application to the investigation of the spatiotemporal behavior of conserved quantities. It is well known[32] that this is reflected in the presence of a second derivative with respect to the coordinate on the right-hand sides of these equations. For a nonconserved quantity η this derivative vanishes, and the diffusion equation (2.51) becomes a relaxation equation of the Landau–Khalatnikov type:

$$\frac{d^{1-D}\eta}{du^{1-D}}=-(\gamma_D t)\eta, \tag{2.57}$$

and the wave equation (2.49) becomes the equation for a harmonic oscillator:

$$\frac{d^{1+D}\eta}{du^{1+D}}+(\omega_D t)^2\eta=0; \tag{2.58}$$

here, as above, $u=t'/t$ is the dimensionless time, and the parameters $\gamma_D,\omega_D\propto[\sqrt{2}(1-\xi)]^{-D}$ determine the relaxation time $\tau_D=\gamma_D^{-1}$ and the oscillator frequency ω_D. The fractal dimension D is a measure of the residual memory of the system: In the absence of memory ($D=1$) both equations (2.57) and (2.58) reduce to a Debye relaxation equation describing the behavior of the simplest thermodynamic systems (here the relation $\gamma_0=\omega_0^2 t$ is satisfied), and in the case of ideal memory ($D=1$) Eq. (2.57) degenerates into an identity and Eq. (2.58) becomes the ordinary oscillator relation.

The exotic nature of the concept of fractional integration and differentiation can lead to the incorrect conclusion that the constructs made above are of purely theoretical interest and do not reflect the experimental situation. We shall show that this is not so. To this end we determine the frequency dependence of the susceptibility $\chi=\partial\eta/\partial h$ of a system to the action of an external field h. When the field is switched on the term $\chi_0(\gamma t)h$, where χ_0 is the isothermal susceptibility, is added to the right-hand side of the regression equation (2.57), and after Fourier transforming we find

$$\chi(\omega)=\frac{\chi_0}{1+(-i\omega/\omega_\nu)^\nu} \tag{2.59}$$

where we have introduced the characteristic frequency $\omega_\nu=(\gamma t)^{1/\nu}/t$ and the fractional exponent $\nu=1-D$. The frequency dependence (2.59), well-known as the empirical Cowle–Cowle expression, was observed in the process of retarded (compared to the Debye exponent) relaxation of the polarization of dielectrics,[33] in spin[18] and structural[20] glasses, in the process of plastic strain,[15] fatigue fracture,[13] and so on.

2.4.2. Fractal kinetics of hierarchically coordinated systems

Consider two thermodynamic phases, one of which is determined by the order parameter η_i (usually $\eta_i=0$) and the other by the value η_f. As the state parameters (for example, the temperature T) varies, the free energy can

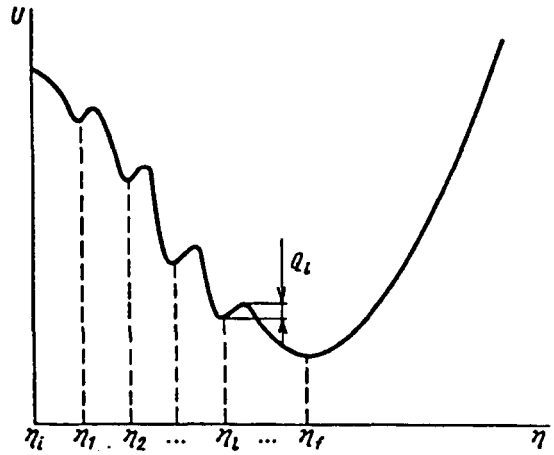

FIG. 14. Diagram illustrating the dependence of the thermodynamic potential on the order parameter for a sequential chain of phase transformations.

satisfy the condition $U(\eta_i)\geqslant U(\eta_f)$, and a phase transition will occur at the point $T=T_c$. If the states η_i and η_f are not separated by an energy barrier, then a second-order transformation mechanism is realized with relaxation time of the nonequilibrium phase

$$\tau_0=\tau_{00}[1-(T/T_c)]^{-1} \tag{2.60}$$

where τ_{00} is the microscopic (Debye) time (of the order of 10^{-12} sec). For a first-order transition between the states η_i and η_f there is a barrier Q, resulting in the fact that the quantity (2.60) increases according to Arrhenius' formula

$$\tau=\tau_0\exp(Q/T), \tag{2.61}$$

where the exponential factor takes into account the probability of overcoming the barrier Q by means of a fluctuation.[34] The time dependence of the order parameter $\eta(t)$, reflecting the kinetics of the transition $\eta_i\to\eta_f$, is described by the very simple regression equation

$$d\eta/dt=-\eta/\tau, \tag{2.62}$$

whose solution leads to the Debye expression

$$S(t)=e^{-i/\tau}, \tag{2.63}$$

for the transition probability

$$\frac{\eta_f-\eta(t)}{\eta_f-\eta_i}=S(t) \tag{2.64}$$

from the initial state η_i into an arbitrary state $\eta(t)$.

The picture presented above is realized in the simplest case, when the function $U(\eta)$ has only two extrema, corresponding to the phase η_i and η_f. Often, as shown in Fig. 14, there are many shallower minima, corresponding to metastable phases, incommensurable structures, and so on, are present between them.[35] For this reason, if the initial state is determined by the parameter η_i, then prior to entering the final state η_f the system passes through a successive chain of transitions $\eta_i\to\eta_1\to\eta_2\to\cdots\to\eta_l\to\cdots\to\eta_f$ between neighboring minima. Each transition is described

by the probability $S_l(t)$ of the transition from the lth into the $(l+1)$st minimum. The expression for this probability is determined by the exponential (2.63) with the relaxation time τ_l, given by the Arrhenius relation (2.61) with barrier height Q_l (Fig. 14). This chain of transitions is characterized by the fact that all barriers heights Q_l are of the same order of magnitude, as a result of which the times $\Delta t_l = t_{l+1} - t_l$ for overcoming the barriers will be comparable. For this reason, over the time $t \gg n/\tau_l$ the system overcomes with probability $1-S(t)$ n barriers, where

$$S(t) = \prod_{i=1}^{n} S_l,$$
$$S_l = \exp(-\Delta t_l/\tau_l), \quad \Delta t_n = t - t_n. \tag{2.65}$$

For $n \gg 1$ the spread in the time intervals Δt_l can be neglected, setting $\Delta t_l = t/n$. Then the relation (2.65) assumes the Debye form (2.63) with the average relaxation time $\langle\tau\rangle$ given by the equation

$$\langle\tau\rangle^{-1} = \frac{1}{n}\sum_{l=1}^{n} \tau_l^{-1}. \tag{2.66}$$

Thus the chain of transitions between the metastable states of the system has been reduced to Debye relaxation with average time $\langle\tau\rangle$. The sequential character of this process is reflected in the multiplicativity of the elementary probabilities $S_l(t)$ and the additivity of the inverse relaxation times τ_l^{-1}. Since according to Eq. (2.61) τ_l^{-1} is proportional to the probability that the interphase barrier Q_l will be overcome by a thermal fluctuation, the indicated additivity means that the fluctuations of the microscopic quantities (for example, the energies of the phases) are independent of one another.

If such a situation is realized at the macroscopic level, then the probabilities (2.63) themselves and not the microscopic quantities τ_l^{-1} are added. This means that the collection of parallel relaxation channels, the existence of which was indicated at the end of Sec. 2.4.1, acts independently. Each such channel corresponds to a statistical ensemble α, realized with probability ω_α. The probability of transition between the channels α and β has, in accordance with Eqs. (2.63) and (2.61), the following form:

$$S_{\alpha\beta}(t) = \exp(-t/\tau_{\alpha\beta}),$$
$$\tau_{\alpha\beta} = \tau_0 \exp(Q_{\alpha\beta}/T), \tag{2.67}$$

where $Q_{\alpha\beta}$ is the height of the barrier separating the channels α and β. The total probability

$$S(t) = \sum_{\alpha,\beta} \omega_\alpha \omega_\beta S_{\alpha\beta}(t) \tag{2.68}$$

describes relaxation due to the entire collection of channels.

Obviously, the channels are connected in parallel, if the probabilities for relaxation of different channels

$$\omega_\alpha \propto \exp(-E_\alpha/T) \tag{2.69}$$

are comparable quantities. Such a situation requires degeneracy with respect to the energy levels

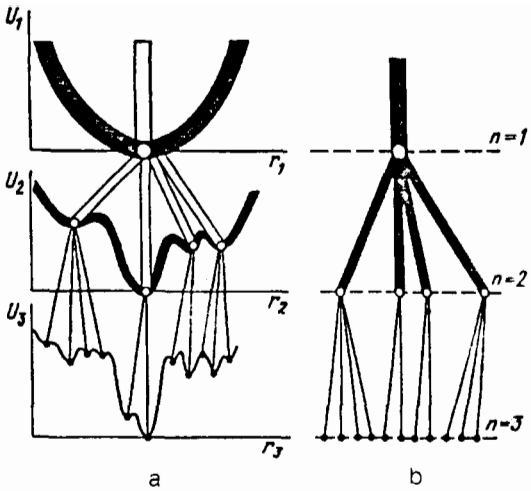

FIG. 15. a—Form of the potential relief on different structural levels. b—Corresponding hierarchical tree.[15]

$$E_\alpha = U(r)\rho_\alpha(r)\mathrm{d}r, \tag{2.70}$$

where $\rho_\alpha(r)$ is the distribution of structural units (for example, atoms) in the αth relaxation channel and $U(r)$ is the potential relief of the system. Since the dome-shaped function $\rho_\alpha(r)$ separates in the integral (2.70) the region of space corresponding to the αth channel, the condition that the energies E_α are comparable implies that minima of the potential relief $U(r)$, differing only insignificantly from one another, should be associated to the different channels α. On the other hand, the existence of a spectrum of relaxation times $\tau_{\alpha\beta}$ in Eq. (2.67) can be guaranteed only if heights $Q_{\alpha\beta}$ of the barrier separating different minima α and β are significantly different. Evidently, these conditions can hold only for a hierarchical structure of the potential relief (Fig. 15a): Shallower minima are superposed on the large-scale minima of the function $U(r)$, even shallower minima are superposed on the shallow ones, and so on. This results in the fractal function $U(r)$ that is strongly reminiscent of the coastline in Fig. 2. It is evident from Fig. 15 that the statistical ensembles α and β can be united into clusters, each of which is characterized by a maximum height $Q_{\alpha\beta}$ of the barrier separating this cluster from other clusters. On the other hand, since the ensembles α and β correspond to nodes of a Cayley tree (Fig. 15b), the points α and β of the ultrametric space, which are separated by a distance $l_{\alpha\beta}$ (see Sec. 2.1.2), can be associated to them. Thus the barrier heights $Q_{\alpha\beta}$ and together with them the relaxation times $\tau_{\alpha\beta}$ are functions of the distance $l_{\alpha\beta}$ in the ultrametric state space. Since the separation of clusters[3)] is guaranteed by the increasing height of the barrier separating the clusters, it can be concluded that the function $Q(l)$ must be monotonically increasing (see below).

Thus it can be concluded that different relaxation channels are guaranteed to operate in parallel only if the corresponding set of statistical ensembles is hierarchically coordinated. This situation is realized in strongly nonequilibrium thermodynamic systems such as spin and structural glasses,[18–20] strongly deformed materials,[12,15,21,22]

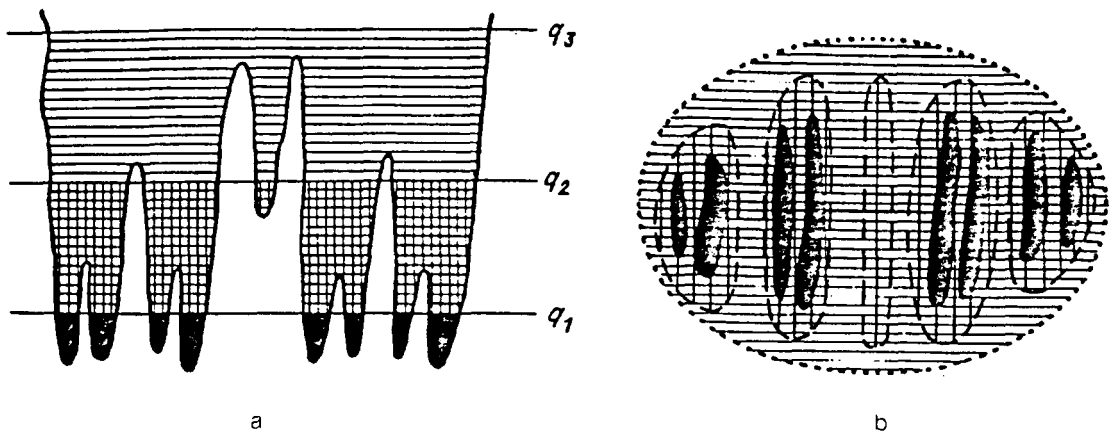

FIG. 16. Diagram illustrating the dependence of the thermodynamic potential on the order parameter for a sequential chain of phase transformations.

polytypic and martensite structures,[23–26] and so on. In a hierarchical system the fastest processes, corresponding to overcoming barriers of minimum height $Q_{\alpha\beta}$, proceed first. In the process, the smallest statistical ensembles merge, and the system passes into a higher hierarchical level of the Cayley tree (Fig. 15b). Next, barriers of large height $Q_{\alpha\beta}$ are overcome, as a result of which the obtained superclusters merge into larger formations, corresponding to the next hierarchical level. This process can continue without bound. Its hierarchical character is expressed in the fact that so long as channels with fixed relaxation time τ_l have not yet been activated, the parallel network of channels of the next level, with relaxation times $\tau_{l+1} \gg \tau_l$, will not come into play. This hierarchical coordination is responsible for the critical retardation of relaxation, resulting, as we shall see below, in transformation of the Debye exponential (2.63) into a more slowly decreasing function.

As already indicated above, the fractal character of a hierarchically coordinated system is manifested in the coordinate dependence of the potential energy $U(r)$ of the system. This apparently means that the set of clusters of statistical ensembles, represented by points of an ultrametric state space, will also exhibit fractal properties. As is evident from Fig. 16, the above-described stagewise merging of clusters results in growth of the overlap parameter[36]

$$q_{\alpha\beta}=\frac{1}{N}\sum_{i=1}^{N}\langle x_i\rangle_\alpha\langle x_i\rangle_\beta, \tag{2.71}$$

where x_i is the hydrodynamic variable at the point r_i, giving on averaging over the αth cluster the order parameter $\eta_\alpha=\langle x\rangle_\alpha$, and N is the number of structural units. Hierarchical merging of clusters is graphically represented by a gradual merging of lagoons filled with liquid with increasing level $q_{\alpha\beta}$ in a vessel whose bottom relief is determined by the function $U(r)$. Evidently, as the relaxation channels come into play successively (see Fig. 14) the clusters do not overlap at all, and the liquid spills successively into increasingly smaller depressions.

In Sec. 3.3.3 we shall show that the set of clusters formed in the state space of the hierarchical system has a stochastic character. This means that, in particular, the parameter (2.71) describing the overlap of clusters will be a random quantity, whose distribution is given by the function

$$P(q)=\sum_{\alpha,\beta} w_\alpha w_\beta \delta(q-q_{\alpha\beta}). \tag{2.72}$$

Then it is easy to see from the definition (2.68) that the probability $S(t)$ for the system to remain in the initial state is expressed in terms of the first moment of the overlap parameter (2.71) as follows:

$$S(t)=1-\int_0^1 qP(q)\,dq=1-\int_0^1 q(Y)\,dY. \tag{2.73}$$

Here we introduced in the second equality the probability

$$Y(q)=\int_q^1 P(q')\,dq' \tag{2.74}$$

that overlappings q' exceeding a prescribed threshold q are realized.

In order to determine the explicit form of the functions (2.68) it is necessary to find the probability distributions $w_\alpha=w_\alpha(l)$, $Q_{\alpha\beta}=Q_{\alpha\beta}(l)$ for the realization of the ensembles α and β and the barrier between the ensembles as a function of the distance l in the ultrametric space. Within the phenomenological approach, we focus our efforts on investigating the possible forms of the time dependence $S(t)$ for different majorants of the distributions $w(l)$ and $Q(l)$. We approximate the decaying probability distribution by the functions

$$w_w(l)\propto\exp(-l/l_0), \quad w_s(l)\propto l^{-D}, \tag{2.75}$$

the first one describing weakly hierarchical systems and the second one describing strongly hierarchical systems (l_0 and D are positive parameters). This is connected to the fact that the exponential function $w_w(l)$, decaying over distances $l\sim l_0$, couples only a small number of hierarchical levels, and the slowly varying power-law function $w_s(l)$ takes into account virtually the entire set of levels. As far as the barrier-height function $Q(l)$ is concerned, we shall approximate it by the three basic forms of increasing functions:

TABLE I. Possible asymptotic forms ($t\to\infty$) of the correlation function $S(t)$.

$S(t)$	$Q_l(l)$	$Q_p(l)$	$Q_l(l)$
$\omega_\infty(l)$	$\exp\left[-\left(\frac{t}{\tau_0}\right)^{\beta}\right]$, $\beta=\left[1+\left(\frac{Q}{T}\right)\right]^{-1}$	$\exp\left[-\left(\frac{T}{Q}\ln\frac{t}{\tau_0}\right)^{1/a}\right]$	$\left(\frac{T}{Q}\ln\frac{t}{\tau_0}\right)^{-1/a}$
$\omega_s(i)$	$t^{-\gamma}$, $g=DT$	$\left(\frac{T}{Q}\ln\frac{t}{\tau_0}\right)^{-D/a}$	$\left[\ln\left(\frac{T}{Q}\ln\frac{t}{\tau_0}\right)\right]^{-D}$

$$Q_l(l)=Q\ln l,\quad Q_p(l)=Ql^{\alpha},\quad Q_e(l)=Qe^{l},\qquad (2.76)$$

where Q is the characteristic height and $a>0$ is an exponent.

Substituting the functions (2.76) into Eq. (2.67) and the result obtained and Eq. (2.75) into the definition (2.68), we find by the saddle point method the asymptotic expressions, presented in Table I, for the limit $t\to\infty$. According to this table, for any combination of approximations (2.75) and (2.76) the relaxation law $S(t)$ loses its Debye form. The weakest retardation is observed for logarithmic growth of heights of the fractal relief in weakly hierarchical systems (so-called Kohlrausch's law, representing an extended exponential due to the exponent $\beta<1$). As the hierarchical coupling increases or a transition occurs to power-law growth of the heights of the reliefs, the function $S(t)$ starts to decay in a power-law fashion. If, however, exponential growth of barriers in weakly hierarchical systems or power-law growth in strongly hierarchical systems is realized, then the relaxation becomes logarithmic. Finally, for strongly hierarchical systems in which the barrier heights grow exponentially, we obtain a double logarithmic delay, i.e., the relaxation process virtually stops.

3. MULTIFRACTALS

A distinguishing feature of the manifolds considered above is that they are represented by a scale factor ξ and a branching j, the set of values of which is characterized by the averages $\langle\xi\rangle$ and $\langle j\rangle$ characteristic of the given fractal. Correspondingly, Eq. (2.11) leads to a unique value of the fractal dimension D, which is why the term monofractal is employed. In the present section we consider the more general case of a multifractal, representing a superposition of several monofractals, characterized by different values of the probabilistic factor $p=j^{-1}$ and geometric factor ξ. The approach employed in Sec. 3.1 is based on the geometric aspect, associated with the distribution of ξ. In Sec. 3.2 we present a thermodynamic method based on analysis of the probabilistic factor p. The relation between these factors is described at the end of Secs. 3.2.1 and 3.2.2.

It is easy to see the difference between the geometric and thermodynamic approaches by comparing the method described in Sec. 2 for constructing a fractal and the so-called curdling method, presented below. The first method is of a purely geometric character—the entire construction reduces to a sequence of $n\to\infty$ cycles of partitioning of the initial fragment into i blocks, subsequent discarding of $i-j$ of them, and deformation ξ of the remaining j blocks. The curdling method, reminiscent of the real process of the curdling of milk, is characterized by a physical aspect, associated with a change in the probabilities of the realization of different fragments of the set.

The crux of the curdling method is most easily represented as follows.[3] Consider a rod of unit length $l_0=1$ and mass $m_0=1$. Correspondingly, the density $\rho=m/l$ will also be one ($\rho_0=1$). Next, we cut the rod in half, so that the masses of the segments are $m_1=m_1^{(1)}=m_1^{(2)}=1/2$. Without changing them, we plastically deform (forge) the obtained pieces, shortening the rods to the same length $l_1=l_1^{(1)}=l_1^{(2)}=1/3$. As a result the density increases to $\rho_1=m_1/l_1=3/2$. Repeating the procedure n times, we obtain $N_n=2^n$ rods of length $l_n=3^{-n}$ and mass $m_n=2^{-n}$, such that their total mass $N_nm_n=1$ does not change. The dependence of the physical characteristics m and ρ of an elementary rod on the length l of the rod (we drop the index n)

$$m=l^{\alpha},\quad \rho=l^{\alpha-1}\qquad (3.1)$$

is determined by the value of the exponent $\alpha=\ln 2/\ln 3$.

It is easy to see that the construction made above is reminiscent of the formation of quantum dust, studied in Sec. 2.1.1. The difference can be expressed graphically by modifying the Cantor construction (see Fig. 6a), increasing the height of the rod fragments so that on each step n the total area would remain constant (see Fig. 6b). Besides this circumstance, which corresponds to the law of conservation of mass, the switch to the convolution procedure is also reflected in a formal manner: instead of the relations (2.7) and (2.5), determining the geometric characteristics of the fractal, we obtain scaling of the dependence (3.1) of the physical quantities, the character of the scaling being determined by the exponent α corresponding to the fractal dimension (2.10).[4)]

The convolution procedure described above makes it possible to construct the so-called devil's staircase, shown in Fig. 17. It represents a plot of the mass

$$m(x)=\int_0^x\rho(x')dx'\qquad (3.2)$$

of the elementary rods, located in the interval $[0,x]$, versus the length x of the rod. Since the density $\rho=0$ outside the rods and $\rho=\infty$ at the points of the Cantor set, which correspond to the arrangement of the rods, the integral

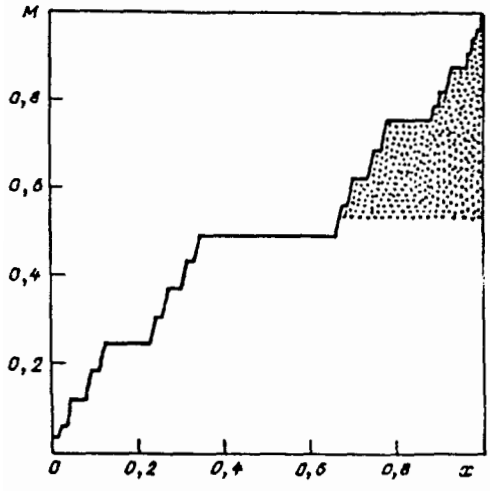

FIG. 17. Mass M of a Cantor rod, shown in Fig. 6b, as a function of the coordinate x measured from the left end.[3]

(3.2) increases only at these points and off these points the integral is constant. A distinguishing feature of the staircase is that the function $m(x)$, while remaining constant at most points of the continuous set [0,1], increases from 0 to 1 due to sharp jumps at the points of the counting edges of the set, whose size is negligibly small compared to the continuum.

3.1. Geometric approach

Before presenting the formal scheme of the representation of multifractal sets (Sec. 3.1.2), we examine the simplest examples of Cantor sequences, which make it possible to demonstrate this scheme graphically.

3.1.1. Cantor multifractals

Monofractal Cantor dust, studied in Sec. 2.1.1, is distinguished by the fact that the segments obtained from each step $n\to\infty$ of division of the initial fragment have the same lengths $l_n=3^{-n}$ and are realized with the same probability $p=1$ (this is indicated by the fact that they have the same measure p). We shall now consider the changes resulting when these restrictions are removed.

If we assume that the lengths ξ_1 and ξ_2 of the left- and right-hand segments are different, then the Cantor set acquires a two-scale character of the type shown in Fig. 18. In order to determine the fractal dimension we must determine the generating function (2.26). Since after n steps we obtain a collection of $i\leqslant n$ segments of length ξ_1 and $n-i$ segments of length ξ_2, the quantity I_i^q must be understood to be the product $I_n^q=\xi_1^{iq}\xi_2^{(n-i)q}$ contained in the sum (2.26) a number of times equal to the number of combinations

$$C_n^i=\frac{n!}{i!(n-i)!},\quad i=0,1,...,n. \tag{3.3}$$

The obtained expression

$$\chi_n(q)=\sum_{i=0}^{n} C_m^i\xi_1^{iq}\xi_2^{(n-i)q}=(\xi_1^q+\xi_2^q)^n \tag{3.4}$$

reduces to Newton's binomial. It assumes a finite value in the limit $n\to\infty$ if

$$\xi_1^q+\xi_2^q=1. \tag{3.5}$$

For prescribed lengths ξ_1 and ξ_2 it determines a unique value $q=0$ of the fractal dimension (for example, for $\xi_1=1/4$ and $\xi_2=2/5$, corresponding to Fig. 18, we obtain $D=0.611$, less than the value $D=0.631$ for a single-scale set). Thus it can be concluded that the nonuniformity in the distribution of the scales ξ only reduces the fractal dimension, leaving it unique and thus not leading to transformation of the monofractal into a multifractal.

We now consider what happens when the measures P_i of the realization of different segments of the set are not constants. To this end, we consider the binomial multiplicative process. The crux of this process reduces to the fact that after each division of the initial segment into two parts a measure $p<1$ is assigned to the left-hand part and a measure $q=1-p$ is assigned to the right-hand part. In other words, the above-indicated curdling process multiplies, but each half-rod, obtained after cutting the initial rod, deforms with different powers p and $q=1-p$. It is easy to see that after the second step the distributions P_n^i of the measure corresponding to a physical quantity, such as the mass, will have the form

$$P_2^i: pp;\ pq;\ qp;\ qq;\quad i=1,2,...,2^n,\quad n=2, \tag{3.6}$$

where the commas separate values of measures of different segments. Correspondingly, after the third step we obtain

$$P_3^i: ppp;\ ppq;\ pqp;\ qpp;\ qpq;\ qqp;\ pqq;\ qqq;$$
$$i=1,2,...,2^n,\quad n=3. \tag{3.7}$$

Figure 19 displays for $p=1/4$ and $q=3/4$ the distribution of measures P_n^i after $n=11$ steps and the corresponding integral measure

$$M_n(x)=\sum_{i=0}^{2^n x} P_n^i \tag{3.8}$$

on the segment $[0,x]$, $x\leqslant 1$. It is easy to see, similarly to the derivation of Eq. (3.4), that we obtain hence explicitly

FIG. 18. Construction of a Cantor set with scales $\xi_1=1/4$ and $\xi_2=2/5$.[3]

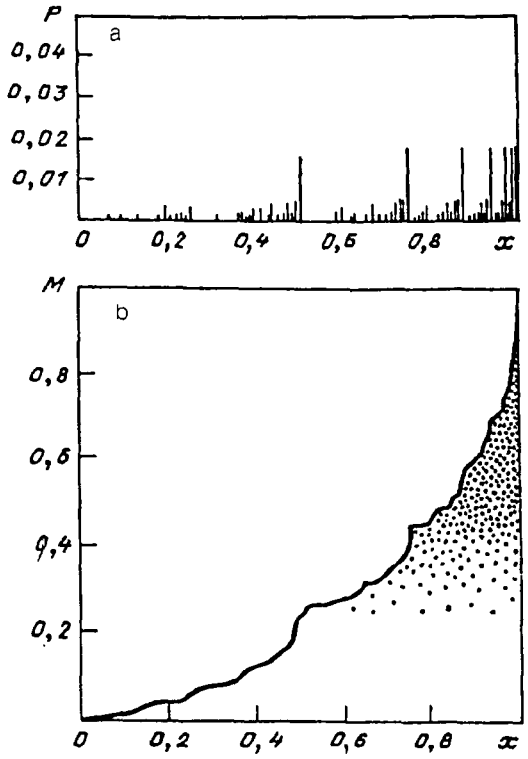

FIG. 19. Distribution of the density of measure (a) and the total measure (b) for a binomial multiplicative process (the number of iterations $n=11$, the probability $p=1/4$, $q=3/4$).[13]

$$M_n(x)=\sum_{i=0}^{nx} C_n^i p^i q^{n-i}. \tag{3.9}$$

Taking into account the condition $p+q=1$ for the total length $x=1$, as should happen, we obtain

$$M_n(1)=(p+q)^n=1. \tag{3.10}$$

It is easy to see from relations of the type (3.6) and (3.7) that after $n\to\infty$ steps we obtain a set of 2^n binary numbers with the values p and q. It is convenient to separate these numbers into groups, each of which contains C_n^i numbers, having i values p and $n-i$ values q [in the sequences (3.6) and (3.7) these groups are divided by a semicolon]. Assuming that the segment of length $l_i\to 0$ covers only one group of n-digit numbers, containing i values of p, we obtain from Eq. (2.26) the generating function

$$\chi_n^i(q)=C_n^i\xi_n^q, \quad \xi_n=(1/2)^n. \tag{3.11}$$

Using in Eq. (3) Stirling's formula

$$n!\approx\exp[-n(1-\ln n)], \tag{3.12}$$

we find that the expression (3.11) assumes a finite value if $q=f(s)$, where the function $f(s)$ of the argument $s=1/n$, determining the fraction of p values in the ith group, has the form

$$f(s)=-\frac{s\ln s+(1-s)\ln(1-s)}{\ln 2}. \tag{3.13}$$

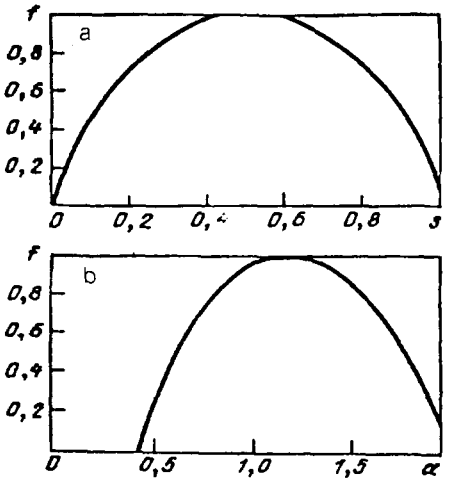

FIG. 20. Spectral function of a multifractal, generated by a binomial multiplicative process, represented in Fig. 19 as a function of the parameter s determining the fraction of the numbers p in the binary representation of points of the set (a) and as a function of the exponent α determined by Eq. (3.17) (b).[3]

Thus the fractal dimension of the binomial Cantor set, corresponding to a finite value of the generating function, has the form

$$D(s)=f(s). \tag{3.14}$$

Since this value corresponds only to the group of n-digit sequences, which is fixed by choosing the number $0\leqslant s\leqslant 1$, the entire collection of the sequences is characterized by the set of quantities $D(s)$, corresponding to different values of s. In other words, the binomial Cantor set is a superposition of monofractals, corresponding to the complete spectrum of dimensions (3.14). This is why the multifractal is employed. Each of the constituent monofractals enters with weight

$$N_n^s=C_n^{sn}=\exp(\ln 2\cdot nf(s)). \tag{3.15}$$

The function $f(s)$ determining it evidently is the spectral distribution of the monofractals over a given multifractal. It is evident from the plot of the function $f(s)$, presented in Fig. 20, that the maximum values $D=1$ and $N_n=2^n$ obtained for the group of sequences that corresponds to topological dimension $d=1$, i.e., for the ordinary, nonfractal set of identical segments of length $l_n=2^{-n}$.

The inconvenience of this scheme lies in the fact that the parameter s is not an observable quantity. For this reason, it is necessary to switch to the exponent α, defined as the equation

$$P(l)=l^\alpha, \tag{3.16}$$

reminiscent of the scaling relations (3.1) for physical quantities. It is obtained from the chain of relations

$$P(s)=M(x(s)+l)-M(x(s))=l^\alpha, \tag{3.17}$$

following from the definition (3.8). For the case of the binomial Cantor set, under consideration here, the switch from the parameter s to the parameter α can be made

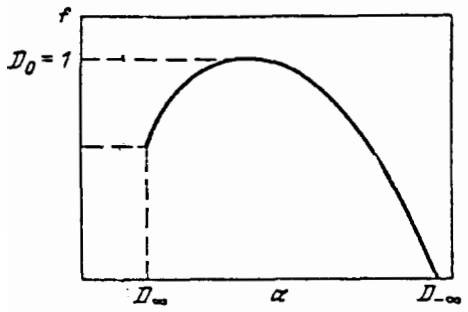

FIG. 21. Spectral function for the two-scale Cantor set of constant length.[10]

explicitly, by using the expression for the measure of the binomial distribution [see Eqs. (3.8) and (3.9)]

$$P_n(s)=(p^s q^{(1-s)})^n \tag{3.18}$$

and the equality $l_n=(1/2)^n$. As a result, the expression (3.16) gives the linear function

$$\alpha=-\frac{s\ln p+(1-s)\ln(1-p)}{\ln 2}. \tag{3.19}$$

Thanks to this, the form of the function $f(\alpha)$ is the same as that of $f(s)$ (see Fig. 20). Nonzero values of f are concentrated in the interval from $\alpha_{\min}=-\ln(1-p)/\ln 2$ to $\alpha_{\max}=-\ln p/\ln 2$, where $p\leqslant 1/2$. The lower limit corresponds to the case $s=0$—the binomial sequence consists only of numbers q and the upper limit corresponds to the opposite case $s=1$, for which the sequence reduces to a collection of numbers p. At the limit points we have $df/d\alpha=\pm\infty$, and the maximum value $f=1$, corresponding to $df/d\alpha=0$, is reached at $\alpha=-[\ln p+\ln(1-p)]/\ln 2$.

It should be noted that the upper limit $\alpha_{\max}$ corresponds to the sequence consisting only of the numbers p, and for this reason $f=0$ always on it. According to Eqs. (3.14) and (3.15), this means that there exists a unique zero-measure set, which is taken as the initial set. At the lower limit $\alpha_{\min}$ a sequence consisting of only the numbers q is realized. For a binomial Cantor set this sequence also reduces to a point ($D(\alpha_{\min})=0$) and it is unique ($N(\alpha_{\min})=1$). If, however, at the upper limit, corresponding to the initial sequence, this situation is natural, then this is not always the case at the lower limit.

For proof, we consider the case when the initial segment is divided into two segments of length ξ_2 and one segment of length ξ_1, and no segment is discarded. The probability p_2 is assigned to the first two segments and p_1 to the remaining segment. Due to the normalization conditions $\xi_1+2\xi_2=1$, $p_1+2p_2=1$. In addition, it is assumed that $\xi_2<\xi_1$ and $p_2/\xi_2>p_1/\xi_1$. The calculation performed in Ref. 10 on the basis of the indicated assumptions gives the spectral distribution $f(\alpha)$ shown in Fig. 21. The characteristic feature of this distribution is that $f\neq 0$ at the lower limit. This means that the sequence corresponding to the condition $s=0$, reducing it to an infinite series only of the numbers p_2, is not the only possible sequence. Evidently, this is connected with the fact that, in contrast to the single-scale Cantor set, here not only the numbers p_1 and p_2 but also segments of different length ξ_1 and ξ_2 can be transposed. This is why the limiting set does not reduce to a point and according to (3.14) $f(\alpha_{\min})\neq 0$.

3.1.2. Formalism of the geometric description of multifractals

Bearing in mind the examples of the simplest Cantor multifractals considered above, we now present the general scheme of the geometric description of an arbitrary fractal set.[3,8,10] The set is formed as a result of $n\to\infty$ divisions of the initial set, leading to the formation of N_n fragments of length l_i ($\to 0$), $=1,2,\ldots,N_n$. The probability of realization of each fragment is determined by the formula [compare with Eq. (3.17)]

$$P_i=l_i^{\infty}, \tag{3.20}$$

where α is the scaling parameter. As in the case of a monofractal, the starting construct is the generating function of measure of the type (2.26):

$$M(q)=\sum_{i=1}^{N_n} P_i^q. \tag{3.21}$$

Substituting Eq. (3.20) into Eq. (3.21) we obtain the definition

$$M(q)=\sum_i l_i^{q\alpha}, \tag{3.22}$$

which differs from the generating function (2.26) of the monofractal by the presence of the variable factor α. From the entire set of N_n fragments a given value of α is realized for

$$N_n(\alpha)=l_n^{-f(\alpha)} \tag{3.23}$$

fragments, where the function $f(\alpha)$, which determines the spectrum of values of α, gives the dimension of the geometric set [the collection of segments l_i on which the distribution of the measure (3.20) is realized]. Using Eq. (3.23) in Eq. (3.22) we obtain the expression

$$M_n(q)=\sum_n l_n^{q\alpha-f(\alpha)}. \tag{3.24}$$

Taking into account the dimension of the distribution of the values of α, it is convenient to rewrite Eq. (3.24) as an integral

$$M_n(q)=\int_{\alpha_{\min}}^{\alpha_{\max}} l_n^{q\alpha-f(\alpha)}\rho(\alpha)\,d\alpha, \tag{3.25}$$

where the function $\rho(\alpha)$ describes the distribution of segments l_n over the parameter α.

Since the length l_n is very small, the values of α corresponding to the minimum exponent in the integrand will make the largest contribution to the integral (3.25). Hence there follow the relations

$$\left.\frac{df}{d\alpha}\right|_{\alpha=\alpha(q)}=q,\quad \left.\frac{d^2f}{d\alpha^2}\right|_{\alpha=\alpha(q)}<0, \tag{3.26}$$

which make it possible to find, from a given spectrum $f(\alpha)$, the relation $\alpha(q)$ for the scaling exponents. The integral (3.25) itself can be reduced, by the steepest-descent method, to the form

$$M_n(q) \approx l_n^{q\alpha(q)-f(\alpha(q))}. \tag{3.27}$$

The obtained measure $M(q)$ enables finding the spectrum of dimensions $D(q)$ of the multifractal. In order to find the relations relating these quantities, we consider the monofractal measure $P=l^d$, defined in a Euclidean space of dimension d. Dividing it into $N=l^{-d}$ cells of volume $l^d \to 0$, we obtain from the definition (3.21)

$$M(q) = \sum_{i=1}^{N} l^{qd} = N l^{qd} = l^{(q-1)d}. \tag{3.28}$$

Since for the simple case at hand the fractal dimension $D(q)$ reduces to the topological dimension d, the obtained result (3.28) makes it possible to introduce the following definition

$$D(q) = \lim_{l \to \infty} \left(\frac{1}{q-1} \frac{\ln M(q)}{\ln l} \right). \tag{3.29}$$

It can be written in an exponential form of type (3.28)

$$M(q) \approx l^{(q-1)D(q)}, \quad l \to 0. \tag{3.30}$$

Comparing this result to Eq. (3.27), we obtain an expression for the fractal dimension in terms of the spectral functions $\alpha(q)$ and $f(\alpha(q))$:

$$D(q) = (q-)^{-1}(q\alpha(q) - f(\alpha(q))). \tag{3.31}$$

On the other hand, if the spectrum of dimensions $D(q)$ is known, then the spectral function can be easily found with the help of Eqs. (3.26) and (3.31):

$$\alpha(q) = \frac{\mathrm{d}}{\mathrm{d}q} [(q-1) D(q)]. \tag{3.32}$$

The definition of measure (3.21), introduced above, has the deficiency that it takes into account only the probabilistic aspect, based on the curdling procedure, and completely ignores the geometric features of a multifractal. Indeed, calculation of the measure according to Eq. (3.21) presupposes that the carrier space is partitioned into blocks i, to each of which the probability P_i is associated. As is evident from the example with the coastline (see Fig. 2), however, some fragments of the fractal can appear in the ith block N_i times, and in Eq. (3.21) the product $N_i P_i$ should appear instead of P_i. For this reason, if the scaling relation $N_i \propto l_i^{-\tau}$, where τ is a corresponding exponent, is assumed, then the definitions (3.21) and (3.22) assumes the form

$$M(q,\tau) = \sum_i P_i^q / l_i^\tau = \sum_i l_i^{q\alpha-\tau}, \quad l_i \to 0. \tag{3.33}$$

Hence we obtain, as done when switching from Eq. (3.22) to Eq. (3.27), the estimate

$$M_n(q,\tau) \approx l_n^{\alpha q - f(\alpha) - \tau}. \tag{3.34}$$

As the fragments decrease in size $l_n \to 0$, the measure (3.34) assumes finite values if the exponent τ reduces to the quantity $\tau(q)$ given by the condition

$$\tau(q) = q\alpha(q) - f(\alpha(q)), \tag{3.35}$$

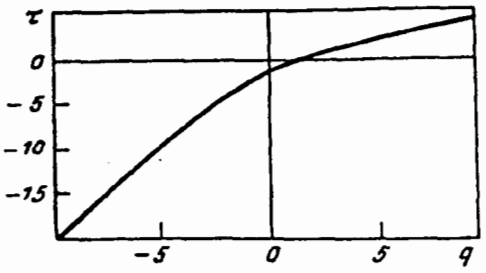

FIG. 22. Distribution of the exponent of the measure (3.33), corresponding to the spectrum of the binomial multiplicative process (see Fig. 20).[3]

where the function $\alpha(q)$ is determined by the relation (3.26). Using Eq. (3.31), we find hence the relation to the fractal dimension

$$\tau(q) = (q-1) D(q). \tag{3.36}$$

Substituting Eq. (3.36) into Eq. (3.32) in turn gives the relation

$$\alpha(q) = \frac{\mathrm{d}\tau(q)}{\mathrm{d}q}. \tag{3.37}$$

The system of equations (3.35) and (3.37) can be regarded as a Legendre transformation, making it possible to switch from one pair of independent variables α, f to another pair q, τ (or vice versa). An arbitrary multifractal is described completely by the spectral function $f(\alpha)$ or by the equivalent function $\tau(q)$, determining, according to Eq. (3.36), the spectrum $D(q)$ of fractal dimensions. In thermodynamics the equation of state of the system corresponds to the functions of $f(\alpha)$ and $\tau(q)$.

3.1.3. Characteristic features of the functions f(q), τ(q), and D(q)

In Sec. 2.1.1 we examined, for the example of a bimodal Cantor sequence, the characteristic features of the dome-shaped function $f(\alpha)$. As is evident from Figs. 20 and 21, the function $f(\alpha)$ assumes positive finite values in the bounded interval $[\alpha_{\min}, \alpha_{\max}]$, at whose limits the derivative of the function is infinite while inside the interval the derivative vanishes, thereby determining the maximum of the function $f(\alpha)$. For convenience, Figs. 22 and 23 display the form of the functions $\tau(q)$ and $D(q)$, corresponding to the spectral curve $f(\alpha)$ in Fig. 20 for a Cantor

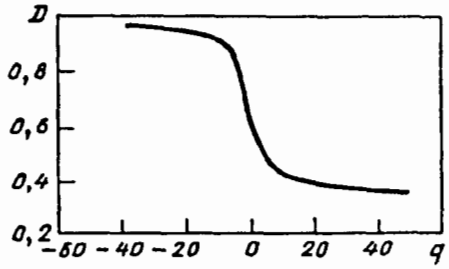

FIG. 23. Spectrum of fractal dimensions for a two-scale Cantor set shown in Fig. 18.[3]

multifractal. It is evident that the exponent $\tau(q)$ grows linearly for large $|q|$, taking on negative values as $q\to-\infty$ and positive values as $q\to+\infty$. Since the multifractal dimension $0<D(q)<\infty$, it is evident from Eq. (3.36) that the exponent $\tau(q)$ changes sign at the point $q=1$. As far as the function $D(q)$ is concerned, it is evident from Fig. 23 that it decays monotonically from the maximum value $D_{-\infty}$, corresponding to $q=-\infty$, to the minimum value $D_\infty\equiv D(q=+\infty)$, and the region where the function $D(q)$ changes most rapidly is concentrated near the value $q=0$.

We now give a more detailed analytical description of these functions. We start with the spectral function $f(\alpha)$. As one can see from Eq. (3.26), the derivative $df(\alpha)/d\alpha=\pm\infty$ at the limits $\alpha_{\min}$ and $\alpha_{\max}$ of the domain of the function $f(\alpha)$, where the parameter q assumes the limiting values $q=\pm\infty$. The right-hand limit, where this derivative is negative, corresponds to the initial value $q=-\infty$ and the left-hand limit, where the derivative is positive, corresponds to the final value $q=+\infty$. Then, using the relation (3.31) it is easy to see that the value of $\alpha_{\max}$ reduces to the maximum dimension $D_{-\infty}$, corresponding to the initial value of the parameter q, and $\alpha_{\max}$ corresponds to the minimum dimension $D_{+\infty}$, corresponding to the final value of q:

$$D_{-\infty}=\alpha_{\max},\quad D_{+\infty}=\alpha_{\min}. \tag{3.38}$$

Besides the limiting points, the spectral distribution $f(\alpha)$ gives a number of physical values of $D(q)$ inside the interval. Thus if we set $q=0$ in the definition (3.22), then summation over all segments i yields the value $M(0)=N_n$. Comparing it to the result (3.30) for $q=0$, we arrive at the relation

$$N_n=l_n^{-D_0},\quad D_0\equiv D(q=0), \tag{3.39}$$

determining, similarly to Eq. (2.7), the total number of segments l_i on which the measure P_i is given. Thus for $q=0$ the distribution $D(q)$ gives the fractal dimension of the geometric set, which is the carrier (domain) of the physical quantities P_i. According to the definition (3.31) at the point $q=0$ we have $D(q=0)=f(\alpha_0)$, where the value $\alpha_0\equiv\alpha(q=0)$ is fixed by the condition $df/d\alpha=0$, following from Eq. (3.26). This means that the fractal dimension D_0 corresponds to the ordinate of the maximum of the spectral function $f(\alpha)$ (Fig. 24).

We now determine the meaning of the value $D_1\equiv D(q=1)$. Since the denominator in Eq. (3.29) contains the factor $q-1$, great care must be exercised in performing the calculation, because one cannot set immediately $q=1$. Taking $q=1+\delta$, $\delta\to0$, we rewrite the definition (3.29) in the form

$$D(1)=\lim_{\substack{\delta\to0,\\ l\to0}}\left[\frac{1}{\delta}\left(\ln\sum_i P_i^{1+\delta}\right)(\ln l)^{-1}\right]. \tag{3.40}$$

Writing the chain of obvious relations

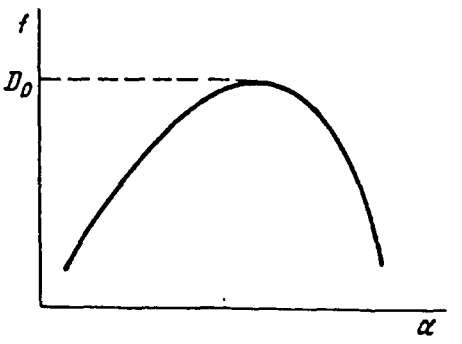

FIG. 24. Diagram showing how to determine the dimension D_0 of the geometric carrier set from the spectrum of the multifractal.[8]

$$\begin{aligned}\ln\sum_i P_i^{1+\delta}&=\ln\left[\left(\sum_i P_i^{1+\delta}-1\right)+1\right]\\ &\approx\sum_i P_i^{1+\delta}-1\\ &=\sum_i P_i e^{\delta\ln P_i}-1\\ &=\sum_i P_i(1+\delta\ln P_i)-1\\ &=\delta\sum_i P_i\ln P_i,\end{aligned}$$

where the normalization condition

$$\sum_i P_i=1$$

is taken into account, we arrive at the expression

$$D_1=-S(l)/\ln l, \tag{3.41}$$

where

$$S=-\sum_i P_i\ln P_i \tag{3.42}$$

is the ordinary entropy.[34] If the iteration process for the set under study reduces to having the segments in steps, then the elementary length $l_n=(1/2)^n$, and Eq. (3.41) assumes the form

$$D_1=s/\ln 2 \tag{3.43}$$

where $s=S/n$ is the entropy per iteration. Since the denominator represents 1 bit$\equiv\ln 2$ of information, it can be concluded that the fractal dimension D_1, corresponding to the parameter $q=1$, reduces to the information entropy.

In order to obtain a geometric interpretation of the dimension D_1 we set $q=1+\delta$, $\delta\to0$, in the definition (3.31):

$$\begin{aligned}D_1&\approx[(1+\delta)(\alpha+\alpha'\delta)-(f(\alpha)+f'(\alpha)\alpha'\delta)]\\ &\approx\alpha+\alpha'(1-f'(\alpha))+\delta^{-1}(\alpha-f(\alpha)),\end{aligned} \tag{3.44}$$

where $\alpha=\alpha(q=1)$, $\alpha'=d\alpha/dq|_{q=1}$, $f'(\alpha)=df/d\alpha|_{\alpha=\alpha(q=1)}$.

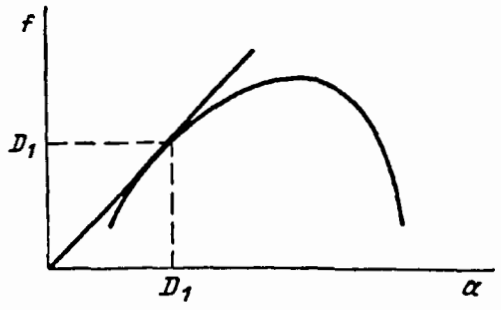

FIG. 25. Diagram showing how to determine the information entropy D_1 from the spectrum of the multifractal.[8]

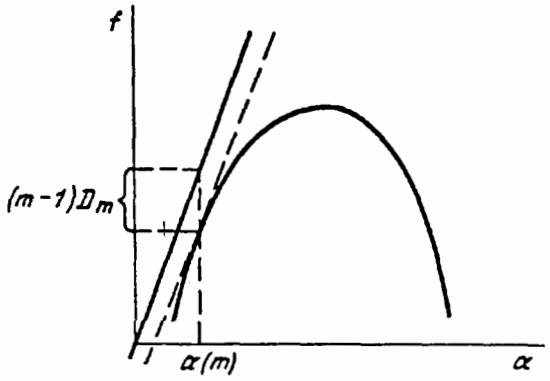

FIG. 26. Diagram showing how to determine the dimension D_m of the exponent m of the partial correlation function.

In order to prevent the expression (3.44) from diverging in the limit $\delta \to 0$ we set

$$\alpha(q=1)=f(\alpha(q=1)). \tag{3.45}$$

On the other hand, the second term in Eq. (3.44) also disappears, since, by virtue of Eq. (3.26),

$$\left.\frac{df}{d\alpha}\right|_{\alpha=\alpha(q=1)}=1. \tag{3.46}$$

As a result, we obtain

$$D_1=\alpha(q=1). \tag{3.47}$$

According to Eqs. (3.45)–(3.47), in order to determine the dimension D_1 we must construct the tangent to the plot of $f(\alpha)$, passing through the origin (Fig. 25). Then the abscissa and ordinate of the point of tangency determine D_1.

The fractal dimension $D_2 \equiv D(q=2)$ is important. It determines the behavior of the correlation function[5)]

$$S(r)=\frac{\langle \rho(r+r')\rho(r')\rangle}{\langle \rho^2(r')\rangle} \propto r^{-(D_0-D_2)}, \tag{3.48}$$

where the fact that the dimension d of the physical space reduces to the fractal dimension D_0 has been taken into account; $\rho(r)$ is the coordinate distribution of the particle density; and, the brackets indicate averaging over the fractal set. The physical meaning of the function (3.48) is that this function determines the conditional probability that a particle has the coordinate $r'+r$ if another particle is located at the point r'. It is easy to show that the Fourier transform of the function (3.48) has the form $S(k) \propto k^{-D_2}$ and thus it reduces to the distribution (2.32) of the intensity of the transmitted radiation.

In order to determine the exponent D_2 we integrate the function (3.48) over a sphere of radius l centered at the point r'. The obtained measure

$$M_2(l) \propto l^{D_2} \tag{3.49}$$

determines the joint probability that both particles are located in the sphere. It can be calculated independently by partitioning the entire space into N spheres of radius l and taking into account the fact that the probability that two particles are simultaneously present in the ith sphere is P_i^2. Then, summing over all spheres, we obtain the desired quantity $M_2(l)$, which, evidently, reduces to the general definition of measure (3.21) with $q=2$. Comparing the result (3.49) obtained above to the expression (3.30) gives the equality $D_2=D(q=2)$, indicating that the correlation exponent D_2 corresponds to the value $q=2$ in the spectral distribution $D(q)$.

Evidently, the procedure performed above can be extended to a correlation function of arbitrary order $m \geqslant 2$, if r in an equation of the type (3.48) is the maximum distance between m particles:

$$S(r_1,r_2,\ldots,r_m) \propto \left\langle \prod_{i=1}^{m} \rho(r_i) \right\rangle \propto r^{-(D_0-D_m)}, \tag{3.50}$$

where $r=\max|r_i-r_j|$, $i,j=1,\ldots,m$. Thus the collection of exponents D_m, which correspond to integer values $q=m$, $m=2,3,\ldots$, determines the rate at which the m-particle spatial correlations decay.

In order to determine the quantities D_m graphically, we start from Eq. (3.31) written for $q=m$:

$$(m-1)D_m=m\alpha(m)-f(\alpha(m)). \tag{3.51}$$

Using the condition

$$m=df/d\alpha|_{\alpha=\alpha(m)}, \tag{3.52}$$

following from Eq. (26), we can see that in order to determine D_m we must construct the straight line $f=m\alpha$, and then displace it parallel to itself until it is tangent to the dome of the spectral function $f(\alpha)$. According to Eq. (3.52) the point of tangency gives $\alpha(m)$, knowing which we determine from Eq. (3.51) the exponent D_m (Fig. 26). The decreasing character of the function $D(q)$ (see below) indicates that the rate of decay of the correlation function (3.50) increases with increasing order m. In the limit $m \to \infty$ the correlation exponent in Eq. (3.50) reaches the final value D_0-D_∞, which, as should happen, does not exceed the dimension D_0 of the space itself in which the correlation is observed.

We now describe the behavior of the function $\tau(q)$. Since the values of the parameter α are limited to the positive values (3.38), it follows from Eq. (3.37) that the

function $\tau(q)$ is monotonically increasing (see Fig. 22). For $|q|\gg 1$ we can take $\alpha(q)\approx D_{\pm\infty}$, and integrating the expression (3.37) gives the linear function

$$\tau(q)\approx C_{\pm}+D_{\pm\infty}q, \quad q\to\pm\infty, \tag{3.53}$$

where $C_{\pm}$ are constants. The behavior of $\tau(q)$ for small values of q is characterized by the fact that τ vanishes for $q=1$. This result follows from Eq. (3.36), if we take into account the fact that the dimension $D(q)$ is always finite. At the point $q=0$ we have $\tau=-D_0$.

Finally, we describe the spectrum of dimensions $D(q)$. Substituting the relation (3.36) into Eq. (3.37) and performing the differentiation, we obtain, using Eq. (3.31),

$$\frac{dD}{dq}=-\frac{d-f(\alpha)}{(q-1)^2}. \tag{3.54}$$

As one can see from Fig. 25, the first term in the numerator of Eq. (3.54) as a function of the parameter α is greater than the second term at all points, except $\alpha=\alpha(q=1)$, where they become equal to one another. Then, however, the denominator of Eq. (3.54) also vanishes, so that $dD/dq\leqslant 0$ always and the function $D(q)$ is monotonically decreasing. According to Eqs. (3.36) and (3.53), for large $|q|$ the dimension D approaches the limiting values $D_{\pm\infty}$ according to the relation

$$D\approx D_{\pm\infty}+(C_{\pm}+1)q^{-1}, \quad |q|\gg 1. \tag{3.55}$$

Correspondingly, for $|q|\ll 1$ Eq. (3.31) yields the linear function

$$D\approx D_0-(\alpha_0-1)q, \quad \alpha_0\equiv\alpha(q=0). \tag{3.56}$$

An example of the dimension $D(q)$ is shown in Fig. 23.

3.2. Thermodynamic description of multifractals

In this section we show that the formalism developed above can be expounded by analogy to the standard apparatus of thermodynamics.[34] In Sec. 3.2.1 we consider the case when the probability P_i in Eqs. (3.33) is constant. The conjugate curdling method in Sec. 3.2.2 will make it possible to extend the results to an arbitrary distribution P_i over fragments in the set.

3.2.1. Multifractal with constant probability distribution of the measure

Taking into account the normalization condition

$$\sum_i^{N_n} P_i=1,$$

we set in Eq. (3.33)

$$P_i=\text{const}\equiv N_n^{-1}, \tag{3.57}$$

where N_n is the total number of fragments in the set, obtained after $n\to\infty$ division steps. Then the condition $M_n(q,\tau)=1$ gives

$$N_n^q=\sum_i l_i^{-\tau}. \tag{3.58}$$

This equation can be put into the canonical form by introducing a parameter of the type inverse temperature

$$\beta=-\tau \tag{3.59}$$

and the analog of the partition function

$$Z=\sum_i l_i^{\beta}\equiv\sum_i e^{-\beta\varepsilon_i} \tag{3.60}$$

where the effective energy levels

$$\varepsilon=-\ln l_i \tag{3.61}$$

are given by the distribution of lengths l_i of the segments in the set. The thermodynamic potential $g=g(\beta)$ for one of the n iterations has the form

$$g\equiv-\frac{1}{n}\ln Z=-\frac{1}{n}\ln\sum_i l_i^{\beta}, \tag{3.62}$$

where g is measured in units of the temperature β^{-1}.

We introduce, in addition, the parameter μ according to the equation

$$N_n=\mu^n. \tag{3.63}$$

Then, using Eq. (3.62), the condition (3.58) gives the expression

$$g=-q\ln\mu, \tag{3.64}$$

where the presence of the logarithm indicates that the parameter μ is an entropy.

For further clarification, we assume that all segments of the set at the nth iteration step have identical lengths

$$li=\xi^n, \tag{3.65}$$

determined by the scale

$$\xi=e^{-\lambda}, \tag{3.66}$$

whose magnitude is set by the Lyapunov exponent λ. In order to clarify its thermodynamic meaning, we determine the partition function (3.60)

$$Z_n=N_n l_n^{\beta}=\mu^n e^{-\beta\lambda}=\exp[n(\ln\mu-\beta\lambda)], \tag{3.67}$$

where Eqs. (3.63), (3.65), and (3.66) are taken into account. Substituting Eq. (3.67) into Eq. (3.62) we obtain the following expression for the specific free energy:

$$g=\beta\lambda-\ln\mu. \tag{3.68}$$

This reduces to the standard definition $G=E-TS$, if the quantity $(n/\beta)g$ is taken to be the total free energy G and the quantity $E=n\lambda$ is taken to be the energy, and finally the entropy is

$$S=ns, \quad s=\ln\mu. \tag{3.69}$$

Thus the fractal set can be described in thermodynamic language, if it is assumed that the number of iterations $n\to\infty$ plays the role of the number of particles, the parameter β is the inverse temperature, the Lagrange multiplier λ is the specific energy, and s is the entropy. Their values are determined by Eqs. (3.59), (3.66), and (3.69), and the energy spectrum ε_i is given by the distribution of the segment lengths (3.61). In this approach the quantity β is a free parameter, and the equation of state establishes the function $g(\beta)$. Using the thermodynamic identity

$$\lambda = dg/d\beta, \tag{3.70}$$

we can switch from the parameter β to the conjugate field λ.[34] Then Eqs. (3.68) and (3.69) give the expression

$$s = \beta g'(\beta) - g(\beta), \quad g' \equiv dg/d\beta \tag{3.71}$$

for the entropy, whose value is determined by the energy λ.

In order to establish the relation between the geometric and thermodynamic approaches the quantities τ, q, α, f, and D, introduced in Sec. 3.1, must be expressed in terms of the parameters β and g employed here. The definition of the first parameter τ is given by the identity (3.59). The expression for the second quantity

$$q = \left(1 - \frac{d \ln g(\beta)}{d \ln \beta}\right)^{-1} \tag{3.72}$$

follows from Eqs. (64), (69), and (71).

For the exponent α we obtain from Eq. (3.47), using Eqs. (3.63), (3.69), (3.65), and (3.66), $P_n = l_n^{g/\lambda}$. Comparing this result to the definition (3.20) we arrive at the desired equality

$$\alpha = \beta - g(\beta)/g'(\beta), \tag{3.73}$$

where Eqs. (3.70) and (3.71) are taken into account. Using the definition (3.20) and (3.23) it is easy to see that the condition (3.57) means that

$$\alpha = f, \tag{3.74}$$

so that Eq. (3.73) also gives f. On the other hand, substituting Eq. (3.74) into the definition (3.31) we arrive at the last of the required geometric characteristics:

$$D = f = \alpha = \beta - [g(\beta)/g'(\beta)], \tag{3.75}$$

where Eq. (3.73) is taken into account.

3.2.2. Thermodynamic description of a multifractal on the basis of the curdling method

A well-known feature of the thermodynamic scheme is that a dual representation of the system is possible—depending on the character of the external condition, within one approach the temperature dependence can be studied and within the conjugate approach the entropy dependence can be studied (in the first case the thermodynamic potential is the Gibbs or Helmholtz free energy and in the second case the thermodynamic potential is the internal energy or enthalpy).[34] Obviously, such a situation can be expected in our case also: in Sec. 3.2.1 the independent parameter reduced to the inverse temperature β, whereas here the independent parameter is the energy λ, which, according to Eq. (3.70), is the conjugate field with respect to the parameter β. The equation (3.70) itself makes it possible to find, for a given value of λ, the parameter $\beta(\lambda)$, substituting which into the relations (3.71)–(3.75) will lead to their expression in terms of the energy λ. In so doing, the entropy $s(\lambda)$ as a function of the energy must play the role of the equation of state, replacing the relation $g(\beta)$ employed above.

With regards to the geometric aspect of the approach expounded, it should be noted that in Sec. 3.2.1 the probability P_i of filling the fragments was assumed to be constant and the dependence of the measure (3.67) on the character of the distribution of fragments, determined by the inverse temperature β, was investigated. The measure determined the free energy (3.62). In the present section, we employ the conjugate curdling method, in which imposition of the condition $\tau = 0$ in Eq. (3.33) leads to a uniform distribution of fragments, and the probability distribution is postulated in the form

$$P_i = Z^{-1} l_i^{\beta}, \tag{3.76}$$

where the normalization condition gives the partition function (3.60). Evidently, here the quantity (3.21) plays the role of measure.

Using Eqs. (3.20), (3.65), (3.66), and (3.62) we obtain from the definition of the probability (3.76) the basic thermodynamic relation of the approach employed:

$$g = \lambda\beta - s(\lambda), \tag{3.77}$$

replacing the relation (3.71). From this equation it is easy to obtain the entire collection τ, q, α, f, and D of geometric characteristics of the multifractal. Since the calculations employed here are identical to the calculations described in the preceding section, we present only the results:

$$\begin{aligned} &\tau = -\beta, \\ &q = 1 - (\lambda\beta/s(\lambda)), \\ &\alpha = f = D = s(\lambda)/\lambda. \end{aligned} \tag{3.78}$$

Replacing λ with β and using the relations (3.70), the relations (3.78) reduce to the equalities (3.59) and (3.72)–(3.75). The last expression in Eqs. (3.78) indicates that on the basis of the thermodynamic approach the dome of the spectral function $f(\alpha)$, characteristic of the geometric picture, is straightened (see Fig. 25). However, according to the second relation in Eqs. (3.78), the parameter q then becomes dependent on one of the thermodynamic quantities λ and β.

3.3. Examples of application of the concept of a multifractal

In this section it will be shown that the concept of a multifractal makes it possible to construct a unified picture of phenomena such as turbulent motion of a liquid and fatigue fracture of materials (Sec. (3.3.1), formation of incommensurate structures and quasicrystals [Sec. (3.3.2)], phase transitions (taking into account critical fluctuations), and formation of hierarchically coordinated structures (Sec. 3.3.3). In this exposition we start from considerations of symmetry of the mapping function, the successive action of which generates the set of points of the multifractal set. Thus, Sec. 3.3.1 is based on the use of a parabolic function, which is the simplest example of a symmetric function. Correspondingly, quasiperiodic sequences, generated by antisymmetric functions, are studied in Sec. 3.3.2. A characteristic feature of the maps employed in Secs. 3.3.1 and 3.3.2 is that at each step of the generation of a fractal set only the two closest levels are coupled. In contrast to this, in Sec. 3.3.3 a non-Markovian chain of

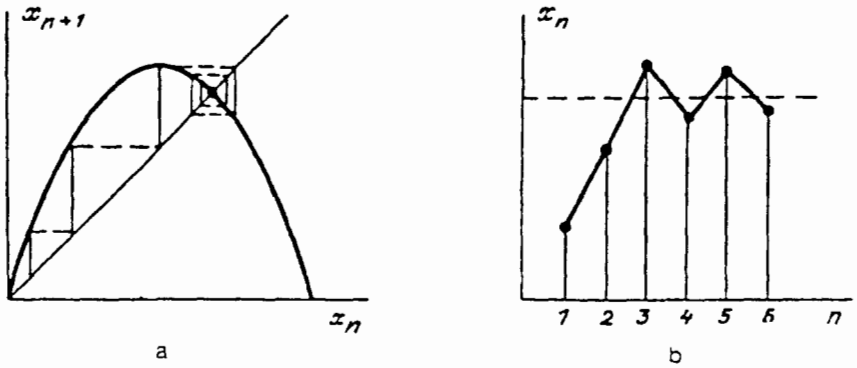

FIG. 27. a—Construction of the logistic sequence (3.79). b—Values $x_1, x_2, \ldots, x_n$ of the coordinates of the logistic sequence which are given by the intersection of the perpendiculars to the axes x_n and x_{n+1} with the parabola (the dashed line indicates the point of intersection of the parabola with the bisector).[40]

linear maps, which couples the three nearest levels, is employed. Evidently, the Markovian sequence corresponds to first-order differential equations reflecting dissipation processes, while the non-Markovian chains correspond to second-order equations of the Schrödinger equation type.

3.3.1. Logistic sequence

In the present section we describe processes that can be represented by a chain of bifurcations, each of which, by dividing the initial fragment in two pieces (see Fig. 7a), represents the simplest mechanism of formation of a fractal set. A well-known example of a physical process that can be described with the help of a chain of bifurcations is the transition to turbulent fluid flow by means of period doubling.[37] The reverse process of pairwise merging of microcracks can be regarded as a possible mechanism of fatigue fracture of solids.[13]

The simplest relation modeling bifurcation of the coordinate x_{n+1} into a pair of values $x_n^{(\pm)}$ is the quadratic function

$$x_{n+1}=1-ax_n^2, \tag{3.79}$$

which generates a logistics sequence, characterized by the parameter α. Iterating it with the help of the graphical procedure shown in Fig. 27a, we obtain the limiting coordinate

$$x_\infty=[(1+4a)^{1/2}-1]/2a. \tag{3.80}$$

A plot of the iteration process is shown in Fig. 27b. The value of the parameter a is chosen so that the iteration process would be similar. This means that the form of the function (3.70) must not change on passing from $n+1$ to $m>n+1$.

In order to determine the value of α we point out that the initial equation (3.79) has real solutions $x_{n+1}=x_n$ for $a\geqslant A_1$, where A_1 is given by the condition $dx_{n+1}/dx_n=-1$. Hence we find $A_1=3/4$. In order to determine the next value A_2 we iterate the map (3.79) twice. It is easy to see that, to within quadratic terms in x_n, the function $x_{n+2}(x_n)$ obtained can be put into the form (3.79), by making the scale transformation

$$x_n\to(1-a)x_n, \quad a\to\varphi(a)\equiv 2a^2(a-1). \tag{3.81}$$

Repeating this operation l times we arrive at a series of successive maps of the form (3.79):

$$x_{n+2^l}=1-a_l x_n^2, \quad a_l=\varphi(a_{l-1}). \tag{3.82}$$

As a result we obtain the chain of equations

$$A_1=\varphi(A_2), \quad A_2=\varphi(A_3),\ldots, \quad A_{l-1}=\varphi(A_l) \tag{3.83}$$

for determining the limiting parameter A_∞. A graphical solution of this chain is obtained by the construction shown in Fig. 28. Using the definition (3.81), we find the limiting value $A_\infty=(1+\sqrt{3})/2\approx 1.37$. It is evident from the chain of equations (3.83) that as $l\to\infty$ we can write

$$\frac{A_{l+2}-A_{l+1}}{A_{l+1}-A_l}=\frac{1}{\delta_l}, \quad \delta_l=\left.\frac{d\varphi}{du}\right|_{a=A_l}. \tag{3.84}$$

Using Eq. (3.81), we obtain hence the limiting value $\delta\equiv\delta_\infty=4+\sqrt{3}\approx 5{,}73$. Thus the condition of self-similarity of the logistic sequence requires that its parameter assume at the step $l\to\infty$ a value a not less than A_l, varying according to the law

$$A_\infty-A_l\propto\delta^l=e^{l\ln\delta}. \tag{3.85}$$

The analytical procedure presented above for studying the logistic sequence reflects the basic characteristics of the process—the presence of a chain of bifurcations, occurring for different values of A_l, and the similarity property, characterized by the exponent $\ln\delta$. For all its convenience,

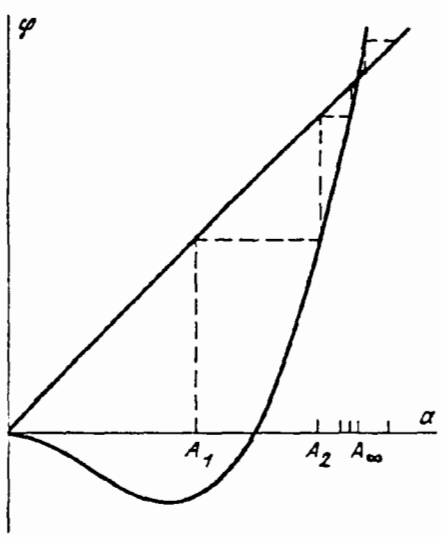

FIG. 28. Graphical solution of the chain of equations (3.83) for the parameter a of the logistic sequence [the function $\varphi(a)$ is given by Eq. (3.81)].[37]

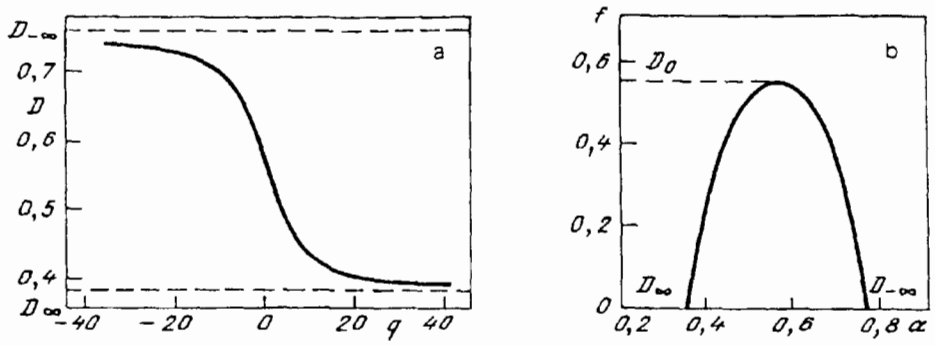

FIG. 29. The spectrum of fractal dimensions (a) and the spectral function (b) for a multifractal set generated by the logistics sequence.[10]

however, this procedure gives only approximate values of δ and A_∞. This is evidently connected with the fact that the terms x_n^k, $k>2$, are dropped when the map (3.79) is iterated. The exact values obtained by repeated iteration on a computer are[38]

$$\delta=4.669, \quad A_\infty=1.401. \tag{3.86}$$

In Ref. 10 a set of values of x_l, obtained as a result of 11 iterations of the logistic sequence (3.79) with the parameter $a=A_\infty$, was investigated numerically. To this end, the measure (3.33) was calculated, and the function $\tau(q)$ was then found from the condition $M_{11}(\tau,q)=1$. Hence the functions $D(q)$ and $f(\alpha)$, presented in Fig. 29, were obtained using the relations (3.35)–(3.37). It was found that the spectrum of fractal dimensions is bounded by the values

$$D_\infty=0.378, \quad D_{-\infty}=0.756, \tag{3.87}$$

which are related by the relation $D_{-\infty}/D_\infty=2$. Using the definition (2.11), where for the bifurcation parameter $j=2$, we see that for $q=\pm\infty$ the scale factor $\xi_{-\infty}=A_\infty-1$, $\xi_\infty=(A_\infty-1)^2$. In other words, if in dividing the initial fragment the scale l is obtained, then the logistic sequence generates a multifractal also containing the scale $l^{1/2}$. The first one corresponds to the densest region of the fractal set, lying near the apex of the parabola (3.79). On shifting to rarefied regions near the points $x_n=0$ and 1, the quadratic function $x_{n+1}(x_n)$ becomes a linear function, and this is what leads to the appearance of the square root $\xi^{1/2}$. We shall use this fact extensively below.

The description presented above was of a geometric character. We now describe the corresponding formalism. To this end, just as in Sec. 3.2.1, we assume that the probability P_i of realization of measure on the ith fragment is a constant. Then it is easy to see that for the logistic sequence (3.79) the probability density must have the form

$$p(x)=\pi^{-1}[x(1-x)]^{-1/2}, \tag{3.88}$$

where the factor π^{-1} takes into account the normalization condition. On a qualitative level this is evident from Fig. 30, which displays the distribution of the coordinates x. In accordance with the distribution (3.88), the branches of the bifurcation chain bunch up on the limits of the interval [0,1]. If the fragments $[0,l]$, $[1-l,1]$ of length $l\to 0$ are separated here, then according to Eq. (3.88) the probability of realization of each of them is

$$P_0=\int_0^l p(x)\mathrm{d}x\approx\pi^{-1}\int_0^l x^{-1/2}\mathrm{d}x=(2/\pi)l^{1/2}. \tag{3.89}$$

For the segment l_i, lying in the interval $[l,1-l]$, we have, correspondingly,

$$P_i=\int_{x_i}^{x_i+l_i} p(x)\mathrm{d}x\approx p(x_i)l_i=\frac{l_i}{\pi}[x_i(1-x_i)]^{-1/2}. \tag{3.90}$$

By virtue of the equally probable character of the distribution $P_i=P_0$, and Eqs. (3.89) and (3.90) lead to the following distribution of the segment lengths

$$l_i=2l^{1/2}[x_i(1-x_i)]^{1/2}, \tag{3.91}$$

according to which the minimum values l_i are realized at the limits of the interval [0,1], and the maximum values are realized at the center.

This result is easy to imagine, if the values of x_i are taken to be the coordinates of the nodes of the Cayley tree corresponding to the logistics chain of bifurcations (see Fig. 30). Then the lengths l_i reduce to the distance between the nodes i and $i+1$.[6)] It is evident from Fig. 7 that if neighboring nodes of the Cayley tree are located at the periphery of the tree, then their nearest ancestor is not significantly removed from them, and at the center it approaches the vertex of the tree. This means that the distances l_i increase as the coordinate x_i of a node approaches

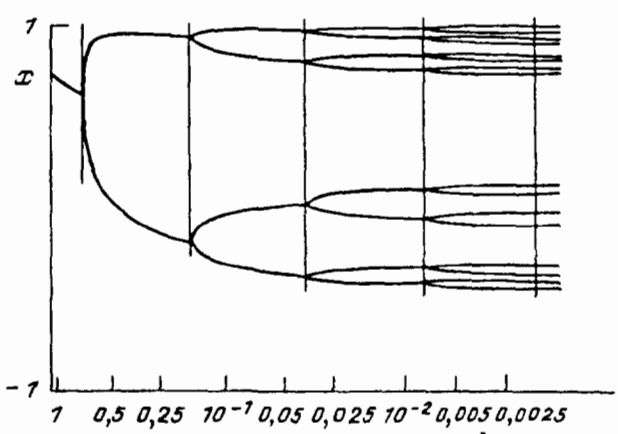

FIG. 30. Chain of bifurcations generated by the logistic sequence (3.79) (the values of the control parameter a are plotted along the abscissa; the vertical lines correspond to the critical values of A_n).[40]

the center of the segment of the ultrametric space corresponding to the initial interval [0,1] in ordinary space. It is this behavior that is provided by the distribution of lengths (3.91). Since it follows from the probability distribution $p(x)$, the indicated correspondence justifies the choice of the function (3.88). On the other hand, and more importantly, we can draw the following conclusion: In order to switch from the analytic description of the sequence of reflections of the type (3.79), which gives the coordinates x_i of the set obtained in ordinary space, to the geometric representation, determined by the distribution of the lengths l_i of the elementary fragments, it is necessary to switch from the ordinary space to the ultrametric space. As shown in Sec. 2.1.2, this transition is achieved formally by switching from the ordinary decimal representation of the numbers x_i [with the help of the series expansion (2.13)] to a j-adic system, where in the continuous space x we pass to the limit $j\to\infty$. Since the system of computer computation, where $j=2$, is based on such a transformation, it is easy to understand why computer modeling is the main tool for investigating different maps.

In order to achieve a comprehensive representation of the logistic sequence (3.79) it is necessary to construct a thermodynamic description, the scheme of which is developed in Sec. 3.2. First we employ the approach (see Sec. 3.2.1) in which the free parameter is the inverse temperature β. The value of β determines the thermodynamic potential $g=g(\beta)$, and the entropy s and energy λ are assumed to be given.

In order to determine the function $g(\beta)$ the distribution of lengths (3.91) must be substituted into the definition (3.62). The expression obtained in so doing reduces to a nonanalytic ratio of γ functions $\Gamma(1+\beta/2)/\Gamma(3/2+\beta/2)$.[39] It is more convenient to use a simplified scheme in which the continuous distribution of segment lengths (3.91) is replaced by a two-scale approximation. On the basis of the arguments presented after Eqs. (3.87), we assume that at the nth step of the logistics map (3.79) the entire set separates into two classes of fragments, whose lengths are $l_n=\xi^n$ and $l_n^{1/2}=\xi^{n/2}$, and the number of fragments in each class is $2^{n-1}\sim 2^n$, where $n\to\infty$. Then the partition function (3.60) is estimated to be

$$Z=\sum_i l_i^\beta \sim 2^{n-1}l_n^{\beta/2}+2^{n-1}l_n^\beta, \tag{3.92}$$

where the first term is determined by the contribution of short lengths l_i, corresponding to the edges of the interval [0,1], and the second term is determined by the inner part of this interval. Substituting the exact distribution (3.91) into Eq. (3.60) shows that the ends of the interval can make a determining contribution only for significant negative values of the parameter β. For this reason, it is more natural to put the estimate (3.92) into the form

$$\begin{aligned} Z_n &\sim 2^n\cdot 2^{-n\beta\lambda} \quad \text{for } \beta<-2,\\ &\sim 2^n\cdot 2^{-n\beta\lambda/2} \quad \text{for } \beta>-2, \end{aligned} \tag{3.93}$$

where the relations (3.65) and (3.66) were used, and the critical temperature $\beta_c=-2$ is determined by the divergence of the exact expression $Z(\beta)\propto(\Gamma(1+\beta/2))^n$. Substituting Eq. (3.93) into Eq. (3.62), we find an estimate of the thermodynamic potential

$$\begin{aligned} g &\sim \lambda\beta-\ln 2 \quad \text{for } \beta<-2,\\ &\sim(\lambda/2)\beta-\ln 2 \quad \text{for } \beta>-2. \end{aligned} \tag{3.94}$$

The entropy (3.71) then assumes the characteristic value $s=\ln 2$, and the definition (3.75) leads to the following geometric characteristics:

$$\begin{aligned} D=f=\alpha &\sim \ln 2/\lambda \quad \text{for } \beta<-2,\\ &\sim \ln 2/(\lambda/2) \quad \text{for } \beta>-2. \end{aligned} \tag{3.95}$$

Thus the two-scale approximation of the distribution (3.91) gives, instead of a continuous set of values of D, f, and α, two discrete values, corresponding to the limits $q=\pm\infty$. Taking into account the existence of a break in the temperature dependence (3.94) of the potential $g(\beta)$, a jump in the fractal dimension (3.95) can be interpreted as a unique first-order phase transition, indicating bunching up of the fractal at the point $\beta=-2$. As the functions $D(q)$ and $f(\alpha)$ in Fig. 29 show, this transition is actually not sharp, but diffuse. This means that the real multifractal reduces to a continuous set of monofractals with the pair (3.95), corresponding to the limits of the spectrum $f(\alpha)$.

Finally, we determine the quantities f, α, and D within the conjugate approach, where the energy λ is an independent parameter, determining the entropy $s(\lambda)$, and the quantities β and $g(\beta)$ are given (see Sec. 3.2.2). Integrating the relation (3.70), we obtain the result $g=\beta\lambda+\text{const}$, substituting which into Eq. (3.77) gives, as above, the constant value $s(\lambda)=-\text{const}\equiv\ln 2$. On the other hand, the two-scale model adopted means that the energy domain is exhausted by the values λ and $\lambda/2$. Then the latter equality (3.78) leads, as should happen, to the spectrum (3.95). The second equality in Eq. (3.78) in turn gives the parameter q as a function of the energy λ:

$$\begin{aligned} q &= 1-(\beta/\ln 2)\lambda \quad \text{for } \beta<-2,\\ &= 1-(\beta/\ln 4)\lambda \quad \text{for } \beta>-2. \end{aligned} \tag{3.96}$$

3.3.2. Quasiperiodic sequencies. In the preceding section we studied for the example of the simplest parabolic function the class of symmetric maps

$$x_{n+1}=\alpha+x_n+f(x_n), \tag{3.97}$$

whose generating function has the property $f(x)=f(-x)$, $\alpha=\text{const}$. In this section we investigate antisymmetric sequences: $f(x)=-f(-x)$. Since an arbitrary function can be represented as a superposition of symmetric and antisymmetric components, it can be expected that, together with the results of Sec. 3.3.1, such an analysis exhausts the description of possible features of multifractal sets generated by chains of bifurcations.

Another feature of the generating function $f(x)$ that makes this function exceedingly important in applications to condensed-matter physics is the condition of irrationality of the ratio $\Omega=1/b<1$ of the length of the interval [0,1], on which the values of x are defined, to the period

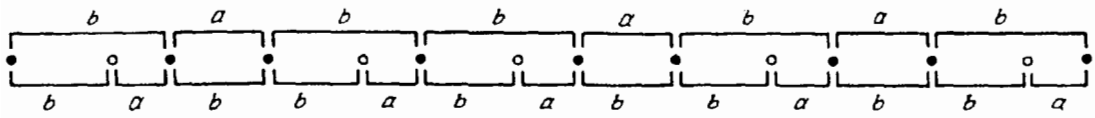

FIG. 31. Scale transformation for a quasiperiodic sequence of atoms of two types (the initial periods a and b are shown at the top; the values of the periods reduced by a factor of τ are shown at the bottom).[11]

$b>1$ of the function $f(x)=f(x+b)$. Physically this means that the characteristic scale b of the response function $f(x)$ is incommensurable to the initial scale 1 of the action of x on a given system.[7)] A classical example of such a situation is the mechanism of appearance of turbulence, in which each bifurcation corresponds to a transformation of a circular trajectory of fluid flow into quasiperiodic motion on the surface of a torus, formed by "swelling" of the initial circle.[37]

In solid state physics this situation arises in the study of long-period structures, whose period b is incommensurable to the period a of the initial lattice. On the basis of the simplest Frenkel'–Kontorova model the map (3.97), which takes into account the main features of the behavior of incommensurable structures,[41] assumes the form

$$x_n=(n+\alpha)a-(K/2\pi)\sin[2\pi n(a/b)+\beta], \qquad (3.98)$$

where $n=0,1,...$ is a series of integers, and a and b are periods, whose ratio $\Omega=a/b<1$ is an irrational number; the constants α and β play the role of initial phases of the short-period distribution and its long-period components; and, K is a coupling constant.

A nontrivial extension of the periodic sequence $x_n=(n+\alpha)a$, having period a, is obtained if the integer part $[x]$ of the variable x (or its fractional part $\{x\}=x-[x]$) is taken as the generating function $f(x)$ in the map (3.97). Then the quasiperiodic sequence obtained has the form[11]

$$x_n=(n+\alpha)a+[(n/\sigma)+\beta](a/\rho), \qquad (3.99)$$

where α and β are the initial phases, and ρ and σ are positive irrational numbers. A characteristic feature of this sequence is that the distances $\Delta x_n=x_n-x_{n-1}$ between nearest neighbors can assume only two values

$$\begin{aligned}\Delta x_n&=a \quad \text{for } [(n/\sigma)+\beta]-[(n-1)\sigma^{-1}+\beta]=0,\\ &=b \quad \text{for } [(n/\sigma)+\beta]-[(n-1)\sigma^{-1}+\beta]=1,\end{aligned} \qquad (3.100)$$

where the period b, irrational with respect to the initial period a, is set by the parameter ρ according to the equation $b=(1+\rho^{-1})a$. On the other hand, it is easy to show by direct calculation that for each value of n for which the upper condition (3.100) holds there are, on the average, $\sigma-1$ values of n satisfying the lower condition. Thus the quantity $1-\sigma^{-1}$ determines the frequency of appearance of the period b.

Given arbitrary irrational values of the parameters σ and ρ it is easy to construct a sequence of segments a and b corresponding to Eq. (3.99). The most important feature of this sequence is that without the periodicity property it, by definition (3.99), is not random. By varying the parameters ρ and σ it is possible to obtain any irrational values of the ratio of the periods $b/a=1+\rho^{-1}$ and frequencies of appearance of the long period $1-\sigma^{-1}$. From this set, corresponding to different values of ρ and σ, we can separate a Fibonacci sequence, which has the property of self-similarity. As explained in Sec. 2.1.1, only such a set exhibits fractal properties, and we must determine next the values of ρ and σ which give these conditions.

They mean, first, that by a simple scale change the Fibonacci sequence can be transformed into a self-similar sequence. For example, by decreasing the periods a and b it is possible to obtain a situation when the length of the period b of the initial sequence transforms into the set of segments $a+b$ and the short period a transforms into b (Fig. 31). This is achieved under the condition

$$\frac{b}{a+b}=\frac{a}{b},$$

which, substituting the relation $b=(1+\rho^{-1})a$, assumes the form of a quadratic equation

$$\rho^2-\rho-1=0. \qquad (3.101)$$

Thus local self-similarity is achieved for values of the scale factor ρ equal to the so-called golden mean[8)]

$$\tau=\frac{\sqrt{5}+1}{2}=1.618. \qquad (3.102)$$

In addition, the segments a and b must make the same contribution to the total length of the sequence. Evidently, this requires that the average lengths a/σ and $b(1-\sigma^{-1})$ of these segments, alternating with frequency σ^{-1} and $1-\sigma^{-1}$, must be equal. From Eq. (3.101) we can see that this condition is satisfied with the frequency factor $\sigma=\tau$. As a result, the Fibonacci sequence, following from Eq. (3.99), assumes the form

$$x_n=(n+\alpha)a+[(n/\tau)+\beta](a/\tau). \qquad (3.103)$$

This sequence was first obtained by the Pisan mathematician Leonardo Fibonacci, who was studying the following graphic situation. Let an adult rabbit a give birth each year to a rabbit b, which during the year reaches reproductive age and transforms from b to a, and then bears progeny similar to his ancestor. Then the chain of multiplication of rabbits can be represented by the Cayley tree presented in Fig. 8. It is evident from Fig. 8 that at each level n one observes an aperiodic sequence

$$abaababaabaab..., \qquad (3.104)$$

whose length N_n is determined by the Fibonacci numbers F_n. The first few numbers are: $F_0=0$, $F_1=1$, $F_2=1$, $F_3=2$, $F_4=3$, $F_5=5$, $F_6=8$, $F_7=13$,... . It is easy to see that the entire collection $\{F_n\}$ can be obtained from the rule

$$F_n=F_{n-1}+F_{n-2}. \tag{3.105}$$

On the other hand, the pair of nearest Fibonacci numbers is related by the relation

$$F_{n+1}/F_n\to\rho \text{ as } n\to\infty, \tag{3.106}$$

substituting which into Eq. (3.105) leads to Eq. (3.101), giving the golden mean (3.102). Writing out the sequence of ratios (3.106) from a given value $n\gg 1$ down to $n=1$ and eliminating the numbers $F_{n-1}, F_{n-2},..., F_2$, it is easy to obtain the equality

$$F_n\approx\tau^n, \quad n\to\infty, \tag{3.107}$$

determining the fractal dimension of the Fibonacci sequence. Indeed, since F_n is the number of points of the set N_n, we obtain, taking into account the definition (3.63) for the entropy $s=\ln\mu$, $s=\ln\tau$. Substituting this value into the last equality in Eq. (3.78), taking into consideration the definition (3.66) for the energy λ, we find

$$D=\ln\tau/\ln\xi^{-1}. \tag{3.108}$$

Since the length ξ actually reduces to the scale factor in Eq. (2.11), the equation (3.108) obtained above and this formula must be identical. Therefore the golden mean (3.102) determines the effective branching ratio $j=\tau$ of the Fibonacci tree (see Fig. 8).

By going through the values $n=0,1,...$ in the relation (3.103) it can be shown that it generates the Fibonacci sequence (3.104) of alternating segments of lengths a and b. The form of the corresponding hierarchical tree, presented in Fig. 8, predicts that at the nth step the sequence (3.103) can be obtained by operating n times with the operator

$$\hat{S}=\begin{pmatrix}1 & 1\\ 1 & 0\end{pmatrix} \tag{3.109}$$

on the column vector, constructed from the segments a and b, as projections:

$$\begin{pmatrix}x_{n+2}\\ x_n\end{pmatrix}=\hat{S}^n\begin{pmatrix}a\\ b\end{pmatrix}. \tag{3.110}$$

Evidently, the operator (3.109) is the generator of a new level of the hierarchical Fibonacci tree.

In the last ten years it was discovered that the sequence (3.103) is not only a curious mathematical construct, but it is also realized in nature in the alternation of atoms of a quasicrystal along a distinguished direction.[11] Such a series is most simply modeled as a projection of the nearest nodes of a rectangular grid with sides $a,b=\tau a$ on a straight line, making an angle of 45° with respect to the axes (Fig. 32). From this construction it is evident, in particular, that in the reciprocal space the sequence (3.103) is a superposition of wave vectors which are multiples of the periods $2\pi/a$ and $2\pi/b$, $b/a=\tau$, each of which corresponds to the

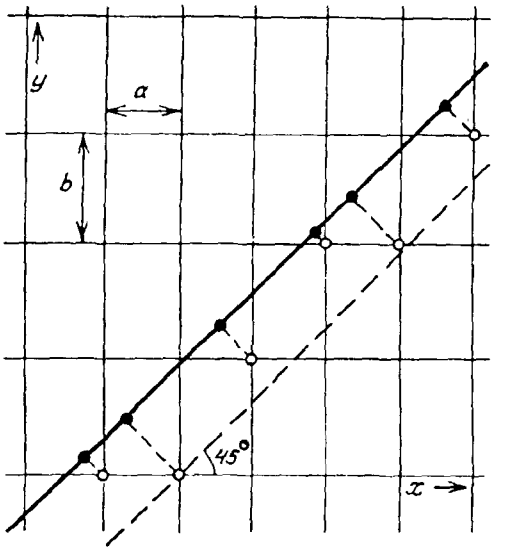

FIG. 32. Diagram showing how to construct the one-dimensional quasiperiodic sequence by the method of projection of the nodes of a rectangular lattice (the nodes lying between the parallel lines, separated along the y axis with period b, are projected).[11]

projection of one of the lattice axes on the distinguished direction. Thus the points of the reciprocal space of a one-dimensional quasicrystal are given by the equation

$$g_{lm}=\frac{2\pi/\alpha}{1+\tau^{-2}}\left(l+\frac{m}{\tau}\right), \tag{3.111}$$

where l and m are integers. We shall show that from their set the values $l=F_n$ and $m=F_{n-1}$, determined by the Fibonacci numbers, are distinguished.

To this end, we rewrite Eq. (3.103) in the form

$$x_n=(1+\tau^{-2})na-\{(1+\tau^{-2})n/\sqrt{5}\}(a/\tau); \tag{3.112}$$

here we introduce the fractional part $\{x\}=x-[x]$ of the number x; the phases α and β are assumed to be zero; and, the fact that $\tau(1+\tau^{-2})=\sqrt{5}$ was used. The form (3.112) is more convenient than the form (3.103) in the sense that the coordinate x_n is represented as a sum of the sequence $(1+\tau^{-2})na=\sqrt{5}n(a/\tau)$ with period a/τ and a periodic function (subtracted) with period a. Since the Fourier representation of periodic functions reduces to a collection of delta-like functions, taken at the points of the reciprocal space (3.111), we can write the amplitudes f of scattering of penetrating radiation with wave vector k by the quasicrystal as

$$f(k)=\sum_{l,m} f_{lm}\delta(k-g_{lm}), \tag{3.113}$$

$$f_{lm}=\lim_{N\to\infty} N^{-1}\sum_{n=0}^{N}\exp(-ig_{lm}x_n). \tag{3.114}$$

In order to calculate the form factor f_{lm} we rewrite the argument of the exponential in Eq. (3.114), regrouping the terms in the series (3.112) and using the definition (3.111):

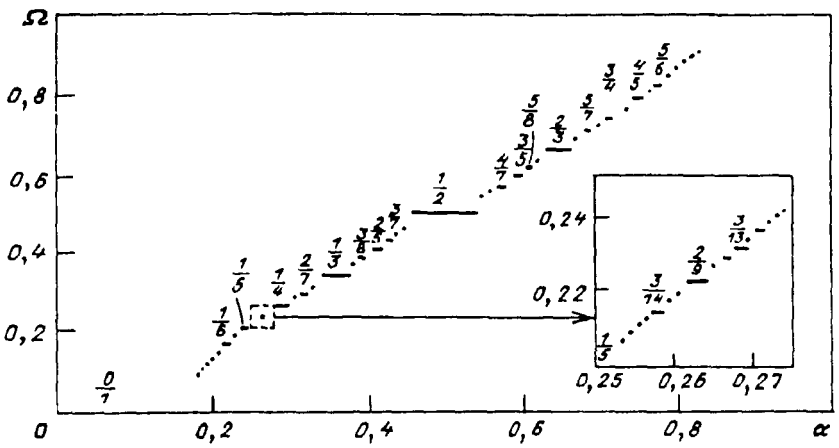

FIG. 33. Devil's staircase, reflecting mode-locking for the quasiperiodic sequence (3.119) (the ratio of the characteristic frequency of the system to the response frequency is plotted along the ordinate: the ratio of the characteristic frequency to the frequency of the external field is plotted along the abscissa).[10]

$$g_{lm}x_n=2\pi(ln+m[n/\tau])+(2\pi m-(g_{lm}/\tau))\{n/\tau\}. \tag{3.115}$$

Since the first term is a multiple of 2π, it can be dropped, and when calculating the contribution to Eq. (3.114) corresponding to the second term (3.115), it is necessary to take into account the fact that as n varies, the fractional function $\{n/\tau\}$ uniformly fills the interval [0,1]. For this reason the sum $N^{-1}\Sigma_n$ in Eq. (3.114) can be replaced by an integral over this interval, as a result of which we obtain

$$f_{lm}=\int_0^1 \exp(-i\varphi_{lm}x)dx$$
$$=\frac{\sin(\varphi_{lm}/2)}{\varphi_{lm}/2}\exp(-i\varphi_{lm}/2), \tag{3.116}$$

where we have introduced the characteristic phase

$$\varphi_{lm}\equiv 2\pi m-g_{lm}(a/\tau)=(2\pi/\sqrt{5})(m\tau-l). \tag{3.117}$$

The interference function (3.116) assumes maximum values near the phase $\varphi_{lm}=0$. Then it follows from the expression (3.117) that the indices l and m, determining the coordinates (3.111) of points in the reciprocal space must be related by the relation $l/m=\tau$, which reduces to (3.106). It can thus be concluded that the maxima of the diffraction pattern of the quasicrystal correspond to points of the reciprocal space

$$g_n=\frac{2\pi/a}{1+\tau^{-2}}\left(F_n+\frac{F_{n-1}}{\tau}\right)\approx\frac{2\pi}{a}F_n, \tag{3.118}$$

where the second equality was written out for large values of n. In contrast to the diffraction pattern of an ordinary crystal, where the reflections are arranged strictly periodically, here their position is completely aperiodic, though regular.

We now discuss the more general maps

$$x_{n+1}=x_n+\alpha-(K/2\pi)\sin(2\pi x_n), \tag{3.119}$$

where, for simplicity, the period a is taken to be one. In comparison to the similar relation (3.98), representing a map of a periodic sequence na into a quasiperiodic sequence x_n, here there is only the stochastic variable $0\leqslant x\leqslant 1$, whose values x_n and x_{n+1} at the nearest levels are related by Eq. (3.119). For transcritical values of the coupling parameter $K>1$ the right-hand side of Eq. (3.119) becomes a nonmonotonic function of x_n; this means that bifurcations appear and therefore chaos is possible. Bearing this circumstance in mind, we assume below that the coupling constant has the critical value $K_c=1$.

We consider first the appearance of mode-locking,[37] corresponding to the map (3.119). It consists of the fact that if a field with frequency ω_1 acts on the system having a characteristic frequency ω_0, then as the ratio $\alpha=\omega_0/\omega_1<1$ changes, the frequency ω of the response will not change continuously but rather in a manner so that the ratio $\Omega=\omega_0/\omega\leqslant 1$ assumes a series of rational values.[9)] As one can see from the corresponding devil's staircase in Fig. 33, the interval of the seed frequency ω_1, in which the response frequency ω is locked with the characteristic frequency ω_0 by fixing the rational number $\Omega=\omega_0/\omega$, will be all the wider the "better" this number is: The widest steps correspond to values $\Omega=0,1$; then follow steps with $\Omega=1/2$, then the pair with $\Omega=1/3$, $2/3$, and so on. According to Ref. 10 the devil's staircase in Fig. 33 is constructed so that its steps are distributed most sparsely near the values of Ω corresponding to the inverse Fibonacci numbers F_n^{-1} [see Eq. (3.107)] and most densely near the values $\Omega=1/n$, $n=1,2,...$, corresponding to a harmonic sequence. In application to spatial structures, where the parameter $\Omega\equiv k/k_0=a/b\leqslant 1$ determines the ratio of the short period a to the long period b,[10)] this fact explains why, on the one hand, quasicrystals, whose characteristic wave numbers k are given by the values (3.118) proportional to the Fibonacci numbers, are so rarely realized, and on the other why n-type long-period structures with wave numbers

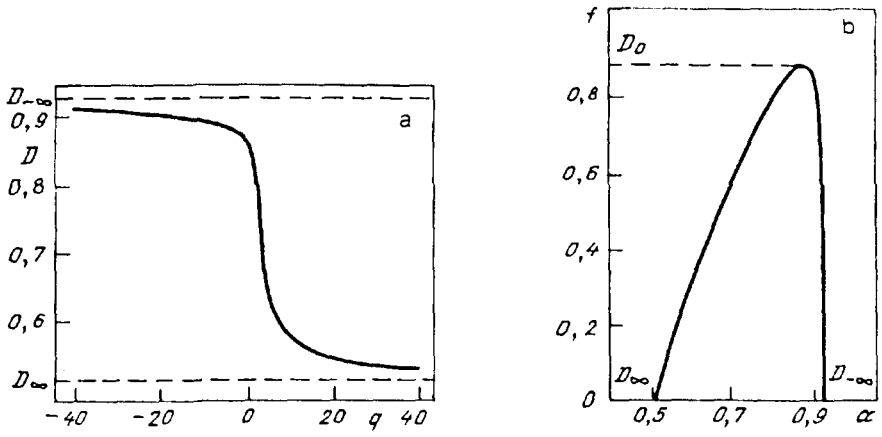

FIG. 34. Spectrum of fractal dimensions (a) and spectral function (b) for a multifractal set of mode-locked frequencies corresponding to the sequence (3.119).[10]

$$k_n=k_0/n=2\pi/na, \quad n=2,3,... \tag{3.120}$$

are encountered so often. In other words, the spatiotemporal structure obtained as a result of the external action, prescribed by the parameters ω_1 and k, on the initial structure, characterized by the scales ω_0 and k_0, is a $(d+1)$-dimensional multifractal, whose free parameters reduce to the set of ratios $\Omega=\omega_0/\omega$; $\Omega_i=k_i/k_0$, $i=1,...,d$. The Fibonacci sequence studied above and the harmonic sequence are limiting sets among all monofractals forming the given multifractal.

The foregoing analysis was based on numerical investigation of the devil's staircase on a set containing 2^n, $n=10$, values of the parameters α and Ω. The differences $\Delta\alpha_i$ and $\Delta\Omega_i$ were measured for each pair i of nearest points. Since the first differences determine the distances l_i between the points of the set and the second differences determine the probabilities P_i of the realization of measure on them, substituting $\Delta\alpha_i$ and $\Delta\Omega_i$ into the definition (3.33) we find from the condition $M_n(\tau,q)=1$ the spectrum of fractal dimensions $D(q)$ presented in Fig. 34. Its upper limit $D_{-\infty}=0.924$ corresponds to the Fibonacci sequence, for which, according to Refs. 42 and 43, the elementary length $l_n\approx F_n^{-\delta}\approx\tau^{-n\delta}$ is determined by the parameter $\delta\approx 2.164$ and the probability has the form

$$P_n\approx\frac{F_n}{F_{n+1}}-\frac{F_{n+1}}{F_{n+2}}\approx\tau^{-2n}, \tag{3.121}$$

where the estimate (3.107) is taken into account. The last equality of Eq. (3.78) shows that for the given monofractal the dimension $D_{-\infty}$ reduces to the exponent α in the definition (3.20):

$$P_n=l_n^D. \tag{3.122}$$

Using this relation we find

$$D_{-\infty}=2/\delta\approx 0.924. \tag{3.123}$$

As far as the lower limit D_∞ is concerned, it corresponds to the harmonic sequence for which, according to Ref. 44, the relation $P_n\approx l_n^{1/2}$ is realized. Then Eq. (3.122) means that

$$D_\infty=1/2. \tag{3.124}$$

The spectral function $f(\alpha)$, determined from the condition $M_n(q)=1$ for the measure (3.22), has the form shown in Fig. 34. Compared to the corresponding function in Fig. 29 for the logistic sequence (see Sec. 3.3.1), the strong asymmetry of the spectrum $f(\alpha)$ is interesting. The gentle slope, bounded by the value D_∞, corresponding to the harmonic sequence, indicates the large content, already mentioned above, of the long-period structures compared to quasiperiodic structures, which correspond to a sparse upper end of the spectrum $D_{-\infty}$.

In conclusion, we now consider the multifractal set generated by the map (3.119) with the critical coupling $K=1$ and response frequency ω corresponding to the golden mean $\omega_0/\omega\equiv\Omega=\tau^{-1}$.[11] Using the numerical procedure of Ref. 10, an initial value of the phase x_1 was chosen, and then the series of values $x_i^{(1)}$, $i=1,2,...,F_{17}$ of the initial level $n=1$ on the set of points i, whose number is equal to the Fibonacci number $F_{17}=2584$, was determined from Eq. (3.119). It was assumed that these points are equally probable: $P_i=F_{17}^{-1}$. As far as the elementary lengths l_i are concerned, since the frequency with which the new level of iteration n appears is bounded by the condition $\omega=\tau$ (we use the characteristic frequency $\omega_0=1$), for the nearest levels we have $x_i^{(n+1)}=x_{i+\tau}^{(n)}$ and on iteration the distance l_i^n must be determined by the equation $l_i^n=x_{i+F_n}^{(1)}-x_i^{(1)}$, $F_n\approx\tau^n$, $n\to\infty$ (in Ref. 10 the value $n=16$ was reached). The measures (3.22) and (3.33) were found on the basis of the distributions P_i and l_i^n obtained, and the functions $D(q)$ and $f(\alpha)$, characterizing the multifractal set, were calculated from the condition that the measures are equal to one. The form of these functions is shown in Fig. 35.

On a qualitative level the basic features of the functions $D(q)$ and $f(\alpha)$ can be determined by analogy to the description of the logistic sequence (3.79) at the beginning of Sec. 3.3.1. It is evident from the plot of the function (3.119), presented in Fig. 36, that the region where the values of x_{n+1} are most sparse is concentrated near the point $x_n=1/4$, where $x_{n+1}\approx\alpha+(2\pi^2/3)x_n^3$. Thus the transition from the maximally rarefied fractal to the maximally bunched fractal corresponds to transformation of the linear function $x_{n+1}(x_n)$ into a cubic function, in connection with

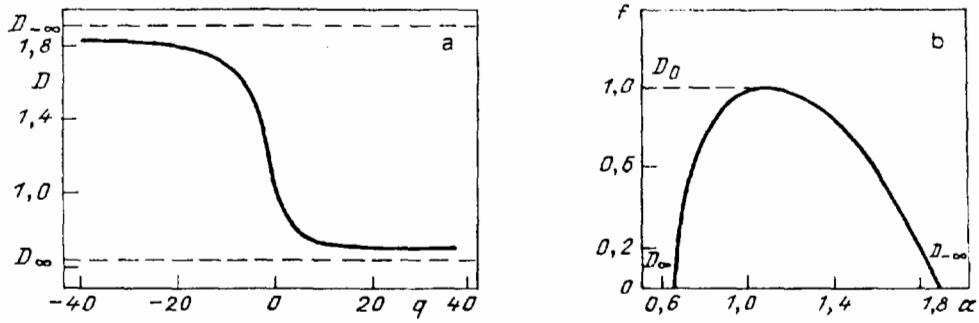

FIG. 35. Spectrum of fractal dimensions (a) and the spectral function (b) for a multifractal set of mode-locked phases corresponding to the sequence (3.119).[10]

which the role of the scale factor switches from ξ to ξ^3. According to the relation (3.108) this gives a minimum dimension $D_\infty = 0.633$ three times smaller than the maximum dimension $D_{-\infty} = 1.898$. It is evident from the plot of the spectral function in Fig. 35 that in contrast to the mode-locking picture the rarefied Fibonacci sequences make the greatest contribution to the formation of the multifractal. This fact can be trivially explained if it is assumed that the density of points of the multifractal set is approximately constant: the sparser the distribution of the monofractal points, the more such points are required in order to form the resulting multifractal.

3.3.3. Multifractal representation of nonergodic systems

It is well known that experimentally measured macroscopic quantities are time averages, while the theory gives averages over a statistical ensemble of microscopic states, simulating real states at different times. Since in ergodic systems all microscopic states are in principle reachable, the two types of averages can be identified with one another, and this is what makes it possible to compare experimentally observed and theoretically determined macroscopic quantities.

In the last few decades, however, interest in disordered systems has increased. Typical examples of disordered systems are Anderson's model[45] for the transition of a charge carrier from the localized into a delocalized state and the model of quenched disorder for spin-glass systems (see Ref. 18). A characteristic feature of disordered systems is the hierarchical distribution of microscopic variables: Thus, for example, in a spin glass, on the one hand, a collection of ordinary (hot) variables is realized, the role of which play the spins $\sigma_i = \pm 1$, distributed over sites i in accordance with the temperature T; on the other hand, a superensemble of cold variables, describing frozen distributions $\{J\}$ and $\{h\}$ of overlap integrals J of wave functions of the nearest sites and the fields h, exerted by the external medium, is superposed on this distribution. The different nature of hot and cold variables is expressed in the fact that the change in temperature T affects the distribution of the former and has no effect at all on the latter quantities. Evidently, such a situation can be realized only for the case of strongly nonequilibrium systems, in whose state space the regions corresponding to different sets $\{J\}$ and $\{h\}$ of cold variables are separated by barriers of height $Q \gg T$.

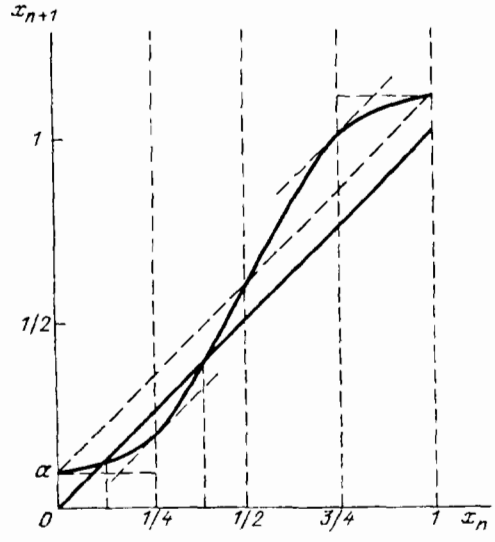

FIG. 36. Plot of the function (3.119) corresponding to a quasiperiodic sequence (the initial phase $\alpha = 0.1$; the coupling constant $K = 0.3\pi$).

Thus it can be concluded that separating the variables of a disordered system into hot and cold results, on the one hand, in nonequilibrium and, on the other hand, nonergodicity. Obviously, comparing physically observable quantities to the statistical theory is a very nontrivial problem. This nontriviality is associated with the complicated character of the separation of the state space into many regions in which the real values of the microscopic variables are concentrated. It will be shown below that the super-ensemble of these regions forms a multifractal set.

The relative simplicity of Anderson's model is connected with the fact that each region corresponds to a set of pure quantum states of an electron, which are realized at zero temperature T. Thus all hot degrees of freedom are frozen out, and the complete collection of microscopic variables reduces to the ensemble $\{h\}$ of fields acting on the electron. The fractal set is completely deterministic. In the case $T \neq 0$, realized, for example, in spin glasses, including the hot variables transfers the pure states, corresponding to this region of allowed values, into mixed states.[34] This means, in particular, that the multifractal set consisting of these regions becomes stochastic—because of the degeneracy of the system different regions α are realized with different probabilities w_α, and averaging over the corresponding states results in a random set η_α of order parameters (see Sec. 2.4.2).

Bearing this circumstance in mind, we consider first

the multifractal set corresponding to Anderson's model.[45] To this end we write the Schrödinger equation for a system of noninteracting electrons with overlapping J of the site wave functions:

$$-(zJ/2)\psi''+h\psi=E\psi. \tag{3.125}$$

Here ψ and E are the wave function and energy of the electron; h is the potential acting on the electron, the magnitude of the potential being distributed randomly in the interval $[-W/2,W/2]$; z is the coordination number; the prime indicates differentiation with respect to the coordinate r; and, the Hartree system of units ($\hbar=m=1$) is used. Numerous investigations of Eq. (3.125) have shown[45–49] that at the center of the band ($E=0$) with a spread of the potential $W<W_c$, where $W_c<zJ$ is the critical value, the electron state is delocalized, and the wave function $\psi(\mathbf{r})$ reduces to a Bloch wave. Correspondingly, for $W>W_c$ it has the localized form

$$\psi\sim\exp(-r/\xi), \tag{3.126}$$

where ξ is the correlation length, characterized by the values $\xi^{-1}=0$ in the delocalized state and $0<\xi^{-1}<\infty$ in the localized state. Thus the transition into a localized state can be associated to the appearance of finite values of the inverse correlation length

$$\xi^{-1}\propto w^{\nu},\quad w=W/W_c-1>0, \tag{3.127}$$

where ν is the corresponding exponent. Away from the center of the band $E\neq 0$ the localization threshold W_c drops, assuming the value $W_c=0$ at the boundaries $E_c=\pm zJ$. According to Ref. 49 the Anderson transition can be represented in the mean-field approximation as a $(2+\delta)$-order phase transformation, where $\delta\to 0$ is a correction corresponding to a logarithmic factor. On the basis of this approach the width W of the potential plays the role of the temperature of the cold variable h, and the displacement of E from band center is the field conjugate to the delocalization parameter. The value of the critical exponent ν in Eq. (3.127) turns out to be 1/2.

Thus on the basis of the mean-field approximation for $W>W_c$ the system can be represented by a collection of identical clusters of localized states of size $\sim\xi\propto w^{-1/2}$. In reality, of course, the situation is not so simple, since even with $w=$const a collection of clusters of the most diverse sizes is realized. This means that the behavior of the system is determined not by a single value of the critical index ν, but rather by an entire collection of values of ν. In order words, we conjecture that the clusters of localized states form a multifractal set, whose spectrum determines a series of possible values of ν.

In order to clarify the situation we write Eq. (3.125) for a one-dimensional lattice model, in which $z=2$, and the second derivative of the wave function ψ_i at the site i is determined by the equation $\psi_i''=(\psi_{i+1}-\psi_i)-(\psi_i-\psi_{i-1})$. Substituting it into Eq. (3.125) and introducing the random variable $v_i=-2h_i/zJ$, which lies in the interval $[-W/zJ,W/zJ]$, and the effective energy $\varepsilon=2[1-(E/zJ)]$, defined in the zone $0\leqslant\varepsilon\leqslant 4$, the Schrödinger equation assumes the form of a second-order map:

$$\psi_{i+1}+\psi_{i-1}+v_i\psi_i=\varepsilon\psi_i. \tag{3.128}$$

In contrast to previously investigated first-order nonlinear sequences [see Eqs. (3.79), (3.97)–(3.99), (3.103), (3.112), and (3.119)] the linear equation (3.128), like the Fibonacci sequence (3.105), couples not two but three nearest sites. Introducing the operator S_i and the vector Ψ_i, defined as

$$\hat{S}_i=\begin{pmatrix}\varepsilon-v_i & -1\\ 1 & 0\end{pmatrix},\quad \Psi_i=\begin{pmatrix}\psi_i\\ \psi_{i-1}\end{pmatrix}, \tag{3.129}$$

the equation (3.128) can be put into the form of a recursion relation

$$\Psi_{i+1}=\hat{S}_i\Psi_i. \tag{3.130}$$

We also introduce the response to the nth action of the operator $\hat{S}$ on the initial function Ψ_i

$$R_i^n\equiv|\Psi_{i+n}|/|\Psi_i|=\mathrm{Sp}\,\hat{S}_i^n, \tag{3.131}$$

where Sp is the trace operator. Being a random number, it characterizes the moment of order q

$$Z_n(q)\equiv\langle(R_i^n)^q\rangle=\lim_{N\to\infty}\left[N^{-1}\sum_{i=1}^{N}(\mathrm{Sp}\,\hat{S}_i^n)^q\right]. \tag{3.132}$$

Suppose that the eigenvalues of the matrix (3.129)

$$s_{\pm}=[(\varepsilon-v)/2]\pm\{[(\varepsilon-v)^2/4]-1\}^{1/2} \tag{3.133}$$

after averaging (3.132) correspond to the quantities $\exp(-\lambda_{1,2})$. Let the maximum eigenvalue be $e^{-\lambda_1}$. Then the definition (3.132) can be put into the form

$$Z_n(q)\approx\exp(-\lambda_1 qn),\quad n\to\infty. \tag{3.134}$$

Since the expression (3.131) determines the manner in which the wave function ψ_{i+n} decays as $n\to\infty$ away from the initial site i, the obtained result (3.134) means that for $q=-1$ the exponent regime (3.126) is realized with the correlation

$$\xi=|\lambda_1|^{-1}\propto w^{-\nu}, \tag{3.135}$$

where the relation (3.127) and the condition $\lambda_1<0$ (see below) are taken into account.

From the set-theoretic standpoint, the definition (3.132) gives a measure of the type (3.60), whose value Z_n determines the analog of the thermodynamic potential

$$g=-\lim_{n\to\infty}(n^{-1}\ln Z_n). \tag{3.136}$$

The simplest approximation (3.134) corresponds to the linear function

$$g=g_0+\lambda_1 q,\quad g_0>0, \tag{3.137}$$

comparing which to Eqs. (3.64) and (3.69) shows that, to within a sign, the exponent $\lambda_1=-s<0$ reduces to the entropy s, determining the increase in information at each step of the map (3.130). In the general case the measure (3.132) can be defined by the expression (3.30), comparing which to Eq. (3.136) leads, using Eqs. (3.65) and (3.66), to the relation

$$g(q)=\lambda(q-1)D(q), \tag{3.138}$$

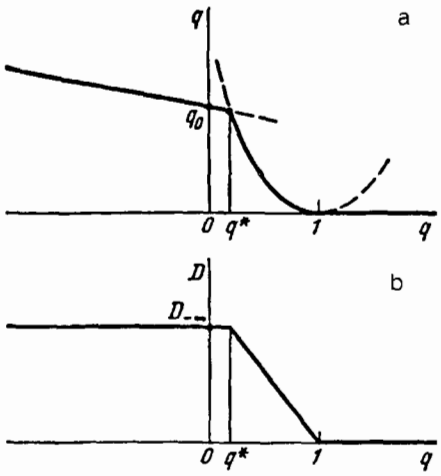

FIG. 37. Effective potential (a) and spectrum of fractal dimensions (b) for a set of clusters of localized states in the Anderson model.

where the parameter $\lambda<0$ determines the effective energy of the set (see Sec. 3.2.1). The equality (3.138) passes into the linear relation (3.137) only for large values of $|q|$, when $D(q)\approx D_{\pm\infty}=\lambda_1/\lambda\propto\xi^{-1}$. Since in the delocalized state $\xi^{-1}=0$, we arrive at an important conclusion: The lower value of the dimension of the fractal set of clusters of localized states is

$$D_{\infty}=0. \tag{3.139}$$

Substituting the upper value $0<D_{-\infty}<d$, as expected, transforms Eq. (3.138) into the linear relation (3.137), where $\lambda_1=\lambda D_{-\infty}$.

In order to determine the function $g(q)$ for moderate values of the parameter q we approximate the monotonically decreasing function $D(q)$ by the linear function

$$D=a-bq, \tag{3.140}$$

where a and b are positive parameters. Substituting Eq. (3.140) into Eq. (3.138) gives a parabola with a minimum at the point $q_0=(a+b)/2b$ and curvature $2b$. Evidently, it is this minimum that corresponds to the delocalized state, in which $D=0$. It can therefore be inferred that the minimum $q_0=(a+b)/2b$ is also the point $q^0=a/b$ where the function (3.140) vanishes, so that $a=b$, $q_0=q^0=1$. As a result the function Eq. (3.138) assumes the final form

$$g=-a\lambda(q-1)^2, \quad \lambda<0, \quad a>0. \tag{3.141}$$

Thus the effective thermodynamic potential $g(q)$, representing the multifractal set of localized states of an electron, has the form shown in Fig. 37a. In the interval $(-\infty,q^*)$ the function $g(q)$ has a linear section (3.137), and a break is observed at the point

$$q^*=\left(1-\frac{D_{-\infty}}{2a}\right)\left[1-\left\{1-\frac{1+(g_0/a\lambda)}{[1-(D_{-\infty}/2a)]^2}\right\}^{1/2}\right] \tag{3.142}$$

after which a parabolic law (3.141) is realized in the interval $(q^*,1)$. Finally, the segment $(1,\infty)$ corresponds to the delocalized state in which by definition $D(q)=0$, so that in agreement with Eq. (3.138) and $g(q)=0$. The spectrum of fractal dimensions $D(q)$, corresponding to the function $g(q)$ is described above, is displayed in Fig. 37b.

As the parameter $w=W/W_c-1$ decreases, the system shifts into a delocalized state, reflected by a decrease in the dimension $D(q)$. According to the calculations of Refs. 47 and 48, performed for the band edge $\varepsilon=4$, the parameter in the functions (3.137) and (3.141) change as follows:

$$\lambda_1\propto w^{1/2}, \quad g_0\propto w^{2/3}, \quad a\propto w^{2/3}, \quad \lambda=\text{const}. \tag{3.143}$$

Correspondingly, the maximum dimension

$$D_{-\infty}=\lambda_1/\lambda\propto w^{1/2}, \tag{3.144}$$

and the characteristic value of the exponent q

$$q^*\propto w^{1/6}. \tag{3.145}$$

This is expressed as a decrease in the height and rate of change of the functions $g(q)$ and $D(q)$ in Fig. 37 as the system approaches the delocalized state. According to the relation (3.144), for large values of $|q|$ the function $D_w(q)$ is characterized by a root singularity, which transforms in the interval $(q^*,1)$ into the relation

$$D(q)=a(1-q)\propto w^{2/3}(1-q), \tag{3.146}$$

which follows from Eqs. (3.138), (3.141), and (3.143).

Using Eqs. (3.136) and (3.138) it is easy to see that as $q\to 0$ the response (3.132) can be put into an exponential form (3.126), where the node number $n\to\infty$ plays the role of the coordinate r and the correlation length ξ is determined by the equality

$$\xi^{-1}=\lambda D_0, \quad D_0=D(q=0). \tag{3.147}$$

As a result Eqs. (3.144) and (3.146) lead to the following values of the critical exponent ν in the expression (3.135)

$$\nu_{-\infty}=1/2, \quad \nu_{\infty}=2/3. \tag{3.148}$$

Thus the multifractal representation of Anderson's transition shows that as the "temperature" W changes, an exponent 2/3, characteristic of the scaling region of the phase transformation, is realized at the lower limit of the dimensions $D_{+\infty}=0$ and the exponent 1/2, characteristic for the mean-field approximation employed far from the transition point,[34] is realized at the upper limit $D_{-\infty}$. Evidently, the approximations (3.137) and (3.141) give only the limiting values (3.148) of the exponent ν. The complete spectrum, however, is described by the function $\nu(q)$ which increases monotonically between these values, the main change in ν occurring in a quite narrow interval of values of q, concentrated in the region of small values of q.

In the discussion above we had in mind only the behavior of the critical exponent ν, determining the temperature dependence (3.135) of the correlation length. It was shown that rarefaction of the fractal set of localized states, reflected by a decrease in the dimension D of the set with increasing parameter q, results in intensification of fluctuations of the delocalized phase, which is what indicates an increase in the exponent ν, resulting in anomalous growth of the correlation length (3.135). Evidently, this intensifi-

TABLE II. Values of the critical indices at phase transitions.

Critical state / Method of determination	α	β	γ	δ	ε	μ	ν	ζ	Dimension of the fractal set
Mean-field theory	0	1/2	1	3	0	1/3	1/2	0	$D_{-\infty} \equiv D_{\max}$
Wilson's method	0,08	0,33	1,26	4,80	0,05	0,40	0,64	0,04	$D_{\infty} < D < D_{-\infty}$
Approximation $\alpha, \zeta = 0$	0	1/3	4/3	5	0	2/5	2/3	0	$D_{\infty} \equiv D_{\min}$

cation of fluctuations will also affect the values of other critical exponents whose set is determined by the following temperature-field relations[34]

$$c \propto |w|^{-\alpha}, \quad \eta \propto |w|^{\beta}, \quad \chi \propto |w|^{-\gamma},$$
$$\eta \propto \varepsilon^{1/\delta}, \quad c \propto \varepsilon^{-c},$$
$$\xi \propto \varepsilon^{-\mu}, \quad \xi \propto |w|^{-\nu}, \quad S(r) \propto r^{-(d-2+\zeta)} \quad \text{at } w=0. \tag{3.149}$$

Here w is the dimensionless temperature, measured from the critical point; ε is the field conjugate to the localization parameter η; c and χ are the susceptibilities to the temperature w and field ε; ξ is the correlation length; $S(\mathbf{r})$ is the correlation function field $\eta(r)$; and, d is the dimension of the physical space. The values of the critical exponents α, β, γ, δ, ε, μ, ν, and ζ are given in Table II. It is evident that the entire collection separates into three groups. The first group consists of the exponents γ, μ, and ν (the dynamical exponent z of Ref. 50 also belongs here), whose values grow monotonically with increasing q between the limits indicated in the first and third rows of Table II. As mentioned, this growth is due to the anomalous intensification of fluctuations of the disordered (delocalized) phase; this intensification is expressed in the decay of the dimension $D(q)$ of the multifractal set of localized states. It is completely clear, however, that such fluctuations should result in a decrease of the localization parameter η, thanks to which the values of the corresponding exponents β and $1/\delta$, which form the second group, decrease. The third group consists of the small exponents α, ε, and ζ. Calculations of their values by Wilson's renormalization group method[51] shows that the critical fluctuations, reflected by the decay of the function $D(q)$, result only in an insignificant growth of $\alpha(q)$, $\varepsilon(q)$, and $\zeta(q)$. Ignoring specific values, the first and third group of exponents, characterized by monotonically increasing functions $\gamma(q)$, $\mu(q)$, $\nu(q)$; $\alpha(q)$, $\varepsilon(q)$, $\zeta(q)$, can be combined.

Evidently, the results presented above can be extended to an arbitrary system undergoing a continuous phase transition. Indeed, although our analysis concerns Anderson's model, it is easy to see that the conclusions concerning the behavior of the critical exponents are based only on the properties of the fractal set of clusters of rarefied states of the system near the transition point. In other words, the picture described is realized for a nonergodic system, clusters of whose states form a self-similar set, where scale invariance is realized.[52] As shown in Ref. 53, even for transitions of the displacement type ergodicity is lost near the transition point (for a system of the order-disorder type ergodicity breaks down at the outset[35]). For this reason, in the critical region, where scale invariance is realized, all systems are nonergodic and thus all conditions on which the picture presented above is based hold.

We now describe a more complicated case, realized in hierarchically coordinated systems of the spin-glass type (see Ref. 18). The simplest Hamiltonian of such a system has the form

$$H_N = -\sum_{i,j}^{N} J_{ij}\sigma_i\sigma_j - \sum_{i}^{N} h_i\sigma_i, \tag{3.150}$$

where the spins $\sigma_i = \pm 1$ consist of a collection of $N \to \infty$ hot variables, while the randomly distributed values J_{ij} of the overlap integrals of the sites i and j and the field h_i are the cold variables. Here the partition function

$$Z_N(T;\{J\},\{h\}) = \langle \exp[-H_N(\{J\},\{h\})/T] \rangle, \tag{3.151}$$

where the averaging is performed over the set $\{\sigma\}$ of hot variables with fixed values $\{J\}$ and $\{h\}$ of the cold variables, plays the role of the measure (3.21). The free energy per spin has the form

$$f(T) = -T \lim_{N\to\infty} (N^{-1} \overline{\ln Z_n(T;\{J\},\{h\})}), \tag{3.152}$$

where the overbar means averaging over the sets $\{J\}$ and $\{h\}$.

A characteristic feature of the expression (3.152) is that the logarithmic function $\ln Z$ must be averaged, which is very inconvenient to do. For this reason, using the limit

$$\ln Z = \lim_{q\to 0} \frac{Z^q - 1}{q}, \tag{3.153}$$

Eq. (3.152) is usually rewritten in the form

$$f(T) = T \lim_{N\to\infty} \lim_{q\to 0} \left[\frac{1}{Nq} (1 - \overline{Z_N^q(T;\{J\},\{h\})}) \right], \tag{3.154}$$

where the averaging is now performed over the powers q of the partition function Z. This means that in the presence of quenched disorder, instead of a single statistical ensemble, a collection of q identical replicas of this ensemble is studied and the averaging is then performed over this ensemble. Setting aside questions associated with the breaking of the symmetry of the replica space in the limit $q \to 0$ (see Ref. 18), we point out that physically the existence of the replicas corresponds to partitioning, owing to the nonergodicity, of the state space into isolated regions of allowed values of the variables (these regions are called states,[54] valleys,[19]

or components[55]). As already mentioned at the beginning of this section and in Sec. 2.4.2, they form a stochastic hierarchically coordinated system of statistical ensembles realized in each valley.

We show first how the set of such ensembles can be generated. To this end we employ the one-dimensional model with overlapping of the nearest sites, for which the Hamiltonian (3.150) assumes the form

$$H_N(\{J\},\{h\}) = -\sum_{i=1}^{N} (J_i\sigma_i\sigma_{i+1} + h_i\sigma_i). \tag{3.155}$$

Correspondingly, the partition function (3.151) can be expressed in the form of a recursion relation of the type (3.132)

$$Z_N(T,q;\{J\},\{h\}) = \left\langle \prod_{i=1}^{N} \hat{S}^q(T;J_i,h_i) \right\rangle, \tag{3.156}$$

whose generator has the form

$$\hat{S}_i = \begin{pmatrix} \exp[(J_i+h_i)/T], & \exp[-(J_i-h_i)/T], \\ \exp[-(J_i+h_i)/T], & \exp[(J_i-h_i)/T]. \end{pmatrix} \tag{3.157}$$

The product of N matrices (3.157), enclosed in the averaging brackets in Eq. (3.156), generates the multifractal set of statistical ensembles corresponding to different values of N. Since its points depend on the choice of cold variables $\{J\}$ and $\{h\}$, this set, in contrast to ordinary systems of the Anderson model type, will be stochastic. An important feature of this set is the self-averaging property. It consists of the fact that if, in the spirit of Eq. (3.152), we defined the random variable

$$f_N(T,q;\{J\},\{h\}) = -(T/N)\ln Z_n(T,q;\{J\},\{h\}), \tag{3.158}$$

then its limiting value

$$f(T) \lim_{N\to\infty} f_N(T,q=1;\{J\},\{h\}) \tag{3.159}$$

will reduce the free energy (3.154), obtained as a result of averaging over the cold variables. In other words, the system of ensembles is ergodic with respect to these variables.

On the other hand, the quantity f can also be determined on the basis of the thermodynamic representation of the obtained set of statistical ensembles (see Sec. 3.2). To this end, we introduce an effective potential of the type (3.136)

$$g(T,q) = -\lim_{N\to\infty} [(T/N)\ln Z_n(T,q;\{J\},\{h\})]. \tag{3.160}$$

Then it follows from Eqs. (3.158) and (3.159) that

$$f(T) = \left.\frac{\partial g(T,q)}{\partial q}\right|_{q=0}. \tag{3.161}$$

Hence one can see, taking into account (3.138), that the free energy f reduces, to within a factor, to the value of D_0 of the spectrum of fractal dimensions $D(q)$ at $q=0$. Since according to the analysis performed in Sec. 3.1.3, the value of D_0 corresponds to the maximum of the spectral function $f(\alpha)$, this means that the observed value of the free energy corresponds to the component of the multifractal of statistical ensembles that has the maximum content. Evidently, this fact is an expression of the property of self-averaging, expressed in the fractal representation.

The method presented above indicates the possibility of describing hierarchically coordinated systems in a manner such that there is no need to employ the replica trick and therefore the difficulties associated with the breaking of the symmetry of the replica space do not arise (see Ref. 18). The crux of the method[56] is that instead of the true free energy (3.152) first the quantity

$$\bar{f}(T,q) = -\lim_{N\to\infty} [(T/N)\ln \overline{Z_n(T,q;\{C\}_a)}], \tag{3.162}$$

is defined, where $\{C\}_a$ denotes sets, enumerated by the suffix a, of cold variables (in Eq. (3.160 they reduce to $\{J\}$ and $\{h\}$). Averaging over these variables is performed in the argument of the logarithm, and for this reason it does not present any difficulties. Next, we introduce the effective potential

$$g(T,q,\{\mu_a\}) = \tilde{f}(T,q) + \sum_a \bar{C}_a\mu_a, \qquad \bar{C}_a = N^{-1}\sum_{i=1}^{N} C_i^a, \tag{3.163}$$

which depends on the fields μ_a conjugate to the cold variables C_i^a. Just as Eq. (3.61), their stationary values $\bar{\mu}_a$ are determined by the condition

$$\left.\frac{\partial g(T,q;\{\mu_a\})}{\partial \mu_a}\right|_{\mu_a=\bar{\mu}_a} = \bar{C}_a, \tag{3.164}$$

where the effective potential is given by the equation [compare to Eq. (3.162)]

$$g(T,q;\{\mu_a\}) = -\lim_{N\to\infty}\left[(T/N)\times\ln Z_n(T,q;\{C_a\})\exp\left(-N\sum_a \bar{C}_a\mu_a\right)\right]. \tag{3.165}$$

Substituting the fields $\bar{\mu}_a = \bar{\mu}_a(T,q)$, found from Eq. (3.164), into Eq. (3.163) we obtain the stationary value

$$g(T,q;\{\bar{\mu}_a(T,q)\}) \equiv g(T,q), \tag{3.166}$$

which is identical to the potential (3.160). Finally, Eqs. (3.166) and (3.161) give the free energy (3.152). In Ref. 56 it was shown that the use of this transition for the Ising model (3.150) with a random field h_i yields results that are identical to the exact calculation. In application to Anderson's model the effective potential (3.165) was found in Ref. 49, where the condition (3.164) determined the displacement $\bar{\mu}$ from the center of the band of localized states as a function of the impurity concentration $\bar{C}$.

The effective potential (3.165) at fixed temperature T describes completely the stochastic multifractal set of the statistical ensembles of the hierarchically coordinated system. Indeed, substituting Eq. (3.165) into Eq. (3.75), taking into account Eq. (3.72), we obtain the spectrum of

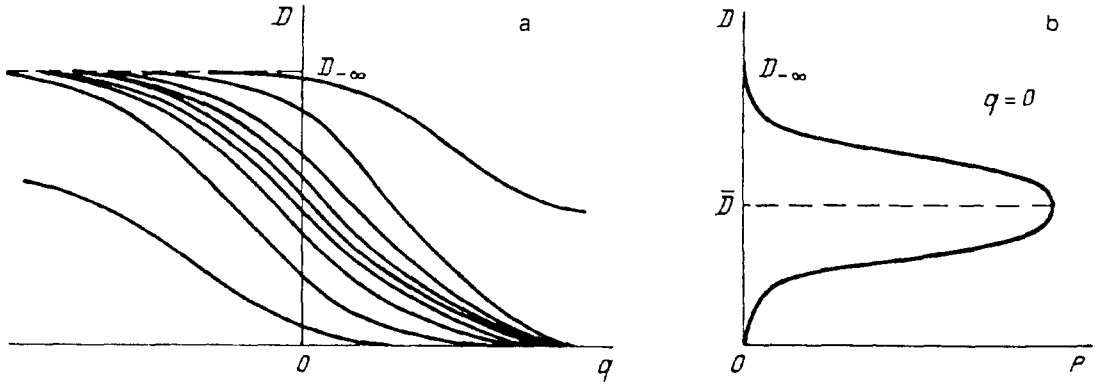

FIG. 38. a—Distribution of the spectra of the fractal dimensions of a hierarchically coordinated system of statistical ensembles of a spin glass. b—Section describing the probability of fluctuations of a monofractal with $q=0$.

fractal dimensions $D(T,q;\{\mu_a\})$, determined by the dependence on the parameter q. According to Eq. (3.164) the component $\bar{D}_T(q)=D(T,q,\{\bar{\mu}_a\})$, corresponding to stationary values $\{\bar{\mu}_a\}$ of the cold fields, is realized with maximum probability. The distribution of the spectra $D(q)$ near this component is described by the functional of probabilities

$$P\{D(q)\}\propto\exp(-g(T,q;\{\mu_a\})), \tag{3.167}$$

where the function $D(q)$ is expressed by Eq. (3.72) and (3.75). Figures 38 display the form of this distribution.

The description of the stochastic multifractal set of statistical ensembles on the basis of the relations (3.162)–(3.167), though it is, in our opinion, most natural, has still not been realized. This is because the description of such a set was first obtained by Parisi with the help of the replica representation.[57] We shall present the corresponding scheme.

As we have already indicated, the stochasticity arising due to the spread in the cold variables is expressed in the random character of the probability w_a of the realization of the ath ensemble and the overlap parameter $q_{\alpha\beta}$ of the ensembles α and β [see the definitions (2.69) and (2.71)]. As a result of this, the function (2.72) of the probability distribution $P(q)$ of the overlap parameters q and the probability $Y(q)$, given by Eq. (2.74), of having overlap q' exceeding a prescribed level q are random functions. The total probability

$$W=\sum_{\alpha} w_\alpha \tag{3.168}$$

of realization of statistical ensembles with overlapping $q_{\alpha\beta}>q$ is also of a random character. Parisi's method made it possible to find the corresponding distribution functions $\Pi_q(Y)$ and $f_q(W)$ of the quantities (2.74) and (3.168) for fixed value of q. Their form is determined by the average value

$$y(q)=\overline{Y(q)}\equiv\int Y(q)\Pi_q(Y)dY \tag{3.169}$$

of the probability of having overlap of ensembles $q^{\alpha\beta}\equiv q(y)$ not less than q. The distribution $\Pi_q(Y)$ is bimodal with maxima at $Y\approx 0.5$ and $Y=1$. The presence of a singularity $\Pi_q(Y)\propto(1-Y)^{-y}$ near the second of these points has the result that the most probable value $Y=1$ is different from the average probability $y<1$. The average distribution $\overline{f_q(W)}$ over clusters of ensembles with a bounded overlap level is also bimodal:

$$\overline{f_q(W)}=\frac{W^{y-2}(1-W)^{-y}}{\Gamma(y)\Gamma(1-y)},\quad y=y(q). \tag{3.170}$$

According to Eq. (3.170) the largest number of clusters is concentrated near the values $W=0$ and $W=1$, and especially near the first value. As the overlapping q increases, the probability $y(q)$ decreases monotonically, as a result of which there is a concentration of the number of clusters with zero probability W of being realized. The form of the inverse function $q(y)$ for the overlap parameter q and the nonergodicity parameter Δ, representing the difference of the static and dynamic susceptibilities (see Ref. 15), is displayed in Fig. 39. The function $q(y)$ is characterized by

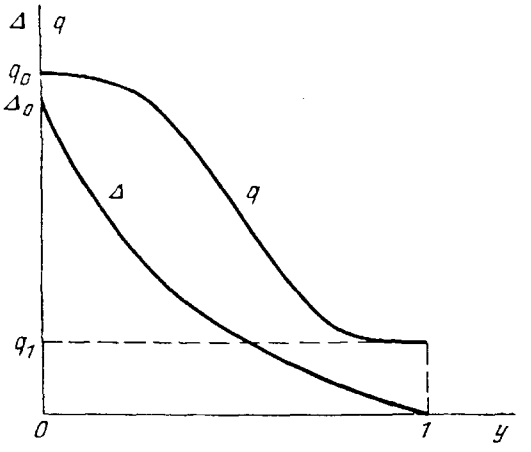

FIG. 39. Distribution of the probability of the overlap parameter q and the nonergodicity parameter Δ.

the presence of two plateaus, lying near the limiting values of the probability $y=0$ and $y=1$, and a monotonic decay in the intermediate region. The nonergodicity parameter decreases monotonically from $\Delta_0 \equiv \Delta(y=0)$ to $\Delta_1 \equiv \Delta(y=1)=0$. Physically, the maximum values q_0 and Δ_0 are determined by processes occurring in the minimal regions of the allowed values of the variables. This means that the points of the fractal set correspond to pure statistical ensembles, whose collection is characterized by the maximum dimension $D_{-\infty}$. The minimum values of the overlapping of the ensembles q_1 and the nonergodicity parameter Δ_1 correspond to the static limit in which all ensembles are united, so that the fractal set reduces to a point and has the minimum dimension $D_\infty=0$. Thus within Parisi's method[57] the monotonically decaying functions $q(y)$ and $\Delta(y)$ correspond to the spectrum of fractal dimensions $D(q)$, which also has a decaying form. Since $\Delta_1=0$ and $D_\infty=0$, but $q_1=0$ does not always hold (see Ref. 15), the correspondence of the functions $\Delta(y)$ and $D(q)$ is more complete than for the pair $q(y)$ and $D(q)$, and the fractal dimension of the set of statistical ensembles can be interpreted as the nonergodicity parameter.

The physical significance of the stochastic scheme presented above lies in the fact that a hierarchical system should be represented not by one statistical ensemble but rather by a collection of such ensembles. The peculiarity of this collection is that the ensembles are not independent but rather overlap with one another with degree $q_{\alpha\beta}$, characterized by Parisi's parameter (2.71). In a hierarchical system stochasticity is manifested not only in the behavior of structural units belonging to a given ensemble but also in the behavior of the ensembles themselves, whose realization probability is given by the distribution w_α. However, if the distribution of structural units in an ensemble is of the ordinary, canonical character,[34] then the distribution of ensembles is determined by the random character of their union into hierarchical clusters—ensembles with maximum overlapping q unite with highest probability, and this probability decreases with q. The character of the hierarchical stochastization is reflected by the distribution $P(q)$ given by Eq. (2.72). Since the latter itself contains the random quantities w_α and w_β, the distribution function $P(q)$ over clusters of the ensembles is also random. Thus hierarchy in the behavior of structural units leads to hierarchy of stochasticities. The ultimate reason for such a situation is that ergodicity in the behavior of the ensemble of structural units breaks down.[55]

The method developed by Parisi,[57] based on the fact noted above that the ensembles correspond to points of an ultrametric space,[17] has made it possible to describe completely hierarchical stochasticity. It is characterized by truncated (with respect to the overlap parameter q) moments $Y(q)$ and W of lowest order [see Eqs. (2.74) and (3.168)] for the distributions $P(q)$ and w_α, respectively. The first moment gives the probability of overlapping of ensembles with overlapping not less than a prescribed value q and the second moment gives the total probability of realization of such ensembles. Clusters with high degree of overlapping q are distinguished because ordinary ergodic systems correspond to the limiting case of the realization of a single ensemble with maximum overlapping $q=1$. A characteristic feature of hierarchical stochasticity is that in a nonergodic system the most probable value of the probability of overlapping of ensembles will be not only the maximum value $Y(q)=1$ but also the intermediate value $Y(q)\approx 0.5$. In other words, the distribution $\Pi_q(Y)$ is bimodal, and is determined by the average probability (3.169). Physically, this indicates a significant probability of realization of ensembles which are weakly dependent on one another even in the statistical sense (for example, dislocations belonging to different small-angle walls belong to practically different nonoverlapping statistical ensembles). On the other hand, if we talk about the number of different clusters of ensembles characterized by the distribution (3.170), then the fact that the integral of (3.170) over all values W diverges means that the total number of possible variants of unification of ensembles into hierarchical clusters is infinite. However, they are formed mainly from ensembles with low realization probability W. This means that rarely realizable structures, belonging to large-scale levels (disorientation boundaries, blocks, grains, and so on) are most prone toward hierarchical coordination. On the other hand, the region of large values of W will make the main contribution to the average value of W with weight $f_q(W)$. Thus, although most structural units enter into statistical ensembles characterized by significant probabilities W, hierarchical structures are formed only by the most rarely realized structural units.

With regard to the distribution of the energies E of the clusters of states, we note that it has a quasi-Gibbsian form, reflecting the independence in the spread in the values of E. If, however, for a minimum cluster corresponding to maximum overlapping $q=1$ we have a purely Gibbsian distribution $n_1(E)=\exp[-(E-\Phi)/T]$, where the energy E is measured from the thermodynamic potential Φ, then as a cluster grows with decreasing overlapping $q<1$ we arrive at the nonequilibrium distribution

$$n_q(E)=\exp[-(1-y(q))(E-E_q)/T]. \qquad (3.171)$$

Here the minimum energy E_q of a cluster is higher than its thermodynamic value $E_1=\Phi$.

Having described the distribution of clusters of statistical ensembles, we now return to the description of the distribution of the structural units, forming these ensembles, themselves. This means that we must, on the one hand, find the distribution $F(\eta)$ of the order parameter η and, on the other, the distribution $N_q(h)$ of the conjugate field h, acting in a cluster with overlapping exceeding q.[54] The nodes i at which the field h_i assumes a value in the interval from h to $h+\Delta h$ form a cell C_h, whose volume for given overlapping q is $|C_h|=NN_q(h)\Delta h$. In this cell ensembles with overlapping exceeding a given value q behave independently and are characterized by the same distributions

$$F_q(\eta,h)=\frac{1}{|C_h|}\sum_{i\in C_h}\delta(\eta-\langle x_i\rangle_\alpha), \qquad (3.172)$$

where x_i are spin-type variables [see Eq. (2.71)]. Then the desired distribution of the order parameter has the form

$$F(\eta)=\int N_q(h)F_q(\eta,h)\mathrm{d}h. \tag{3.173}$$

The average value $\bar{\eta}$ and the overlap parameter q are expressed in terms of the value $\eta_q(h)$ of the order parameter in a cluster with overlapping q and field h:

$$\bar{\eta}=\int F(\eta)\eta\mathrm{d}\eta=\int N_q(h)\eta_q(h)\mathrm{d}h,$$

$$q=\int N_q(h)\eta_q^2(h)\mathrm{d}h; \tag{3.174}$$

$$\eta_q(h)=\int F_{\tilde{q}}(\eta,h)\eta\mathrm{d}\eta.$$

As we have already noted, the conditional distribution (3.172) represents the contribution made by structural units which are acted upon by the field h in clusters of states with overlapping not less than q. These clusters are singled out because the ordinary ergodic representations can be employed in them. The equation (3.173) makes it possible to switch, if the distribution $N_q(h)$ of clusters over values of the field h is known, from the conditional distribution $F_q(\eta,h)$ to the complete distribution $F(\eta)$. They differ in that the latter distribution gives, as the first-order moment (3.174), the average order parameter $\bar{\eta}$, while the first one gives the contribution $\eta_q(h)$ owing to clusters in the field h with overlapping q [see the last equation of Eqs. (3.174)]. Once the field distribution $N_q(h)$ is known, the specific value $\eta_q(h)$ makes it possible to find the quantities $\bar{\eta}$ and q according to the first of the relations in Eq. (3.174).

As far as the function $N_q(h)$ is concerned, for a given spread in the interaction of structural units it can be determined by the method of Ref. 58, developed for amorphous solid solutions. The crux of the method, which is a natural generalization of the standard mean-field theory, consists of establishing a relation not between the field h itself and the interaction parameter of the structural units, but rather between the distribution functions.[20]

We now describe, in conclusion, the evolution of a hierarchical ensemble of structural units. To this end, we take into account the fact that on transferring to a higher degree of overlapping $q'>q$ the cell C_h fragments into parts $C_{hh'}$. The probability that a node i is present in the subcell $C_{hh'}$

$$\frac{|C_{hh'}|}{|C_h|}=G_{qq'}(h,h')\Delta h' \tag{3.175}$$

gives a relation between the distributions of the order parameter in the cell and the subcell

$$F_q(\eta,h)=\int G_{qq'}(h,h')F_{q'}(\eta,h')\mathrm{d}h', \tag{3.176}$$

whose volume is

$$|C'_{h'}|=N\Delta h'\cdot N_q(h)G_{qq'}(h,h')\mathrm{d}h. \tag{3.177}$$

The operator $G_{qq'}(h,h')$ of evolution of the hierarchical structure gives complete information about the distribution of the clusters of states:

$$N_q(h)=G_{0q}(0,h), \tag{3.178}$$

$$F_q(\eta,h)=\int G_{q1}(h,h')\delta(\eta-\tanh(h'/T))\mathrm{d}h', \tag{3.179}$$

$$\eta_q(h)=\int G_{q1}(h,h')\tanh(h'/T)\mathrm{d}h'. \tag{3.180}$$

According to Eq. (3.178), giving the distribution function $N_q(h)$ of the field in clusters is equivalent to determining the evolution from a collection of isolated ensembles into a cluster characterized by overlapping q and field h. The existence of the factor $\tanh(h/T)$, characteristic of the ordinary mean-field theory, in Eqs. (3.79) and (3.180) means that a pure statistical ensemble, in which the order parameter is determined by the standard self-consistency condition[35]

$$\eta=\tanh[(\eta+h)/T], \tag{3.181}$$

is realized in the cluster with maximum overlapping $q=1$. The relation (3.179) means that the conditional distribution function $F_q(\eta,h)$ is obtained by smearing the delta-function-like distribution corresponding to the condition (3.181), on transferring from a pure statistical ensemble to a collection of clusters characterized by a degree of overlapping not less than q. According to Eq. (3.180) the order parameter then transforms from Eq. (3.181) into the conditional value $\eta_q(h)$, determined by the contribution of the indicated collection of clusters.

Thus once the operator $G_{qq'}(h,h')$, representing the evolution of a hierarchical system, are known, the ordering process determined by this evolution can be completely described. The restructuring itself is represented as a Markovian diffusion process on a Cayley tree.[54] This means, in particular, that the binary evolution operator gives a distribution over the number $n\geqslant 2$ clusters, containing $m\geqslant n$ ensembles

$$F_{q_1q_2\ldots q_m}(\eta_1,\eta_2,\ldots,\eta_m)$$

$$=\prod_{\alpha=1}^{m}\int \mathrm{d}h_\alpha G_{q_{\alpha-1}q_\alpha}(h_{\alpha-1},h_\alpha)Fq_\alpha(\eta_\alpha,h_\alpha), \tag{3.182}$$

where $q_0=0$, $G_{qq}(h,h')=\delta(h-h')$, and the parameter q_α gives the overlapping of the states α and $\alpha+1$ (since some pairs of states can have the same overlapping q_α, the number of n of such states can be less than the number of ensembles m).

If the structure is multilevel, then the corresponding discrete ultrametric space can be regarded as being continuous, and transitions between levels are continuous. Then the evolution operator is determined by the Fokker–Planck equation[54]

$$\frac{\partial G}{\partial q}=\frac{1}{2}\frac{\partial^2 G}{\partial h^2}+\frac{\partial \ln Z}{\partial h}\frac{\partial G}{\partial h}, \tag{3.183}$$

where the overlap parameter q and the field h play the role of the time and the coordinate, and the auxiliary function $Z=Z_q(h)$ satisfies the equation

$$\frac{\partial Z}{\partial q}=\frac{1}{2}\frac{\partial^2 Z}{\partial_h{}^2}+\frac{N_q(h)}{1-y(q)}Z\ln Z \qquad (3.184)$$

with the initial condition $Z_1(h)=\tanh h$. If, however, the number of structural levels is small, then transitions between them acquire a discrete character, and the differential equation (3.183) must be replaced by a more complicated kinetic equation[59]

$$\frac{\partial G_{q_0q}(h_0,h)}{\partial q}=\int (G_{q_0q}(h_0,h')w(h',h) - G_{q_0q}(h_0,h)w(h,h'))\mathrm{d}h', \qquad (3.185)$$

where $w(h,h')$ is the probability that the field changes from h to h' with a unit change in overlapping q. In order to determine the function $w(h,h')$ it is necessary to consider specific models of the formation of the macrostructure of the ordered phase.

4. CONCLUSION

Following the situation that has evolved in the scientific literature, we have constructed the review so that it would contain all necessary information on fractals. This, naturally, resulted in a long review. From the table of contents one could get the erroneous impression that the general information, to which all sections are devoted, excepting Secs. 2.4 and 3.3, occupies a special place. In reality, however, this is not so: only part 3 of the review contains material that can be found in the difficult-to-obtain reviews Refs. 8 and 9 and the book Ref. 3, which immediately became a bibliographic rarity; the main volume of the review contains original material on the application of fractals in the theory of condensed media. In expounding the general theoretical questions we strived, keeping in the mind the abstractness of the concept of a fractal, primarily to introduce the new concept and demonstrate it in a clear manner or with a straightforward physical examples. This resulted, naturally, in an abundance of figures, but given the nature of the object being described it would probably be naive to expect to achieve a clear representation of the geometric image of a fractal without a graphic image of the fractal.

With these prerequisites, we described in detail a scheme for constructing the simplest Koch and Cantor fractal sets. Throughout the review the Cantor sets play the role of the initial geometric image, by generalizing which it is possible to introduce the basic characteristics of a multifractal (see Sec. 3.1.1). Another central concept, representing the metric of a fractal set, is the Cayley tree described in Sec. 1.1.2. The Cayley tree gives a graphic representation of an ultrametric space. We note that the relation between fractal sets and the space of ultrametric topology has not been discussed at all in the literature available to us on fractal sets. We not only describe this relation in detail, but we also introduce the concept of fractal and multidimensional hierarchical trees. The problem of determining the main characteristic of a set—its fractal dimension—is studied from both the theoretical (Sec. 2.2) and experiment (Sec. 2.3) points of view. In describing the first aspect, we started from the convenient example of determining the area of an ordinary surface: by covering it with a broken line, squares, or cubes and counting the corresponding total length, area, and volume, we introduce the important concept of the measure of a fractal set. As far as the representation of experimental methods for determining the fractal dimension is concerned, here we confine our attention only to listing the best known methods, presenting for each method the basic working formula. The description of multifractals is given on the basis of both the geometric method (Sec. 3.1), where the distribution of measure over points of the set is assumed to constant, and on the basis of the thermodynamic formalism (Sec. 3.2), which is formally identical to the apparatus of ordinary thermodynamics. The use of the latter apparatus opens up, besides the familiar description, the possibility of representing the evolution of the set as a fractal phase transition. This observation makes it possible, in particular, to solve a well-known problem arising in the description of the evolution of the defect structure of a solid during plastic strain (see Ref. 12): By observing the pattern of restructuring of one type of distribution of defects into another (see, for example, Fig. 4) it became completely clear that a unique phase transition occurs, but it was impossible to define in the standard manner the corresponding order parameter, thermodynamic singularities, critical exponents, and so on.[35] The formalism described in Sec. 2.2 shows that restructuring of the defect structure is a transformation of one monofractal into another with different dimension D.

As we have already mentioned, in this exposition we concentrated mainly on the use of the concept of a fractal in problems of condensed-state theory, which have been studied in recent years. Thus in Sec. 2.4.1 it was shown that if a medium has partial memory, then it can be represented as a chain of parallel processes, some of which proceed in accordance with the principle of mechanical reversibility and for this reason preserve the memory of the system, while others are realized according to a thermodynamic scenario, where dissipation leads to complete loss of memory. It turned out that such a system can be represented by a fractal set of statistical ensembles, the description of which leads to the concept of a fractional integral (derivative as a result of the change in the ratio of the fractions of the mechanical and thermodynamic channels, diffusion-type equations transform into wave-type equations. Section 2.4.2 is devoted to investigation of the temporal behavior of the observed quantities in the indicated systems. Their characteristic feature lies in the hierarchical coordination of the statistical ensembles, until equilibrium is reached in clusters with maximum overlapping; groups of ensembles with smaller overlapping are not included in the structural relaxation process. It is shown that as a result of such hierarchical ordering the Debye relaxation law transforms into more slowly decaying extended Kohl-

rausch exponential, power-law, logarithmic, and double logarithmic functions.

These systems are described on the basis of a monofractal presentation. More complicated examples, requiring the use of the concept of a multifractal set, are studied in Sec. 3.3. Thus a scenario of appearance of turbulent fluid flow via period doubling is studied in Sec. 3.3.1. It is shown that the corresponding set is engendered by a logistic chain of bifurcations, whose mapping function has the simplest parabolic form. The simplest analytical investigation of this mapping makes it possible to establish the characteristic values of the spectrum of the fractal dimensions. It turns out that its main feature is determined by the presence of two characteristic similarity scales, which are connected in a root manner. The exact form of the spectrum of fractal dimensions $D(q)$ and the spectral function $f(\alpha)$ is established on the basis of numerical methods of modeling of the map. The thermodynamic method of description of a given multifractal makes it possible to represent the transition from one scale to another as a first-order phase transition, accompanied by a jump in the information entropy.

In Sec. 3.3.2 we examined quasiperiodic sequences, generated by an antisymmetric map function. Physical examples of such sets are incommensurable and long-period structures as well as the important case of quasicrystals. It is shown that the long-period structures correspond to points of a monofractal set maximally contained in the given multifractal. The quasicrystalline sequence, on the other hand, is realized least often and is represented by the well-known Fibonacci sequence. A regular method for constructing this sequence was described and the distribution of wave vectors, at which the maxima of the diffraction pattern for radiation penetrating through the quasicrystalline lie, was found. In concluding the section the characteristic values of the fractal dimensions were found and the spectral functions $D(q)$ and $f(\alpha)$ were constructed. Both the case of locking of phases, which represents the spectrum of frequencies of one of the scenarios for the appearance of turbulence and the case of representing the phases themselves were studied.

The final section, Sec. 3.3.3, is devoted to multifractal representation of nonergodic systems. The analysis is given for the examples of Anderson's model and a spin glass. The relative simplicity of the first example is associated with the fact that even though the multifractal set of clusters of localized states is nonergodic, hierarchical coordination does not arise. The existence of a nontrivial spectrum of fractal dimensions means that far from the transition point an ensemble of clusters that has the minimum dimension behaves in accordance with the mean-field approximation. As the transition point is approached, critical growth of fluctuations of the delocalized phase occurs, indicating a decrease of the fractal dimension. The values of the critical exponents change accordingly. The described picture, evidently, corresponds not only to Anderson's transition, but also to any phase transformation. Thus the fact that the critical exponents are different from the values given by Landau's theory is represented as the existence of a spectrum of fractal dimensions of a set of fluctuations of the new phase. The characteristic feature of spin glass is that the ensemble of variables is divided into hot variables (spin) and cold variables (overlap integral and local values of the field conjugate to the spin). Accordingly, the system becomes not only nonergodic but also hierarchically coordinated. It was found that the uniquely determined spectrum of fractal dimensions is smeared into a stochastic collection of such spectra. An original method for describing the ensemble of spectra as a generalization of the thermodynamic representation of a multifractal is developed. The method is compared to Parisi's well-known replica representation. In conclusion the stochastic picture of the description of the system based on the Fokker–Planck equation is presented.

Of course, the examples considered in this review do not cover all static systems that can be understood on the basis of the concept of a fractal. Such systems include, evidently, models of associative memory, which are currently under development (see Ref. 60). It is easy to give other possible applications, but we hope that the material described in this review is sufficient to convince the reader that the concept of a fractal plays a central role in the description of the collective behavior of complicated systems.

It is our pleasant duty to thank V. G. Bar'yakhtar, who supported this work and A. V. Paul', who convinced us of the need for such a review for solid state physicists. The discussion of the review at the 11th School-Seminar on the Spectroscopy of Molecules and Crystals (Khar'kov, May 1993) also played an important role. We thank the participants and organization committee for their interest. Finally, we thank D. O. Kharchenko and O. P. Zhurke for assistance in processing the paper.

[1)]Topological equivalence of two figures means that one can be transformed into the other by means of a continuous change of the characteristic dimensions. Thus, for example, a ring can be transformed into a topologically equivalent circle by decreasing the thickness of the ring.

[2)]A. V. Paul' pointed out this method to us.

[3)]In order to avoid misunderstandings, we note that we have in mind clusters of statistical ensembles in an ultrametric space. They do not necessarily correspond to clusters of structural units in r space.

[4)]Evidently, the relation $j=\xi^{-1}$ is satisfied under curdling, and Eq. (2.11) gives $D=1$. Similarly, $\alpha=1$ was used for a monofractal within the geometric approach [see Eq. (2.27)].

[5)]In similarity theory the exponent ζ, defined by the relation $C(r) \propto r^{-(d-2-\zeta)}$, is usually employed.[34] Comparing it to Eq. (3.48), we obtain the relation $D_2=2-\zeta$. As a rule, ζ is small: Thus, for thermodynamic systems undergoing a phase transition (see Table II and Sec. 3.3.3), we have $\zeta<0.1$ and therefore $D_2\approx 2$.

[6)]As shown in Sec. 2.1.2, they represent the distance between different points x of the ultrametric space.

[7)]The role of such an action does not necessarily reduce to an external field. It can also be a self-consistent field, arising as a result of self-organization processes inherent in the system itself.[40]

[8)]In the English terminology the term golden mean is used. It is well known that the proportions of Hellenic temples determined the golden mean.

[9)]On the basis of synergetic ideology, mode-locking is associated with the nonequilibrium system falling into metastable minima of the synergetic potential $V(\omega)$ as a function of the frequency.[40] The corresponding analytic analysis can be found, for example, in Sec. 3 of Ref. 37. The devil's staircase, presented in Fig. 33 and reflecting mode-locking graphically, is obtained numerically in Ref. 10.

[10)]We call attention to the fact that the parameters α and Ω for the

temporal and spatial sequences (3.119) are defined differently (in the first case the index n determines discrete points on the time axis and in the second case it determines discrete points on the spatial axis). For the temporal sequence the quantities α and Ω represent the ratios of the characteristic frequency ω_0 to the frequencies ω_1 and ω of the external action and response, respectively. For the spatial structure, however, these ratios must be inverted, and the quantities α and Ω are found to be proportional to the wave numbers k_1 and k of the external action and response (of course, in a self-organizing long-period structure the scale k_1 may not appear).

[11)]Since we investigated the same map (3.119) previously, in order to avoid misunderstandings it should be noted that the set presented above characterized the spectrum of the spatiotemporal structure, while in what follows the distribution of phases x realized on this spectrum will be investigated.

[1]B. B. Mandelbrot, Science **155** 636 (1967).
[2]B. B. Mandelbrot, *The Fractal Geometry of Nature*, Freeman, New York, 1982.
[3]E. Feder, *Fractals*, Plenum Press, New York, 1988.
[4]L. Pietronero and E. Tosatti [Eds.], *Fractals in Physics*, North-Holland, N.Y., 1986.
[5]B. M. Smirnov, *Physics of Fractal Clusters* [in Russian], Nauka, Moscow, 1991.
[6]B. M. Smirnov, Usp. Fiz. Nauk **149**, 177 (1986) [Sov. Phys. Usp. **29**, 481 (1986)].
[7]R. Jullien, Comm. Mod. Phys., Part B, Vol. 13, No. 4 (1987), pp. 177–205.
[8]J. L. McCauley, Phys. Rep. **189**, 225 (1990).
[9]G. Paladin and A. Vulpiani, Phys. Rep. **156**, 147 (1987).
[10]T. C. Halsey, M. N. Jensen, L. P. Kadanoff, I. Procaccia, and B. I. Shraiman, Phys. Rev. A **33**, 1141 (1986).
[11]D. Levine and P. J. Steinhardt, Phys. Rev. B **34**, 596 (1986). J. E. Socolar and P. J. Steinhardt, Phys. Rev. B **34**, 617 (1986).
[12]*Structural Levels of Plastic Strain and Fracture* [in Russian], Nauka, Novosibirsk, 1990.
[13]*Synergetics and Fatigue Fracture of Metals* [in Russian], Nauka, Moscow, 1989.
[14]V. E. Panin, V. A. Likhachev, and Yu. V. Grinyaev, *Structural Levels of Deformation of Solids* [in Russian], Nauka, Novosibirsk, 1985.
[15]A. I. Olemskoi and I. A. Sklyar, Usp. Fiz. Nauk. **162**, 29 (1992) [Sov. Phys. Usp. **35**, 455 (1992)].
[16]R. R. Nigmatullin, Teor. Matem. Fiz. **90**, 354 (1992).
[17]R. Rammal, G. Toulouse, and M. A. Virasoro, Rev. Mod. Phys. **58**, 765 (1986).
[18]K. Binder and A. P. Joung, Rev. Mod. Phys. **58**, 801 (1986).
[19]S. L. Ginzburg, *Irreversible Phenomena in Spin Glasses* [in Russian], Nauka, Moscow, 1989.
[20]A. I. Olemskoi and E. A. Toropov, Fiz. Met. Metalloved., No. 9, 5 (1991).
[21]A. I. Olemskoi, Fiz. Tverd. Tela **30**, 3384 (1988) [Sov. Phys. Solid State **30**, 30, 1944 (1988)].
[22]A. I. Olemskoi and I. I. Naumov in Ref. 13, p. 200.
[23]A. I. Olemskoi, Fiz. Met. Metalloved. **68**, 56 (1989).
[24]A. I. Olemskoi and Yu. I. Paskal', Preprint No. 30, Institute of Physics and Applied Mathematics, Tomsk Affiliate of the Siberian Branch of the USSR Academy of Sciences, Tomsk, 1988.
[25]A. I. Olemskoi and E. A. Toropov, Fiz. Met. Metalloved., No. 7, 32 (1991).
[26]D. Adelman, C. P. Burmester, L. T. Wille, P. A. Sterne, and R. Gronsky, J. Phys.: Condensed Matter **4**, L585 (1992).
[27]J. Kjems and T. Freltoft, *Scaling Phenomena in Disordered Systems*, Plenum Press, New York, 1985.
[28]G. Porod, *Small Angle X-Ray Scattering*, Academic Press, New York, 1983.
[29]S. G. Samko, A. A. Kilbas, and O. I. Marichev, *Integrals and Derivatives of Fractional Order and Their Applications* [in Russian], Nauka i tekhnika, Minsk, 1987.
[30]D. Forster, *Hydrodynamic Fluctuations, Broken Symmetry, and Correlation Functions*, W. A. Benjamin, Reading, MA, 1975.
[31]D. N. Zubarev, *Nonequilibrium Statistical Thermodynamics* [in Russian], Nauka, Moscow, 1971.
[32]A. I. Olemskoi, I. V. Koplyk, I. A. Sklyar, E. A. Toropov, and A. Ya. Flat, Izv. Vyssh. Uchebn. Zaved., Fiz., No. 1, 90 (1993).
[33]A. K. Jonscher, *Dielectric Relaxation in Solids*, Chelsea Dielectric Press, London, 1983.
[34]L. D. Landau and E. M. Lifshitz, *Statistical Physics*, Pergamon Press, New York, 1977.
[35]A. A. Katsnel'son and A. I. Olemskoi, *Microscopic Theory of Inhomogeneous Structures* [in Russian], Moscow State University Press, Moscow, 1987.
[36]G. Parisi, Phys. Rev. Lett. **50**, 1946 (1983).
[37]L. D. Landau and E. M. Lifshitz, *Fluid Mechanics*, Pergamon Press, New York, 1989.
[38]M. J. Feigenbaum, J. Stat. Phys. **19**, 25 (1978); 21, 668 (1979).
[39]M. Abramovitz and I. Stegan [Eds.], *Handbook of Special Functions*, Dover Press, New York.
[40]H. Haken, *Synergetics*, Springer-Verlag, New York, 1983; *Advanced Synergetics: Instability Hierarchies of Self-Organizing Systems and Devices*, Springer-Verlag, New York, 1983.
[41]P. Bak, Rep. Prog. Phys. **45**, 587 (1981).
[42]M. H. Jensen and P. Bak, Phys. Rev. A **30**, 1960, 1970 (1984).
[43]P. Svitanovic, M. H. Jensen, L. P. Kadanoff, and I. Procaccia, Phys. Rev. Lett. **55**, 343 (1985).
[44]S. J. Shenker, Physica D **5**, 405 (1982).
[45]P. W. Anderson, Phys. Rev. **109**, 1492 (1958).
[46]*Disordered Systems and Localization. Lecture Notes in Physics*, Springer-Verlag, New York, 1981, Vol. 149.
[47]B. Derrida and E. Gardner, J. de Phys. Paris **45**, 1283 (1984).
[48]G. Parisi and A. Vulpiani, J. Phys. A. **19**, L425 (1986).
[49]A. I. Olemskoi, Phys. Status Solidi **160**, 569 (1990).
[50]E. M. Lifshitz and L. P. Pitaevskii, *Physical Kinetics* [in Russian], Nauka, Moscow, 1979.
[51]K. G. Wilson and J. Kogut, Phys. Rep. C **12**, 75 (1974).
[52]A. Z. Patashinskii and V. L. Pokrovskii, *Fluctuation Theory of Phase Transitions*, Pergamon Press, N.Y., 1979.
[53]V. L. Aksenov, M. Bobeth, N. M. Plakida, and I. Schreiber, J. Phys. C. **20**, 375 (1987).
[54]M. Mezard and M. A. Virasoro, J. de Phys. Paris **46**, 1293 (1985).
[55]R. G. Palmer, Adv. Phys. **31**, 669 (1982).
[56]M. Serva and G. Paladin, Phys. Rev. Lett. **70**, 105 (1993).
[57]G. Parisi, J. Phys. A **13**, 1101 (1980).
[58]J. M. Bell, N. E. Frankel, and S. Inawashiro, Phys. Rev. B **33**, 476, 487 (1986).
[59]V. V. Gnedenko, *Course in Probability Theory* [in Russian], Nauka, Moscow, 1988.
[60]D. J. Amit, H. Gutfreund, and H. Sompolinsky, Ann. Phys. **173**, 30 (1987).

Translated by M. E. Alferieff